

**Self-action of laser beams in
photorefractive crystals with external
applied AC or DC electric fields**

DISSERTATION

Zur Erlangung des akademischen Grades

Doctor rerum naturalium (Dr. rer. nat.)

vorgelegt dem Rat der
Physikalisch-Astronomischen Fakultät
der Friedrich-Schiller-Universität Jena

von

Diplom-Ingenieur Oleg Kashin
geboren am 16. Juni 1981 in Asino, Russland

Gutachter:

1. Prof. Dr. Richard Kowarschik

Institut für Angewandte Optik

Friedrich-Schiller-Universität Jena

2.

3.

Tag der Disputation:

Contents

| | |
|--|-----------|
| 1 Introduction | 1 |
| 2 Self-action of laser beams due to the photorefractive effect..... | 6 |
| 2.1 Control of the photorefractive response | 8 |
| 2.1.1 Applied DC electric field..... | 9 |
| 2.1.2 Applied AC electric field..... | 12 |
| 2.2 Beam propagation equation for slowly varying amplitudes..... | 14 |
| 2.3 Laser beam propagation in uniaxial crystals | 15 |
| 2.3.1 (1+1)D case | 15 |
| 2.3.2 (2+1)D case | 16 |
| 2.4 Laser beam propagation in cubic crystals..... | 18 |
| 2.4.1 Base equations | 18 |
| 2.4.2 (1+1)D laser beam propagation | 19 |
| 2.4.3 (2+1)D laser beam propagation | 21 |
| 2.5 Self-bending of the laser beam | 23 |
| 3 Beam self-trapping and self-bending dynamics in a SBN crystal | 28 |
| 3.1 Experimental results | 28 |
| 3.2 Theoretical model | 31 |
| 3.3 Conclusion | 34 |
| 4 Self-action of light beams in sillenites | 36 |
| 4.1 Self-action of light beams in (110)-cut sillenites..... | 36 |
| 4.1.1 Theoretical model | 36 |
| 4.1.2 Numerical simulation | 45 |
| 4.1.2 Conclusion..... | 56 |
| 4.2 Self-action of light beams in (112)-cut sillenites..... | 57 |
| 4.2.1 Theoretical model | 57 |
| 4.2.2 Numerical simulation | 58 |
| 4.2.3 Conclusion | 60 |

| | |
|--|-----------|
| 5 Self-bending of laser beams in photorefractive crystals | 61 |
| 5.1 Self-bending in BaTiO ₃ | 61 |
| 5.1.1 Basic equations | 61 |
| 5.1.2 Results and discussion | 64 |
| 5.1.3 Conclusion | 68 |
| 5.2 Self-bending in cubic photorefractive crystals | 68 |
| 5.2.1 Theoretical model | 68 |
| 5.2.2 Results of numerical analysis | 69 |
| 5.2.3 Experimental results | 80 |
| 5.2.4 Conclusion | 83 |
| 6 Conclusion | 84 |
| References..... | 88 |

Chapter 1

Introduction

The phenomenon of self-action of coherent light in light-sensitive media is a basis of nonlinear optics. This phenomenon is used widely in industry for the production of different high-technological equipments. During the self-action process the light changes the refractive index of the medium that by turn influences the propagating beam. This effect is very important for the developing of optical devices to control light with light as optical switches, optical memories and dynamic waveguides. The most popular media used in such optical devices are electro-optic crystals. The electro-optic effect is connected with the change of the refractive index of the medium under light illumination in the presence of an external applied electric field. The change of the refractive index due to the electro-optic effect occurs by means of linear (Pockels) and quadratic (Kerr) effects. Crystals with Kerr nonlinearity require a higher intensity of the propagating light (about 1 W) to observe the self-action of laser beams while crystals with photorefractive nonlinearity require only powers of 1-10 μ W. The last fact makes photorefractive crystals very attractive media to investigate different phenomena of the beam self-action as self-trapping and self-bending.

The self-trapping process is interesting due to the possibility to observe spatial solitons. Under spatial solitons one understands the propagation of focused laser beams in nonlinear media when the essential diffraction is compensated by the focusing nonlinearity. Spatial solitons in photorefractive crystals have been studied already since 1993 [1-11] after their first experimental confirmation [1, 2]. In contrast to spatial solitons in Kerr media photorefractive spatial solitons are stable in both transverse dimensions (two-dimensional waveguides) [12, 13]. Therefore they have great potential for the application in optical telecommunication devices. The main idea of such devices is based on the fact that the soliton is a fundamental mode of the optical waveguide induced in the photorefractive medium. The ability to generate two-dimensional waveguide structures by the spatial soliton has an application in optical writing or reconfigurable interconnections if solitons

can be switched electrically, optically, or by other soliton beams. Frequency mixing can also be realized in such waveguides if they are part of the wavelength conversion process or are induced additionally. The main advantage of the frequency mixing in photorefractive optical waveguides is the ability to vary the waveguide diameter and to change the propagation constants of the interacting guided beams. This is not possible in a structured waveguide where the propagation constants and dimensions are fixed.

The linear electro-optic effect can be observed in crystals with no center of symmetry only. Among these crystals one can single out single-axis crystals and cubic sillenite crystals of the group 23 and $\bar{4}3m$ which are used generally in experimental works. Single-axis photorefractive strontium barium niobate crystals (SBN) are appropriate materials for the investigation of the photorefractive beam self-trapping and photorefractive solitons. The corresponding pioneer works were published in [2, 7, 14]. By studying the dynamic evolution [15-17] of solitons and their temporal development [18, 19] in photorefractive crystals it became possible to obtain conditions for stabilized solitons in common [20, 21] as well as in dissipative [22] photorefractive systems and finally the properties of quasi-steady-state solitons could be described as well [23, 24]. In spite of the great number of works dealing with the photorefractive self-trapping effect in photorefractive crystals the influence of external parameters as the electric field, the input beam intensity and the input beam diameter (FWHM) were not studied in detail.

Thanks to good photorefractive properties for the visible range, cubic $\text{Bi}_{12}\text{TiO}_{20}$ (BTO) and $\text{Bi}_{12}\text{SiO}_{20}$ (BSO) crystals from the sillenite family are rather popular nonlinear media for the study and implementation of different effects of light beam self-action (see, e.g., [4, 25, 26-32]). When choosing the directions of light beam propagation and application of an external electric field used to increase the nonlinear response, one should take into account the anisotropy of the electro-optic properties of sillenites belonging to the class of 23 symmetry of cubic systems. Conventionally, a light beam propagates along the (110) crystallographic direction under an applied external electric field along the axes (001) [4, 25, 27, 31, 33], (111) [29], or (110) [27, 29]. The equations describing the self-action effects for an arbitrary orientation of the applied field in a plane orthogonal to the (110) light propagation direction are presented in [29, 31]. However, only the simple electro-optic mechanism of the photorefractivity has been taken into account. It is believed that the spatial variations in dielectric permittivity are primarily caused by the electrooptic contribution of the space-charge field which is formed in a crystal.

Nevertheless, the additional elasto-optic contribution to the dielectric permittivity changes of the photorefractive grating was taken into account [34] and [35]. More recently Gunter and Zgonik [36] considered the roto-optic contribution that is evident in crystals with strong linear birefringence only. Both the elasto-optic and roto-optic contributions are associated with the inhomogeneous elastic field induced by the piezoelectric effect in a non-centrosymmetric crystal during photorefractive grating formation. In addition, a nonuniform piezoelectric polarization of the effective static dielectric constant [34-37] of the medium must be taken into consideration that influences on the condition of trap saturation. The influence of the elasto-optic effect on Bragg diffraction, two-wave mixing, and beam fanning has been experimentally verified in various photorefractive crystals such as LiNbO_3 [34], $\text{Bi}_{12}\text{GeO}_{20}$ [38], $\text{Bi}_{12}\text{SiO}_{20}$ [39-41], $\text{Bi}_{12}\text{TiO}_{20}$ [35, 42-45], GaAs [46], KNbO_3 [47], and BaTiO_3 [47-49].

The cut (110) of sillenite crystals is not unique for implementation of light self-action effects. It is known that cubic photorefractive crystals of {112}-cuts have the feasibility of implementation of a counter light-beam interaction on holographic gratings [50], which is absent in samples of the conventional {110}-cuts.

At the same time the effect of laser beam self-focusing is accompanied by the bent of the trajectory of the light propagation (self-bending). Self-bending of light beams occurs when they propagate in single-axis photorefractive crystals with a nonlocal nonlinearity of a diffusion type [51-54, 92]. In barium titanate (BaTiO_3) and strontium-barium niobate (SBN) this effect is strong due to large values of their electro-optic coefficients. However, only the simple electro-optic mechanism of photorefractivity has been taken into account [3, 54-58, 60] in the analysis of this effect without considering the anisotropy of the additional photoelastic contribution to the modulation of the optical properties of the medium by the space-charge field induced by a light beam.

In cubic sillenite-type crystals the effect of the self-bending is much weaker. However, it is well known that the nonlocal nonlinearity in these crystals is strongly amplified by an external alternating field [61]. Self-bending of a light beam propagating in a cubic photorefractive crystal with an applied square-wave electric field was considered by Borodin *et al.* [62], who disregarded the optical activity of the crystal. At the same time, it is well known [64] that cubic crystals of point group 23 have a considerable rotary power at the wavelength of a helium-neon laser in the range from 6 deg/mm in $\text{Bi}_{12}\text{TiO}_{20}$ (BTO) to 22 deg/mm in $\text{Bi}_{12}\text{SiO}_{20}$ (BSO) and $\text{Bi}_{12}\text{GeO}_{20}$ (BGO). The rotation of the polarization

plane can affect considerably the self-action of a light beam due to the anisotropy of the electro-optic effect.

The aim of this work is to study theoretically and experimentally the influence of the additional photoelastic contribution to the modulation of the optical properties by the space-charge field as well as the effect of the optical activity on self-focusing and self-bending of laser beams. An accounting of the additional photoelastic contribution allows to separate the influence of effects of the induced birefringence and the formed space-charge field on the optical properties of the medium. It is not possible to separate these effects in existing theoretical models that lead to the strong distortion of the theoretical beam intensity distribution and of the beam polarization state. The influence of the optical activity on the nonlocal photorefractive response of cubic crystals gives an opportunity to predict and observe new effects of laser beam self-bending.

The dissertation work has six chapters. The **second chapter** gives a brief review of self-action effects of the focused laser beam propagation in different photorefractive crystals. We discuss existing theoretical models describing beam self-focusing and self-bending, and show their restrictions.

For the study of additional self-action effects of the light beam propagation in photorefractive crystals we present in the **third chapter** basic experimental and theoretical investigations of the self-trapping and the self-bending of a laser beam with different input diameters in a photorefractive SBN-crystal in dependence on the applied electric field, the input beam intensity and the input beam diameter (FWHM).

In the **fourth chapter** we develop a theoretical model of self-action of one-dimensional light beams in (110)-cut sillenite crystals. The model takes into account the vector nature of the light field, the gyrotropy of the medium, the linear birefringence induced by the external field, and the additional photoelastic contribution to the modulation of the optical properties by the space-charge field.

The considered cut (110) of sillenite crystals is not unique for the implementation of light self-action effects. Further we are going to derive equations with which we can analyze the self-action of light beams with a one-dimensional input intensity distribution propagating along the crystallographic [112] axis of 23 symmetry crystals.

The **fifth chapter** is aimed at studying self-bending of light beams in single-axis BaTiO₃ crystals and in cubic photorefractive crystals of (110)-cut by considering the optical activity of the crystals. Following the simple model of Lyubomudrov and Shkunov

[56], we investigate theoretically the trajectories of the self-bending for extraordinary speckle-beam in BaTiO₃ considering the elasto-optic contribution to the changes of the dielectric permittivity for the photorefractive response. We neglect the roto-optic contribution because of the weak linear birefringence of BaTiO₃. We present also experimental results of the laser beam self-bending in the BTO.

The **last chapter** summarizes the main results of this dissertation.

Chapter 2

Self-action of laser beams due to the photorefractive effect

Self-action of the light in photorefractive materials has a great interest in optical processing technologies [65-67]. Thanks to the high nonlinear optical susceptibilities and the ability to maintain holograms for long periods of time [68] have made them attractive in dynamic holography [69-71], laser coupling [72-80] and nonlinear optical imaging [81, 82]. The photorefractive effect is connected with processes of the charge redistribution on trapped hole centres under inhomogeneous light illumination. For the case with electronic conductivity the light produces charges from donor impurity in the conducting band. The drift of free charges in the external and internal electric fields, the diffusion and photovoltaic effect lead to an inhomogeneous space-charge distribution after charges have been recombined on the trapped hole centres. The created electrostatic field of the space-charges leads to the change of the optical properties of the crystal due to the linear electro-optic effect of Pockels [83]. The form of the created electrostatic field is characterized by the distribution of the light intensity. Hereby induced perturbations in the medium by the laser beam excite changes in the initial light field and so one observes self-action effects of the light due to photorefractive nonlinearity.

Processes of self-action lead to the self-focusing (defocusing) and self-bending of laser beams. The most interesting field of the experimental and theoretical investigation of the laser beams self-action is the self-focusing because of the possibility to produce stable optical waveguides in photorefractive crystals. If the diameter of such a waveguide keeps itself stable along the laser beam propagation distance it calls – optical soliton. Optical solitons exist also in media with Kerr nonlinearity but they require a rather large power of the input beam about 400 kW or higher however photorefractive optical solitons can be realized with input beam powers of the order 10 μ W.

Self-trapping of the laser beam in photorefractive crystals first time was predicted by M. Segev *et al.* [1] and B. Crosignani *et al.* [2] as a process of the screening of the internal electric field by the external applied voltage based on the Pockels effect. Photorefractive solitons can exist in two different stages: quasy-steady-state and steady-state. Quasi-steady-state solitons can be trapped only during short time periods and then suffer diffraction, break-up and fanning [14]. This first type of photorefractive solitons was predicted and observed as bright and dark self-trapped beams in one and two transverse directions [14, 33, 84]. Such types of self-trapped beams are of interest only for the study of the temporal dynamics of the self-focusing effect.

The other type of photorefractive solitons is based on the so-called screening nonlinearity. Waveguide structures formed by the screening self-focusing exist as long as the corresponding experimental conditions remain constant. In comparison also with the Kerr nonlinearity photorefractive screening solitons are supported in both transverse directions. The idea of screening solitons is based on the fact that an artificial background illumination helps to inhibit the quasi-steady-state configuration [4]. This fact was also confirmed in some experimental works [7, 85]. The runaway increase of the charge density leads to a quasi-steady-state regime. The background illumination helps to decrease the charge density due to the charge recombination at the edge of the propagating beam. This is the result of the low dark conductivity in the dark region of the crystal. An artificial increase of the crystal conductivity by means of homogeneous dark irradiance of the whole sample leads to the stable dark current that suppresses the unrestrained increase of charges in the conducting band. The resulting electric field in the crystal, screened by the external applied voltage, depends only on the ratio of the intensity of the propagating beam to the background illumination. By means of the linear electro-optic effect the resulting refractive index change gives rise to a stable self-lensing effect [85]. The exact balance between the essential diffraction and the self-trapping is generally referred as an *optical soliton*.

Photorefractive screening solitons have been observed in different configurations and in different media as bright 1D slab solitons [4], as dark (1+1)D slabs [6, 86], as bright (2+1)D needle solitons [12, 13], and even as dark needles [87]. The self-trapping solitons were experimentally detected in SBN [12, 13] and BTO [4, 88] crystals.

The common experimental setup realizing self-trapped beams in photorefractive crystals is shown in figure 2.1. Polarizer P controls the input polarization of the laser beam. The beam is focused by the lens L1 on the input face of the crystal. The external electric

field U_0 is applied along the optical axis c . Changing the appropriate ratio of the laser beam intensity to the background illumination it becomes possible to find experimentally conditions under which one can observe the self-trapped beam as an optical soliton. The output face of the crystal is observed by means of lens L2 and a CCD camera. The experimental setup is a common scheme to realize all experiments dealing with self-action of the laser beams such as self-focusing, self-bending, interaction of solitons and solitonic lattices.

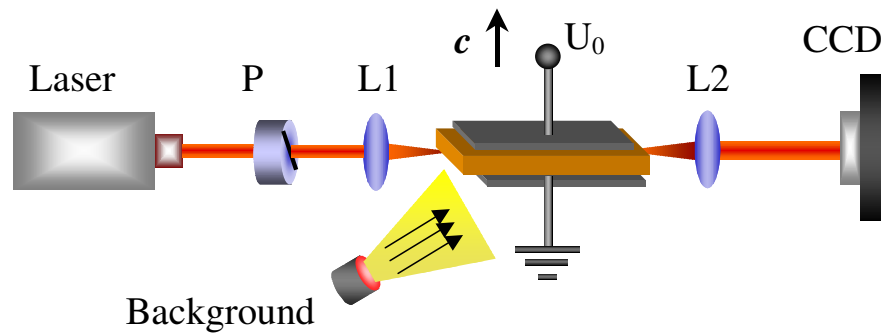


Figure 2.1: Typical experimental setup to realize self-trapped beams in photorefractive crystals.

In this chapter we discuss the theoretical base to study the self-action of laser beams in photorefractive single-axis and cubic crystals. The main equations to control the photorefractive response in the media will be presented. We observe effects of self-focusing and self-bending, and show base mechanisms to control these nonlinear processes.

2.1 Control of the photorefractive response

The fundamental advantage of photorefractive crystals is the ability to provide nonlinear response of the medium under the light illumination with powers of order of $10 \mu\text{W}$. The control of the photorefractive response of a crystal is realized by applying an external alternating (AC) or direct (DC) electric field. Under an applied DC electric field photoinduced electrons drift in one direction of the applied voltage and pass at an average the same length L_0 (drift length) till they will be trapped by ionized donors. The diffusion of electrons occurs due to thermal processes and has a great magnitude particularly in single-axis crystals. In cubic electro-optic crystals the magnitude of the diffusion can be enhanced by applying an AC electric field [61]. These two mechanisms of the control of

the photorefractive response let to observe effects of the self-focusing (self-defocusing) and the self-bending of laser beams, and could be described by means of the one level transport model of Kukhtarev *et al.* [89]:

$$\frac{dN_D^+}{dt} = s(I_d + I)(N_D - N_D^+) - \gamma_R n N_D^+, \quad (2.1)$$

$$\nabla \cdot (\hat{\epsilon} \mathbf{E}) = \rho, \quad (2.2)$$

$$\frac{\partial}{\partial t} \rho + \nabla \cdot \mathbf{J} = 0, \quad (2.3)$$

$$\rho = e(N_D^+ - n - N_A), \quad (2.4)$$

$$\mathbf{J} = e\mu n \mathbf{E} + \kappa_B T \mu \cdot \text{grad}(n), \quad (2.5)$$

where I – optical intensity, \mathbf{E} – the space-charge field, N_D^+ and n_e – concentrations of ionized donors and free charges; N_D – full concentration of donor centers; N_A – concentration of acceptors compensating the charge of ionized donors in the dark; s – photoionization cross-section; γ_R – two-particle recombination constant; $\hat{\epsilon}$ – low frequency dielectric constant; ρ – density of the space-charge field; e – charge of the electron; μ – mobility of photoelectrons in the conducting band; κ_B – Boltzmann's constant; T – absolute temperature.

2.1.1 Applied DC electric field

The first theoretical prediction [1] of the (1+1) D self-focusing of the laser beam in photorefractive crystals under the applied direct electric field was the base for a number of theoretical (for example [2-9, 1110, 85]) as well as experimental (for example [8, 12-14, 33, 84, 86-88, 90]) works studying these effects in different crystals. The nature of the space-charge distribution depends on experimental conditions. The first experimental paper [14] has demonstrated the possibility of the laser beam self-focusing in the medium with photorefractive nonlinearity where a one-dimensional light distribution is focused by a cylindrical lens on the input face of the crystal. In this case the space-charge distribution has also one-dimensional nature. If the input laser beam has a two-dimensional light distribution the induced space-charge field depends in this case also on the transverse coordinate and the theoretical model of Kukhtarev *et al.* has to be considered for the (2+1)D cases.

The speed of the space-charge field formation depends on the relaxation time of the electric field which has different magnitudes for different crystals types. Generally this task is solved for stationary conditions suggesting that the process of the charge redistribution reaches saturation. In this chapter we consider only steady-state conditions and present the exact solution of the amplitude of the space-charge field for (1+1)D cases and the common analytical solution for the (2+1)D cases.

One dimensional case

Under steady-state conditions the set of Kukhtarev equations (2.1)-(2.5) in the one dimensional case takes the form:

$$\frac{dN_D^+}{dt} = s(I_d + I)(N_D - N_D^+) - \gamma_R n N_D^+, \quad (2.6)$$

$$\frac{dE_{SC}}{dx} = \frac{e}{\epsilon_0 \epsilon_r} (N_D^+ - n - N_A), \quad (2.7)$$

$$\frac{d}{dx} [e\mu n E_{SC} + \kappa_B T \mu \cdot grad(n)] = 0, \quad (2.8)$$

where ϵ_0 – dielectric constant; ϵ_r – relative dielectric conductivity in the crystal along the direction of the applied electric field. The spatial dependence of all variables on the propagation coordinate is ignored, while they vary much rapidly in transverse direction. Thus the contribution of the electric field to the modulation of optical properties of the medium along the propagating distance can be neglected.

The estimation of the space-charge field can be simplified if the laser beam propagates in the photorefractive crystal under steady-state conditions [69-71]. In this case the amplitude of the space-charge field E_{SC} is described by the nonlinear differential equation [76]:

$$E_{SC}(x) = E_0 \frac{I_\infty + I_d}{I + I_d} \left(1 + \frac{\epsilon_0 \epsilon_r}{e N_A} \frac{dE_{SC}}{dx} \right) - \frac{\kappa_B T}{e} \left(\frac{1}{I + I_d} \frac{dI}{dx} \right) + \frac{\kappa_B T}{e} \frac{\epsilon_0 \epsilon_r}{e N_A} \left(1 + \frac{\epsilon_0 \epsilon_r}{e N_A} \frac{1}{I + I_d} \frac{dE_{SC}}{dx} \right)^{-1} \frac{d^2 E_{SC}}{dx^2}. \quad (2.9)$$

The inequality $e N_A \gg \epsilon_0 \epsilon_r \frac{dE_{SC}}{dx}$ satisfies the condition if the traps saturation is absence in the crystal. Under this condition and in the linear approximation the equation (2.17) can be reduced to the simpler form:

$$E_{\text{SC}}(x) = E_0 \frac{I_\infty + I_d}{I + I_d} - \frac{\kappa_B T}{e} \left(\frac{1}{I + I_d} \frac{dI}{dx} \right). \quad (2.10)$$

The obtained solution of the one dimensional space-charge field distribution describes the contribution of the local and nonlocal response of the photorefractive medium when the laser beam propagates through the crystal. The term $E_0 \frac{I_\infty + I_d}{I + I_d}$, corresponding to the local response of the medium, is responsible for the self-focusing and the self-defocusing of the light beam. The self-bending effect arises due to the influence of the second term in equation (2.10). In cubic photorefractive crystals of the sillenite family the second term vanishes due to small values of the electro-optic coefficient if the direct electric field is applied to the crystal. However it is well known [61] that the nonlocal response in cubic photorefractive crystals can be enhanced by applying an alternating electric field.

Two dimensional case

Photorefractive optical spatial solitons are of great interest because of the possibility to form two-dimensional waveguide structures. The created waveguide possesses the fundamental mode parameters of the spatial soliton. In this case the set of Kukhtarev equations has to be solved in frameworks of the (2+1)D model.

The solution for the set of Kukhtarev equations for the vector of the space-charge field \mathbf{E} cannot be found in explicit form. On the other side the dimensionless potential of the static electric field φ is a scalar value and under the standard assumptions $N_A \gg n_e$, $N_D^+ \gg n_e$ it can be reduced to a nonlinear partial differential equation [98].

Introducing the amplitude of the space-charge field by the relation $\mathbf{E} = \nabla_\perp \varphi + \mathbf{E}_0$, where $\nabla_\perp = (\partial/\partial x, \partial/\partial y)$, and under the above assumptions equations (2.1)-(2.5) can be reduced after some manipulations to:

$$\varepsilon_0 \varepsilon_r \frac{\partial}{\partial t} \nabla_\perp^2 \varphi + e\mu \{ \nabla_\perp \cdot [n_e (\nabla_\perp \varphi - \mathbf{E}_0)] \} + \mu \kappa_B T \{ \nabla_\perp \cdot (\nabla_\perp n_e) \} = 0. \quad (2.11)$$

The density of charge carriers n_e can be expressed in the exact form:

$$n_e = s(N_D - N_A)(I + I_d) \tau_R \left(1 + \frac{\varepsilon_0 \varepsilon_r}{e N_A} \nabla_\perp \cdot \mathbf{E} \right)^{-1}, \quad (2.12)$$

where $\tau_R = (N_A \gamma_R)^{-1}$ is the recombination time of free charge carriers. If the power density of the light beam $I(x, y, z)$ varies slowly in both transverse directions x and y , the term

$\left| \frac{\epsilon_0 \epsilon_r}{e N_A} \nabla_{\perp} \cdot \mathbf{E} \right|$ is much less than unity for typical photorefractive media. By substituting

(2.12) in (2.11) the equation for the potential of the space-charge electric field yields:

$$\begin{aligned} \frac{1}{I + I_d} \tau \frac{\partial}{\partial t} \nabla^2 \varphi + \nabla^2 \varphi + \nabla \ln(I + I_d) \cdot \nabla \varphi = \\ E_0 \frac{\partial}{\partial x} \ln(I + I_d) + \frac{k_B T}{e} \left[\nabla^2 \ln(I + I_d) + \{ \nabla \ln(I + I_d) \}^2 \right] \end{aligned} \quad (2.13)$$

where $\tau = \epsilon_0 \epsilon_r / \epsilon \mu n_0$ is the characteristic relaxation time of the electric field. The diameter of the input beam is much smaller than the crystal width and so the power density $I(x, y, z)$ vanishes at the crystal borders that is $I(x \rightarrow \pm\infty, y \rightarrow \pm\infty, z) = 0$. The potential $\varphi(x, y, t)$ is a function of two transverse components of the spatial electric fields E_x and E_y and depends on time.

2.1.2 Applied AC electric field

The control of the nonlinear response in the photorefractive medium can be realized also by means of an applied AC electric field [61]. This technique allows significantly increase the nonlinear response of photorefractive crystals. This effect is especially strong in widegap-semiconductors and sillenite crystals possessing a long drift length of the charge carriers. The applied AC electric field increases significantly two-wave-mixing gain [61, 91-95], improves the beam fanning and phase conjugation efficiency [96, 97], lets to observe spatial subharmonics [98-100] and photorefractive surface waves [101, 102].

If the external square-wave electric field is applied to the photorefractive crystal and the focused laser beam propagates perpendicularly to the direction of this bias field the set of Kukhtarev equations can be solved for the (1+1)D case neglecting the diffusion of charge carriers [37]. Under standard assumptions mentioned in section 2.1 for the steady-state and taking into account only linear and quadratic terms relative to the space-charge field the (1+1)D set of Kukhtarev equations (2.6)-(2.8) can be reduced to two nonlinear equations:

$$\tilde{E}_{SC} - \frac{\tau_d I_d L_E}{I_d + I} \frac{d\tilde{D}_{SC}}{dx} + \frac{k_B T}{e} \left[\frac{1}{I_d + I} \frac{dI}{dx} - \frac{L_A}{E_0} \frac{d^2 \tilde{E}_{SC}}{dx^2} \right] \times \left(1 - \frac{L_A}{E_0} \frac{d\tilde{E}_{SC}}{dx} \right) = 0, \quad (2.14)$$

$$\begin{aligned} & \tilde{D}_{SC} \left(1 + \frac{L_A}{E_0} \frac{d\tilde{E}_{SC}}{dx} \right) - L_E \frac{\tilde{E}_{SC}}{E_0} \frac{d\tilde{D}_{SC}}{dx} - \frac{L_A}{\tau_d} \frac{d\tilde{E}_{SC}}{dx} - L_D^2 \frac{L_A}{E_0} \frac{d^2 \tilde{D}_{SC}}{dx^2} \\ & + L_D^2 \frac{L_A}{E_0} \frac{d\tilde{D}_{SC}}{dx} \frac{d^2 \tilde{D}_{SC}}{dx^2} = -\frac{I}{I_d \tau_d} E_0 \end{aligned}, \quad (2.15)$$

where $\tau_d = \varepsilon / \sigma_d$ is the dielectric relaxation time in the dark area of the crystal, $L_E = \mu \tau_R E_0$ is the drift length, $L_A = \varepsilon E_0 / (e N_A)$ is the length of the electron tightening by the electric field E_0 , and $L_D = (\mu \tau_R \kappa_B T / e)^{1/2}$ is the diffusion length. The equation for the \tilde{E}_{SC} can be obtained from equations (2.14) and (2.15) excluding \tilde{D}_{SC} . If the drift length L_E exceeds the lengths L_D , L_A and the Debye screening length $L_S = [\kappa_B T \varepsilon / (e^2 N_A)]^{1/2}$ then the nonlinear equation for the time-averaged space-charge field takes the form [37]:

$$\begin{aligned} & 2L_S^2 L_E \frac{\tilde{E}_{SC}}{E_0} \frac{d^3 \tilde{E}_{SC}}{dx^3} - \\ & \left[L_E L_A \left(1 - \frac{\tilde{E}_{SC}^2}{E_0^2} \right) + L_S^2 + L_D^2 - 2 \frac{L_S^2 L_E}{E_0} \left(\frac{d\tilde{E}_{SC}}{dx} + \frac{\tilde{E}_{SC}}{I_d + I} \frac{dI}{dx} \right) \right] \frac{d^2 \tilde{E}_{SC}}{dx^2} \\ & - \left\{ 2(L_E - L_A) \frac{\tilde{E}_{SC}}{E_0} + L_E (2L_E - L_A) \frac{\tilde{E}_{SC}}{E_0} \frac{d\tilde{E}_{SC}}{dx} \right. \\ & - \left[L_E - L_A \left(1 - \frac{\tilde{E}_{SC}^2}{E_0^2} \right) + 2L_S^2 + 3L_D^2 \right] \frac{1}{I_d + I} \frac{dI}{dx} \left. \right\} \frac{d\tilde{E}_{SC}}{dx} \\ & + \left[1 - \frac{1}{I_d + I} \left(L_E \frac{\tilde{E}_{SC}}{E_0} \frac{dI}{dx} + 2L_D^2 \frac{d^2 I}{dx^2} \right) \right] \tilde{E}_{SC} + \left(L_E E_0 + \frac{\kappa_B T}{e} \right) \frac{1}{I_d + I} \frac{dI}{dx} = 0 \end{aligned} \quad (2.16)$$

Here it is assumed that the following inequalities are satisfied

$$\frac{L_A}{a} \ll 1, \quad \frac{L_S}{a} \ll 1, \quad \frac{L_D}{a} \ll 1, \quad (2.17)$$

which allow to take into account terms that are linear and quadratic relative to the small parameters L_A/a , L_S/a , L_D/a .

If the diameter of the input beam is small enough to neglect terms involving L_A^2 , L_D^2 , L_S^2 and much smaller than the transverse dimension of the crystal the equation (2.16) can be simplified as:

$$L_E L_A \left(1 - \frac{\tilde{E}_{SC}^2}{E_0^2} \right) \frac{d^2 \tilde{E}_{SC}}{dx^2} + \left[2(L_E - L_A) \frac{\tilde{E}_{SC}}{E_0} + 2L_E L_A \frac{\tilde{E}_{SC}}{E_0} \frac{d\tilde{E}_{SC}}{dx} - L_E L_A \left(1 - \frac{\tilde{E}_{SC}^2}{E_0^2} \right) \frac{1}{I_d + I} \frac{dI}{dx} \right] \frac{d\tilde{E}_{SC}}{dx} - L_E E_0 \frac{1}{I_d + I} \frac{dI}{dx} - \tilde{E}_{SC} = 0 \quad (2.18)$$

In the linear approximation and in the absence of traps saturation ($L_A = 0$), equation (2.16) can be expressed in the explicit form:

$$\tilde{E}_{SC} = \frac{L_E E_0}{I_d + I} \frac{dI}{dx}. \quad (2.19)$$

In this work we will use applied dc and ac electric fields to control the nonlinear response in photorefractive crystals. The applied dc voltage is used to control the local and nonlocal response of the medium in single-axis photorefractive crystals. The applied ac electric field provides a strong nonlinear response in cubic crystals to observe self-bending of laser beams.

2.2 Beam propagation equation for slowly varying amplitudes

Consider the propagation of the laser beam in a photorefractive crystal along the z axis that has the essential diffraction in both transversal x and y directions. For simplicity we assume that the beam is linearly polarized along the optical axis coincident with the coordinate x . The electric-field component of the optical beam field \mathbf{E} satisfies the Helmholtz equation:

$$\nabla^2 \mathbf{E} + (k_0 n_e')^2 \mathbf{E} = 0, \quad (2.20)$$

where $k_0 = 2\pi/\lambda_0$ and λ_0 are the wave number and the wave length in free-space of the propagating beam and n_e is the unperturbed extraordinary refractive index. Expressing the

electric-field component in the form $\mathbf{E} = \bar{x}A_x(x, y, z)e^{ikz} + \bar{y}A_y(x, y, z)e^{ikz}$ and in terms of slowly varying amplitudes A_x and A_y equation (2.20) yields:

$$\left[i \frac{\partial}{\partial z} + \frac{1}{2k_0 n_e} \nabla_{\perp} \right] A_i(x, y, z) - \frac{k_0}{n} \Delta n_{ij} A_j(x, y, z) = 0, \quad (2.21)$$

where ∇_{\perp} is the transversal Laplace operator.

By studying the dynamic evolution [15-17] of solitons and their temporal development [18, 19] in photorefractive crystals it became possible to obtain conditions for stabilized solitons in common [20, 21] as well as in dissipative [22] photorefractive systems and finally to describe the properties of quasi-steady-state solitons [23, 24].

2.3 Laser beam propagation in uniaxial crystals

The photorefractive SBN and LiNbO₃ crystals belong to the class of single-axis ones. The maximal value of the electro-optic coefficient in these crystals can reach values up to 30 pm/V in LiNbO₃ [64] and up to 200 pm/V in SBN [103] along the direction of the optical axis. The nonlinear response in LiNbO₃ crystals occurs due to the photovoltaic effect that requires no applied external electric field. However effects of the beam self-action in SBN crystals are possible only under an applied voltage. In this case the maximal photorefractive response is achieved if the direction of the bias field is along the optical axis. This condition lets to consider only the perturbation of the space-charge field along the direction of the applied voltage that simplifies the task of the theoretical investigation of the laser beam propagation in single-axis photorefractive crystals.

2.3.1 (1+1)D case

The consideration of the process of the laser beam self-action in frameworks of a one-dimension model supposes that the laser beam is focused by a cylindrical lens on the input face of the crystal. The induced space-charge field in this case depends only on the x coordinate that corresponds to the direction of the optical axis (Equation 2.10). For the linearly polarized beam along the optical axis (Equation 2.21) the process of a self-action of the laser beam in photorefractive media under the applied external electric field in the steady-state regime is described by [7]:

$$i \frac{\partial A}{\partial z} + \frac{1}{2k_0 n_0} \frac{\partial^2}{\partial x^2} A - \frac{k_0 n_e^3}{2} r_{33} \left[E_0 \frac{I_d}{I_d + I} + \frac{\kappa_B T}{e} \frac{1}{I + I_d} \frac{dI}{dx} \right] A = 0. \quad (2.22)$$

The bright soliton solution can be obtained from equation (2.22) by expressing the beam amplitude in the form $A = r^{1/2} y(s) \exp(i\nu z)$, where $s = x/x_0$ is a dimensionless coordinate, x_0 is an arbitrary spatial width, $y(s)$ is the normalized function that has to be integrated in the interval $[0, 1]$ and ν presents the nonlinear shift of the propagation constant. The quantity r is the ratio of the maximal input beam intensity $I_{\max} = I(0)$ to the dark irradiance I_d , $r = I_{\max} / I_d$.

The first attempt to solve this problem taking into account no diffusion nonlinearity is shown in [7] where the amplitude profile for a bright soliton beam has the form close to the Gauss beam:

$$(2\beta)^{1/2} s = \pm \int_y^1 \frac{r^{1/2} dy}{[\ln(1 + ry^2) - y^2 \ln(1 + r)]^{1/2}}, \quad (2.23)$$

where $\beta = (k_0 x_0)^2 (n_e^4 r_{33} / 2) E_0$ and y corresponds to the normalized amplitude of the solution of the soliton beam profile. The width of the input beam depends on the ratio r and the magnitude of the applied electric field E_0 .

The existing soliton curve presented in [7] shows that for the ratio r from 0.1 till 100 the beam diameter remains relatively constant and the existence of bright spatial solitons is always possible if E_0 is a positive quantity.

By taking the nonlocal response into account, the solution of equation (2.22) was in detail considered by Krolikowski *et al.* [104] and Jinsong *et al.* [62]. The authors have shown that the beam center follows a parabolic trajectory and in the biased crystal the solution has the form of an Airy function.

2.3.2 (2+1)D case

Observing theoretical works [9, 11, 105] trying to describe the propagation of the laser beam with transverse intensity distribution in uniaxial PR crystals we can see that this problem requires considerable efforts to find any analytical solution. The first analytical solution was considered by Zozulya *et al.* [9] where authors took into account the anisotropic nature of the photorefractive medium. However, as it was mentioned by

Crosignani *et al.* [11], these results predict no possibility to observe experimentally a self-trapped propagating beam maintaining an axially symmetric invariant diameter. But the theoretical approach developed by Crosignani *et al.* [11] showed that in the low-intensity regime the RP crystal can support circular solitons but after short propagation distance they evolve into an elliptical beam that agrees with the published experimental results (for example [12, 13]).

The propagation of the laser beam focused by a spherical lens on the input face of the biased single-axis photorefractive crystal requires the taking into account of the isotropy of the linear electro-optic effect. However if the input light is linearly polarized along the optical axis it becomes possible to consider the change of the refractive index Δn_{ij} only along the direction of the applied electric field. Under these assumptions the equation (2.21) yields:

$$\left[i \frac{\partial}{\partial z} + \frac{1}{2k_0 n_e} \nabla_{\perp} \right] A - \frac{k_0 n_0^3}{2} r_{33} [\mathbf{x} \cdot \mathbf{E}_{\text{SC}}(x, y, z)] A = 0, \quad (2.24)$$

where $\mathbf{E}_{\text{SC}}(x, y, z) = \mathbf{x}E_{\text{SC}}^x(x, y, z) + \mathbf{y}E_{\text{SC}}^y(x, y, z)$ is the space-charge field amplitude, \mathbf{x} and \mathbf{y} are unit vectors parallel and perpendicular to the optical axis.

The potential equation (2.13) of the induced space-charge field for the (2+1)D case cannot be solved analytically but under steady-state conditions the time derivative vanishes and the equation can be rewritten as:

$$\begin{aligned} & \nabla^2 \varphi + \nabla \ln(I + I_d) \cdot \nabla \varphi = \\ & E_0 \frac{\partial}{\partial x} \ln(I + I_d) + \frac{k_B T}{e} \left[\nabla^2 \ln(I + I_d) + \{ \nabla \ln(I + I_d) \}^2 \right]. \end{aligned} \quad (2.25)$$

The bright (2+1)D solitons were in detail discussed by Crosignani *et al.* [11]. Authors have presented the existence curve and shown that solitons do not exist for the low-intensity regime when the maximal beam intensity is much smaller than that of the dark irradiance. For the high-intensity regime when I_{max} / I_d is large or equal to 1 the self-trapped beam can support screening solitons that was confirmed by Shih *et al.* [12, 13].

We are going to investigate the self-trapping and the self-bending of a laser beam with different input diameters in a photorefractive SBN-crystal in dependence on the applied electric field and the input beam intensity.

2.4 Laser beam propagation in cubic crystals

The propagation of laser beams in cubic photorefractive crystals is studied already since 1994 after their first experimental observation in $B_{12}TiO_{20}$ [4]. When choosing the directions of light beam propagation and application of an external electric field used to increase the nonlinear response, one should take into account the anisotropy of the electro-optic properties of sillenites belonging to the class of 23 symmetry of cubic system. The other problem is the presence of the natural optical activity that makes it necessary to take into account the rotation of the polarization plane and the birefringence of cubic crystals. The first theoretical models for the (1+1)D case were suggested by Singh *et al.* [25] and Krolkowski *et al.* [106] only for the case when the external electric field is applied along crystallographic axes [001] and $[1\bar{1}0]$ when the laser beam propagates along [110]. Five years later in 2002 this problem was considered again by Fazio *et al.* [27]. Authors developed a (2+1)D theoretical model for the orientations of the external electric field along [001] and $[1\bar{1}0]$ axes, and demonstrated experimentally the adequacy of the suggested model [33].

The first attempt to take into consideration the arbitrary orientation of the applied external electric field was made by Shepelevich *et al.* [29] for the (1+1)D case. Authors showed theoretically and experimentally that a maximal nonlinear response of the photorefractive cubic medium can be observed at the orientation of the bias field along $[1\bar{1}1]$ axis. Wiedner *et al.* confirmed this fact experimentally for the (2+1)D case [32].

2.4.1 Base equations

The set of coupled equations describing the laser beam propagation in optical active photorefractive cubic crystals can be obtained from equation (2.21). The natural optical activity is taken into account by an additional term specifying the rotation of the polarization plane [106]:

$$\left[i \frac{\partial}{\partial z} + \frac{1}{2k_0 n_e} \nabla_{\perp} \right] \bar{A}(x, y, z) - \frac{k_0}{n} \Delta n \bar{A}(x, y, z) + i \rho [\vec{e}_z, \bar{A}(x, y, z)] = 0, \quad (2.26)$$

where \vec{e}_z corresponds to the unit vector along the direction of the propagation z , ρ is the specific optical rotation.

2.4.2 (1+1)D laser beam propagation

The set of coupled equations describing the propagation of laser beams in cubic photorefractive crystals under an applied external electric field takes the form [26]:

$$\begin{aligned} i \frac{\partial A_x}{\partial z} + \frac{1}{2k_0 n_0} \frac{\partial^2 A_x}{\partial x^2} - \frac{k_0 n_0^3}{2} r_{41} E_{SC} A_x + i \rho A_y &= 0, \\ i \frac{\partial A_y}{\partial z} + \frac{1}{2k_0 n_0} \frac{\partial^2 A_y}{\partial x^2} - \delta \frac{k_0 n_0^3}{2} r_{41} E_{SC} A_y - i \rho A_x &= 0, \end{aligned} \quad (2.27)$$

where r_{41} is the value of the linear electro-optic coefficient, and E_{SC} is the magnitude of the space-charge field and the parameter δ determines the orientation of the external electric field:

$$\begin{aligned} \delta &= 0 \text{ for } \mathbf{E} \parallel [00\bar{1}], \\ \delta &= -1 \text{ for } \mathbf{E} \parallel [1\bar{1}0]. \end{aligned} \quad (2.28)$$

If $\delta = 0$ only the A_x component of the optical electric field gives the contribution to the nonlinear properties of the medium. The presence of the optical activity leads to the redistribution of the energy between both components of the polarization and the efficiency of the nonlinear response in this case reduces. Such interconnection between both components makes it impossible to observe the spatial soliton regime, especially if $\delta = -1$.

A theoretical model for arbitrary orientations of the external electric field was presented by Shepelevich *et al.* [29]. The orientation of the coordinate system in this case is presented in figure 2.2 where e_x and e_y are unit vectors along axes x and y . The external electric field is applied along x making an angle θ with the crystallographic direction $[1\bar{1}0]$. The set of coupled equations takes the form:

$$\begin{aligned} i \frac{\partial A_x}{\partial z} + \frac{1}{2k_0 n_0} \frac{\partial^2 A_x}{\partial x^2} - \frac{k_0 n_0^3}{2} r_{41} E_{SC} (\mu_1 A_x + \mu_2 A_y) - i \rho A_y &= 0, \\ i \frac{\partial A_y}{\partial z} + \frac{1}{2k_0 n_0} \frac{\partial^2 A_y}{\partial x^2} - \frac{k_0 n_0^3}{2} r_{41} E_{SC} (\mu_2 A_x + \mu_3 A_y) + i \rho A_x &= 0, \end{aligned} \quad (2.29)$$

where coefficients μ_i are:

$$\begin{aligned} \mu_1 &= 3 \sin \theta \cos^2 \theta, \\ \mu_2 &= \cos \theta (1 - 3 \sin^2 \theta), \\ \mu_3 &= \sin \theta (1 - 3 \cos^2 \theta). \end{aligned} \quad (2.30)$$

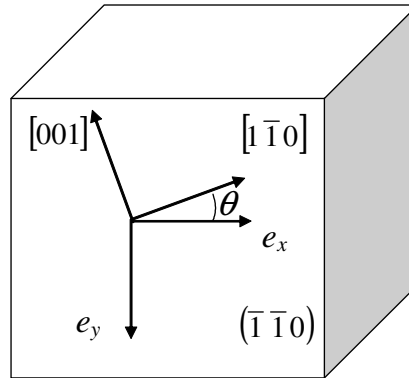


Figure 2.2: Orientation of the coordinate system relative to the crystallographic directions.

Coefficients μ_1 and μ_1 are responsible for the nonlinear response of the medium and are responsible for the self-action process of the light. The coefficient μ_2 specifies the cross-nonlinear coupling between x - and y -components of the polarization. The dependence of coupling coefficients on angle θ is shown in figure 2.3. It is easy to see that for the orientation of the applied voltage along the crystallographic axis $[1\bar{1}1]$ ($\theta = 35.26$) the coefficient μ_1 reaches its maximal value ($\mu_1 = 1.16$) and coefficient μ_2 corresponding to the cross-nonlinear coupling between both components of the vector amplitude is zero. In this case the direction of the polarization vector has to coincide with the direction of the applied voltage while the negative magnitude of coefficient μ_3 ($\mu_3 = -0.58$) can defocus the y -component of the polarization vector. The third term in the second equation (2.29) corresponds to the self-action of A_y component and the sign of coefficient μ_3 gives the negative contribution to the beam self-action process. The first experimental observation of spatial solitons in cubic photorefractive $B_{12}TiO_{20}$ crystals of (110)-cut under the applied electric field along the crystallographic axis $[1\bar{1}1]$ was demonstrated by Shepelevich *et al.* [29]. Authors have shown that in comparison with conventional orientations $[00\bar{1}]$ and $[1\bar{1}0]$ the considered one $[1\bar{1}1]$ requires much smaller magnitude of the bias field to observe the same nonlinear response of the medium.

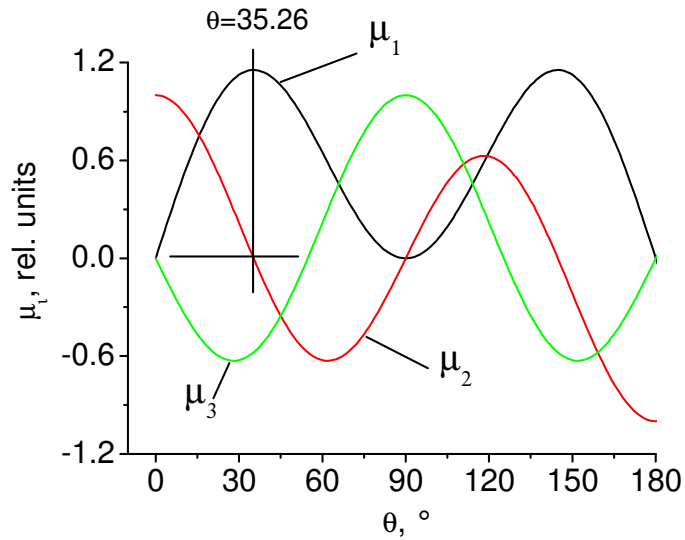


Figure 2.3: Dependence of the coefficients μ_1, μ_2, μ_3 on the orientation angle θ .

2.4.3 (2+1)D laser beam propagation

The propagation of two-dimensional laser beams in cubic photorefractive crystals was considered first time by Fazio *et al.* [27] if the external electric field is applied along directions $[001]$ and $[110]$. Authors have demonstrated theoretically and experimentally the existence of (2+1)D solitons in media with large optical activity and absorption. They have investigated the dependence of the soliton features on different parameters and have shown that solitons are transversely modulated (breathing) due to the combined action of effects of optical activity and absorption. The breathing period is not constant, but depends on the experimental conditions, as it was analytically described. The existence of (2+1)D solitons requires a more limited range of experimental parameters than for the (1+1)D case. The dependence of the normalized experimental beam waists versus the signal/background intensity ratio r , at $E_0 = 40$ kV/cm, together with the analytical and numerical solutions has shown that for the same external electric field, both the numerical integration and the experimental data show a minimum (2+1)D soliton width at $r = 0.8$, which cannot be predicted by the analytical solutions. The further growth of the ratio from about $2 I_0/I_B$ till $10 I_0/I_B$ does not influence on the normalized soliton width.

The arbitrary orientation of the external electric field for the (2+1)D case was considered by Shepelevich *et al.* [31]. The theoretical model takes also into account the complex behavior of the space-charge field (Equation 2.13) obtained from the two-

dimensional Kukhtarev model. The set of coupled equations developed by Shepelevich *et al.* is:

$$\begin{aligned}
 & i \frac{\partial A_x}{\partial z} + \frac{1}{2k_0 n_0} \left(\frac{\partial^2 A_x}{\partial x^2} + \frac{\partial^2 A_x}{\partial y^2} \right) - \frac{k_0 n_0^3}{2} \left\{ r_{41} \left[\left(E_0 - \frac{\partial \varphi}{\partial x} \right) (\mu_1 A_x + \mu_2 A_y) \right. \right. \\
 & \left. \left. - \frac{\partial \varphi}{\partial y} (\mu_2 A_x + \mu_3 A_y) \right] \right\} - i \rho A_y = 0 \\
 & i \frac{\partial A_y}{\partial z} + \frac{1}{2k_0 n_0} \left(\frac{\partial^2 A_y}{\partial x^2} + \frac{\partial^2 A_y}{\partial y^2} \right) - \frac{k_0 n_0^3}{2} \left\{ r_{41} \left[\left(E_0 - \frac{\partial \varphi}{\partial x} \right) (\mu_2 A_x + \mu_3 A_y) \right. \right. \\
 & \left. \left. - \frac{\partial \varphi}{\partial y} (\mu_3 A_x + \mu_4 A_y) \right] \right\} + i \rho A_y = 0
 \end{aligned} \tag{2.31}$$

The transversal component of the space-charge field $E_y = -\partial \varphi / \partial y$ is taken here into consideration.

In frameworks of the two-dimensional model authors showed that for the orientation of the bias field along $[1 \bar{1} 1]$ axis the x -polarized input light provides the quasi-soliton propagation of the laser beam in the crystal. They have calculated the existence curve for two-dimensional spatial solitons taking into account the optical activity of the medium. The presence of the optical activity makes it necessary to increase the amplitude of the external applied voltage to reach a quasi-soliton regime, while the rotation of the polarization plane violates the optical self-focusing. However the higher magnitude of the biased field, the weaker the influence of the optical activity and at about 30 kV/cm it does not influence on the waist radius of the quasi-soliton. This phenomenon is connected with the increasing of the rotation speed of the polarization plane that is allowed to consider the propagated beam as a circular polarized light. Later Weidner *et al.* [32] have shown that the circularly polarized beam in a BTO crystal (with length 21 mm and with an optical activity 6 °/mm at the wavelength 633 nm) has a circular cross-section on the output face of the crystal in the quasi-steady-state regime.

However the main problem of existing theoretical models is the impossibility to separate the effects of the birefringence and the induced space-charge field that distorts the behaviour of the beam polarization and makes it impossible to consider beam self-action effects independently of the birefringence induced by the external applied voltage. It is also well known that the additional photoelastic contribution to the modulation of the optical properties of the medium by the space-charge field has to taken into consideration [107].

So we will consider a model taking into account separately the linear birefringence induced by the external field, the additional contribution of the photoelastic effect to the modulation of the optical properties of the crystal by the space-charge field, and the natural optical activity.

The (110)-cut is not the unique orientation of sillenite crystals for the implementation of the light self-action effects. Plesovskikh *et al.* [50] have shown that cubic photorefractive crystals of {112}-cuts give the feasibility of the implementation of a counter light-beam interaction at reflective holographic gratings. *In this work, we derive equations with which we can analyze the self-action of light beams with one-dimensional input intensity distribution propagating along the crystallographic [112] axis in cubic crystals of 23 symmetry classes. The external electric field orientation is assumed to be arbitrary in a plane perpendicular to the propagation direction.*

2.5 Self-bending of the laser beam

Self-bending of light beams occurs when they propagate in single-axis photorefractive crystals with the nonlocal nonlinearity of a diffusion type [3, 56, 57, 108]. This effect has a rather high magnitude in barium titanate (BaTiO_3) and strontium-barium niobate (SBN) crystals characterized by large values of the electro-optic coefficients.

Various theoretical models have been applied for the investigation of these phenomena. In 1982, Feinberg [54] explained the asymmetric beam fanning by using the diffraction integral for a TEM_{00} Gaussian laser beam which itself deflects from a created transverse gradient of the refractive index. The evolution problem of one-dimensional Gaussian beams propagating in photorefractive crystals was considered in the paraxial approximation by Christodoulides *et al.* [3] and by Esayan *et al.* [55]. Any noise fanning effects have been neglected in these works. In addition of the noise to the system, it is possible to describe the fanning effect both for linear [58, 59] and nonlinear models [59] of material response in the case when the propagated beam has a wide size. In 1994, Lyubomudrov and Shkunov [56] introduced a theoretical model of self-bending with the assumption of a speckled structure of the input beam. This model describes a beam with a Gaussian shape of the angular spectrum. The photorefractive interaction between angular components with random phases causes energy redistribution and the bending of the beam

trajectory in a crystal. Using such approach, the trajectories of the whole beam with a strong curvature (without the frame of paraxial approximation) can be considered.

In single-axis crystals as BaTiO₃ and SBN with the strong diffusion mechanism of the photorefractive nonlinearity the radius of the trajectory curvature typically reaches several centimetres. This process is accompanied by an asymmetric beam fanning. A reduction of the spot size of the beam weakens the fanning. A narrow Gaussian beam with the waist of 15 μm at the entrance face of a BaTiO₃ crystal [58] can have only a wave front tilting of about 0.2° with a small change of the beam shape after the propagation of ~ 5 mm.

The strong anisotropy of a photorefractive response in BaTiO₃ influences both the quantitative parameters and the qualitative peculiarities of the self-bending phenomenon [54-59]. However, a simple electro-optic mechanism of photorefractivity has been taken into account [54-57] and [58-60] in the analysis of this effect. The spatial variations of dielectric permittivity are primarily due to the electro-optic contribution of the space-charge field which is formed in the crystal.

Nevertheless, the additional elasto-optic contribution to the changes of the dielectric permittivity during the process of the photorefractive grating writing was taken into account in [34, 35]. More recently Gunter and Zgonik [36] considered the roto-optic contribution that is evident in crystals with strong linear birefringence only. Both the elasto-optic and roto-optic contributions are associated with the inhomogeneous elastic field induced by the piezoelectric effect in a non-centrosymmetric crystal during photorefractive grating formation. In addition, a nonuniform piezoelectric polarization of the medium must be taken into consideration of the effective static dielectric constant [34-37] of the medium must be taken into consideration that influences the condition of trap saturation. The influence of the elasto-optic effect on Bragg diffraction, two-wave mixing, and beam fanning has been experimentally verified in various photorefractive crystals such as LiNbO₃ [34], Bi₁₂GeO₂₀ [38], Bi₁₂SiO₂₀ [39-41], Bi₁₂TiO₂₀ [35, 42-45], GaAs [46], KNbO₃ [47], and BaTiO₃ [47-49].

Following the simple model of Lyubomudrov and Shkunov [56], we investigate theoretically the trajectories for a selfbent extraordinary speckle-beam in BaTiO₃, considering the elasto-optic contribution to the changes of the dielectric permittivity for the photorefractive response. We neglect the roto-optic contribution because of the weak linear birefringence of BaTiO₃.

In cubic photorefractive sillenite crystals the nonlocal response of the medium can be enhanced by applying an external alternating-sign electric field [64]. Self-bending of a light beam propagating in a cubic photorefractive crystal with an applied square-wave electric field was considered by Borodin *et al.* [62], who disregarded the optical activity of the crystal. At the same time, it is well known [64] that cubic crystals of point group 23 have considerable rotary power at the wavelength of a helium-neon laser lying in the range from 6 deg/mm in $\text{Bi}_{12}\text{TiO}_{20}$ (BTO) to 22 deg/mm in $\text{Bi}_{12}\text{SiO}_{20}$ (BSO) and $\text{Bi}_{12}\text{GeO}_{20}$ (BGO). The rotation of the polarization plane can affect considerably the self-action of a light beam due to the anisotropy of the electro-optic effect. *We are going also to study theoretically and experimentally the self-bending of light beams in cubic photorefractive crystals with allowance for the optical activity of crystals. Experimental results have to confirm developed theoretical models for the investigation of laser beam propagation in cubic photorefractive crystals.*

As we have shown effects of the laser beam self-action are investigated in two different kinds of photorefractive media: in single-axis and cubic crystals. Both media are suitable to realise the self-focusing as well as the self-bending effects under applied external dc or ac electric fields. If the essential diffraction of the laser beam in the crystal can be exact compensated by nonlinear self-focusing, the propagated beam calls – *spatial soliton*.

From the literature it is known that photorefractive solitons can be generated in single-axis photorefractive SBN-crystals with input beam powers of 1-10 μW , applied fields of 1-7 kV/cm and background illuminations in the order of 1 mW/cm^2 [109-111]. Under a photorefractive soliton one understands generally a self-trapped beam, which diameter remains equal along the whole propagation distance in a PR-crystal. *We are going to investigate the self-trapping and the self-bending of a laser beam with different input diameters in a photorefractive SBN-crystal in dependence on the applied electric field and the input beam intensity.*

Due to their good photorefractive properties, cubic $\text{Bi}_{12}\text{TiO}_{20}$ (BTO) and $\text{Bi}_{12}\text{SiO}_{20}$ (BSO) crystals from the sillenite family are rather popular nonlinear media for the study and implementation of different effects of the light beam self-action (see, e.g., [4, 25-31, 106]). When choosing the directions of the light beam propagation and application of an external electric field to increase the nonlinear response, one should take into account the anisotropy of the electro-optic properties of sillenites belonging to the 23 symmetry class of cubic system. Conventionally, a light beam propagates along $[110]$ crystallographic direction when the external electric field is applied along axes $\langle 001 \rangle$ [4, 25, 27-29], $\langle 111 \rangle$ [31], or $\langle \bar{1}10 \rangle$ [27, 31]. The equations describing the self-action effects for an arbitrary orientation of the applied field in a plane orthogonal to the $\langle 110 \rangle$ light propagation direction are presented in [29, 31]. However theoretical models developed by Shepelevich *et al.* [29, 31] cannot separate influences of the induced birefringence and the formed space-charge field than strongly distorts the properties of the propagated beam. It is also well known that the additional photoelastic contribution to the modulation of the optical properties of the medium by the space-charge field has to be taken into consideration [107]. *So we will consider a model taking into account separately the linear birefringence induced by the external field, the additional contribution of the photoelastic effect to the modulation of the optical properties of the crystal by the space-charge field, and the natural optical activity.*

However, the (110)-cut is not the unique orientation of sillenite crystals for the implementation of the light self-action effects. Plesovskikh *et al.* [50] have shown that cubic photorefractive crystals of $\{112\}$ -cuts give the feasibility of the implementation of a counter light-beam interaction at reflective holographic gratings. *In this work, we derive equations with which we can analyze the self-action of light beams with one-dimensional input intensity distribution propagating along the crystallographic $[112]$ axis in cubic crystals of 23 symmetry classes. The external electric field orientation is assumed to be arbitrary in a plane perpendicular to the propagation direction.*

The other phenomenon of the beam self-action is connected with the bending of the beam trajectory due to the nonlocal response of the media. Due to the high magnitude of the electro-optic coefficients this effect can be observed in single-axis photorefractive crystals under applied dc electric field. *Following the simple model of Lyubomudrov and Shkunov [56], we investigate theoretically the trajectories for a selfbent extraordinary*

speckle-beam in $BaTiO_3$, considering the elasto-optic contribution to the changes of the dielectric permittivity for the photorefractive response. We neglect the roto-optic contribution because of the weak linear birefringence for $BaTiO_3$.

In cubic photorefractive sillenite crystals the nonlocal response of the medium can be enhanced by applying an external alternating-sign electric field [64]. Self-bending of a light beam propagating in a cubic photorefractive crystal with an applied square-wave electric field was considered by Borodin *et al.* [62], who disregarded the optical activity of the crystal. At the same time, it is well known [64] that cubic crystals of point group 23 have considerable rotary power at the wavelength of a helium-neon laser lying in the range from 6 deg/mm in $Bi_{12}TiO_{20}$ (BTO) to 22 deg/mm in $Bi_{12}SiO_{20}$ (BSO) and $Bi_{12}GeO_{20}$ (BGO). The rotation of the polarization plane can affect considerably the self-action of a light beam due to the anisotropy of the electro-optic effect. *We are going also to study theoretically and experimentally the self-bending of light beams in cubic photorefractive crystals with allowance for the optical activity of crystals. Experimental results have to confirm developed theoretical models for the investigation of laser beam propagation in cubic photorefractive crystals.*

Chapter 3

Beam self-trapping and self-bending dynamics in a SBN crystal

We present in this chapter base experimental and theoretical investigations of the self-trapping and the self-bending of a laser beam with different input diameters in a photorefractive SBN-crystal in dependence on the applied electric field, the input beam intensity and the input beam diameter (FWHM). The diameter of the input beam varies from 18 μm till 40 μm . For the input beam diameter 25 μm with different values of input intensity (270, 210, 130, 100 mW/cm^2) and under an applied external electric field in the range from 1.5 till 5 kV/cm we obtain experimentally saturation times that correspond to the maximal focusing of the propagated beam. The self-focusing of the light with different input beam diameter in dependence on the applied voltage was investigated under saturation conditions.

3.1 Experimental results

The experimental setup is shown in figure 3.1. A He-Ne laser is used as a source of the monochromatic wave (633 nm). The lens L focuses the beam onto the front surface of the SBN:60 crystal ($5 \times 5 \times 20 \text{ mm}^3$) doped with 0.2-mol.% Ce. The beam profile on the rear surface is taken by a CCD-camera with the help of a micro objective MO. The optical axis c of the crystal is directed parallel to the applied electric field. A white light emitting diode realizes the background illumination.

The peak intensity of the input beam is varied from 100 mW/cm^2 up to 270 mW/cm^2 . Before focusing the beam by the lens L it is transformed into a Gaussian beam by a system of lenses and a pinhole so that the maximum of the intensity distribution can be derived from the initial beam power. The applied electric field is taken in the range from 1 kV/cm

up to 5 kV/cm, the background illumination amounts to 1 mW/cm², the input beam diameter takes values between 18 μm and 40 μm (FWHM).

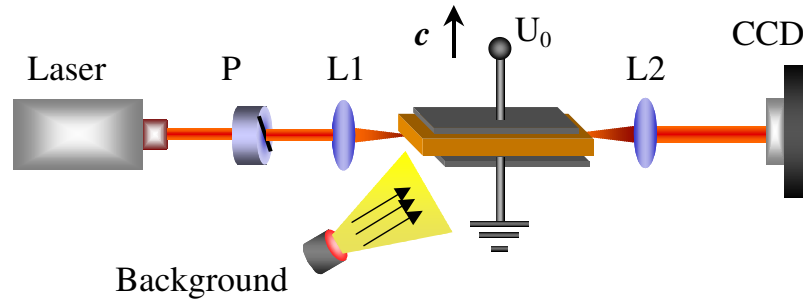


Figure 3.1: Typical experimental setup to realize self-trapped beams in photorefractive crystals.

The output beam size is measured parallel and perpendicularly to the applied electric field and in dependence on the saturation time. In this work we consider only the time period before the maximal focusing and take it as the saturation time (Figure 3.2). One can see that with the increasing of the input beam intensity the saturation time decreases. This can be explained with the increasing density of free charges caused by the stronger laser beam. The general tendency of the decreasing of the saturation time with the increasing applied field is due to the faster recombination rate of the excited charges.

The output beam profile is in general anisotropic and has an elliptic form with the short axis along the applied field (Figure 3.3). This behaviour corresponds to the observations described in [109]. For values of the applied electric field lower than 1.5 kV/cm the effect is weak. For values higher than 5.0 kV/cm the probability of breakdown increases.

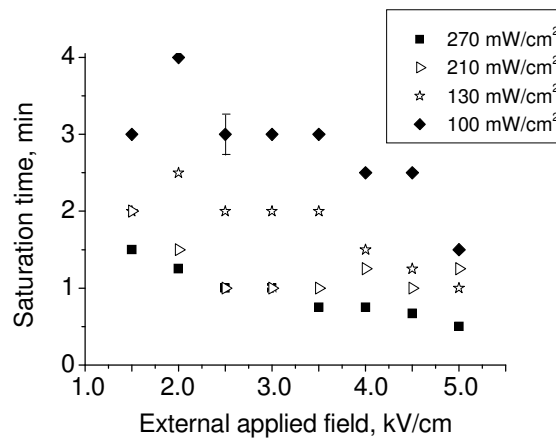


Figure 3.2: Saturation time for beam intensities 100 mW/cm², 130 mW/cm², 210 mW/cm² and 270 mW/cm² and an input diameter FWHM = 25 μm.

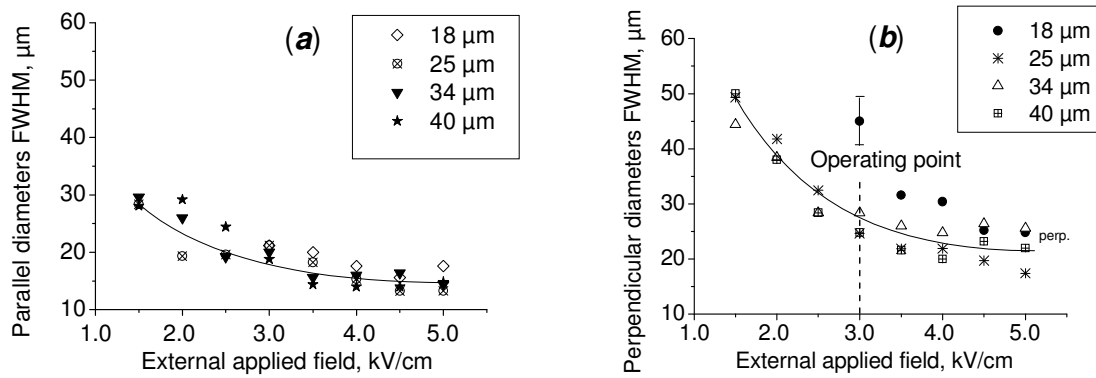


Figure 3.3: Experimental values and average fit of the output beam size parallel (a) and perpendicular (b) to the applied electric field for input beam diameters (FWHM) 18 μm , 25 μm , 34 μm , 40 μm and an input intensity of 130 mW/cm^2 .

We did not notice any essential difference of the output beam size in dependence on the input beam diameters, so that the output beam size decreases exponentially versus applied electric field and reaches a stable form at about 3 kV/cm , where the length of the small axis lies between 18 μm and 22 μm (Figure. 3.3.a), and the length of the large axis varies between 25 μm and 30 μm (Figure. 3.3.b). Out of these observations we can suppose that independently of the input diameter the beam is focused within the crystal always to the same optimal width at least along the optical axis (*optimal focusing*).

Figure 3.4 shows that the beam, as a rule, deviates stronger from the initial direction with increasing of the applied electric field.

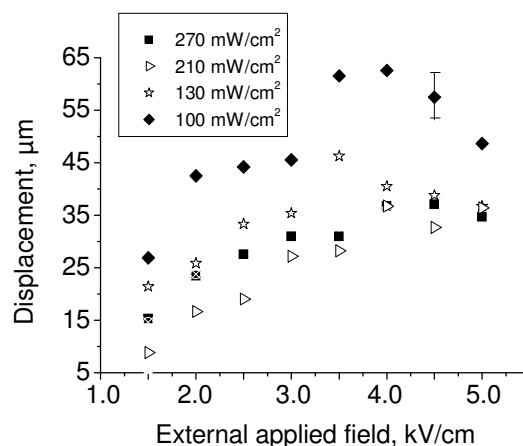


Figure 3.4: Beam displacement in the saturation case as a function of external applied field for beam intensities 100 mW/cm^2 , 130 mW/cm^2 , 210 mW/cm^2 and 270 mW/cm^2 and an input diameter FWHM = 25 μm .

These results coincide completely with similar observations in [109]. But it should be taken into account that there are two different simultaneous temporal processes in the experiment – beam focusing and beam self-bending. Their competition determines the final result. If the beam bending process is faster than the focusing (e. g., low voltage, small intensity), a monotone focusing of the bent beam occurs. In the opposite case (high voltage, high intensity), if the focusing is faster, a collapse of the structures takes place connected with the focusing of the deviated beam at a new place.

3.2 Theoretical model

To check the fact of *optimal focusing* we compared the experimental results with the theoretical ones.

The theoretical description of a laser beam propagating in a monoaxial photorefractive crystal is based on the paraxial wave equation:

$$i \frac{\partial A}{\partial z} + \frac{1}{2k_0 n_0} \left(\frac{\partial^2}{\partial x^2} + \frac{\partial^2}{\partial y^2} \right) A - \frac{k_0 n_0^3}{2} r_{33} \left(\frac{\partial \varphi}{\partial x} - E_0 \right) A = 0, \quad (3.1)$$

where A is the amplitude of the optical field, z is the direction of the beam propagation, x and y are the transverse coordinates, k_0 is the vacuum wave number, and n_0 is the index of refraction. The internal electric field (with potential φ) and the external electric field (with amplitude E_0) influence on the modulation of the refractive index inside the crystal via the linear electro-optic effect with the coefficient r_{33} . The potential φ of the induced space charge field from [60] is given by:

$$\begin{aligned} & \tau \frac{\partial}{\partial t} \nabla^2 \varphi + \nabla^2 \varphi + \nabla \ln(I + I_d) \cdot \nabla \varphi = \\ & E_0 \frac{\partial}{\partial x} \ln(I + I_d) + \frac{k_B T}{e} \left[\nabla^2 \ln(I + I_d) + \{ \nabla \ln(I + I_d) \}^2 \right], \end{aligned} \quad (3.2)$$

where k_B is the Boltzmann's constant, T is the absolute temperature, e is the charge of the electron, $I = |A|^2$ is the normalized intensity of the beam, $I_d = I_{back}/I_{max}$ is the intensity of the background illumination normalized by the peak intensity of the input beam and τ is the intensity-dependent relaxation time of the crystal.

In the steady-state regime we can neglect the change of the potential in time, assuming that $\frac{\partial}{\partial t} \nabla^2 \varphi = 0$ and obtain the following equation for the potential of the electric field:

$$\begin{aligned} \nabla^2 \varphi + \nabla \ln(I + I_d) \cdot \nabla \varphi = \\ E_0 \frac{\partial}{\partial x} \ln(I + I_d) + \frac{K_B T}{e} \left[\nabla^2 \ln(I + I_d) + \{ \nabla \ln(I + I_d) \}^2 \right]. \end{aligned} \quad (3.3)$$

The propagation equation is solved numerically by means of the Split-Step method and the potential equation is solved using the CGNR method [112]. It is assumed that the input beam has an initial Gaussian amplitude distribution.

Numerical method

If we separate out linear and nonlinear parts of equation (3.1), we get:

$$\frac{\partial A_L}{\partial z} = -\frac{i}{2k_0 n_0} \left(\frac{\partial^2}{\partial x^2} + \frac{\partial^2}{\partial y^2} \right) A, \quad (3.4)$$

$$\frac{\partial A_{NL}}{\partial z} = \frac{k_0 n_0^3}{2} r_{33} \left(\frac{\partial \varphi}{\partial x} - E_0 \right) A. \quad (3.5)$$

The nonlinear part has an analytical solution, but the linear one can be calculated only numerically. If we take a small step along z , then the two parts can be treated separately with only a “small” numerical error. So, for the nonlinear part the solution has the form:

$$A_{NL_i} = A_{NL_{0i}} \cdot \exp \left[\frac{k_0 n_0^3}{2} r_{33} \left(\frac{\partial \varphi}{\partial x} - E_0 \right) \Delta z \right], \quad i=1,2 \quad (3.6)$$

and for the linear part the Fast Fourier transform (FFT) is applied— an efficient algorithm to compute the discrete Fourier transform (DFT) and its inverse. For the direct Fourier transformation we substitute the Fourier-function with:

$$A_L(z, x, y) = \int_{-\infty}^{\infty} \int_{-\infty}^{\infty} A_L^*(z, \omega_x, \omega_y) \exp[-2\pi i(\omega_x x + \omega_y y)] d\omega_x d\omega_y, \quad i=1,2, \quad (3.7)$$

where ω_x and ω_y are the projections of the Fourier-transformation frequency on the x - and y -axes. Finally, the solution of the linear part is:

$$A_{L_i}^* = A_{L_{0i}}^* \cdot \exp \left[-\frac{2\pi^2}{k_0 n_0} (\omega_x^2 + \omega_y^2) \Delta z \right], \quad i=1,2. \quad (3.8)$$

The distribution of the intensity on the input face of the crystal has a Gaussian function:

$$I = I_0 \exp\left(-\frac{x^2 - y^2}{FWHM^2} \log(16)\right), \quad (3.9)$$

where I_0 is the initial value of the beam intensity, $FWHM$ is the half width at the half maximum of the laser beam.

Numerical simulation

The numerical calculations are performed according to the experimental values of input beam diameters, external applied voltage, and the ratio of the intensities of the background illumination and the peak intensity of the input beams. The value of the linear electro-optic coefficient is $r_{eff} = 237 \text{ pm/V}$ and the index of refraction is $n=2.3$.

The average dependences of the output beam diameter versus applied voltage are shown in figure 3.5. One can see that the output diameter along the optical axis has the tendency to converge to the common value of about $20 \mu\text{m}$ beginning with applied voltages in the range of about 3 kV/cm which coincides with the experimental results at least for the “parallel” configuration. According to our experience an external electric field of 3 kV/cm is the most suitable for the generation of photorefractive solitons in SBN, what is confirmed by the theory.

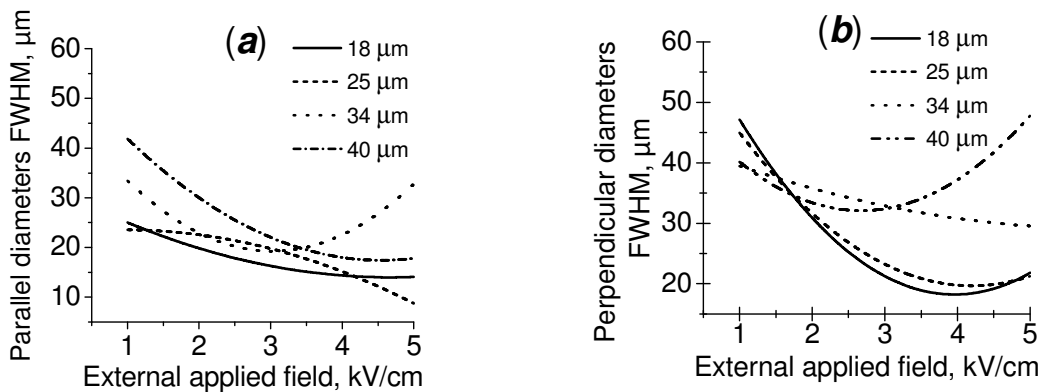


Figure 3.5: Theoretical values of the output beam size parallel (a) and perpendicular (b) to the applied electric field for input beam diameters (FWHM) $18 \mu\text{m}$, $25 \mu\text{m}$, $34 \mu\text{m}$, $40 \mu\text{m}$ and an input intensity of 130 mW/cm^2 .

The theoretical calculation of the displacement is shown in figure 3.6. With increasing applied external field the deviation of the output beam from the initial position also grows in agreement with our experiments. Moreover, the beam with the lower input peak

intensity has a stronger displacement than the beam with higher input peak intensity like in the experiments (Figure 3.4). This behaviour is related to the different magnitudes of the non-local response of the medium for different input beam intensities, which corresponds to the second term on the right part of equation (3). The ratio I_d of the intensity of the background illumination I_{back} to the input peak intensity I_{max} increases with the decreasing of the input peak intensity I_{max} resulting in a growing of the term corresponding to the non-local response of the medium. Moreover, it should be noted that the magnitude of theoretical calculated self-bending is larger than the experimental one, and for some cases (e.g. 5 kV/cm) the difference between theoretical and experimental results can reach up to 50%. Therefore for self-bending we are able to report only about the qualitative agreement between theory and experiment which is confirmed by Ref. [109].

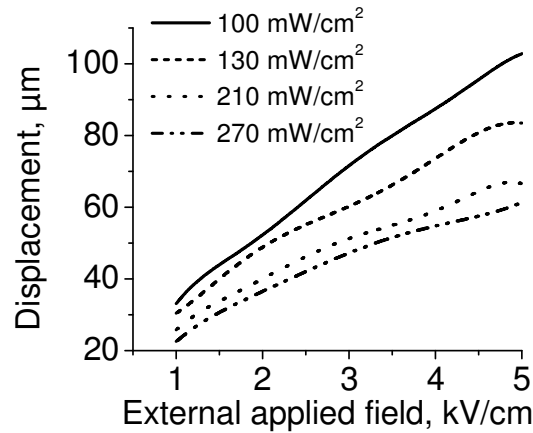


Figure 3.6: Beam displacement versus applied external electric applied field for beam intensities 100 mW/cm², 130 mW/cm², 210 mW/cm², and 270 mW/cm² and an input diameter FWHM = 25 μm.

3.3 Conclusion

In this chapter we have investigated the self-trapping and self-bending of a laser beam in a SBN-crystal for different values of input beam diameter, applied electric field and peak intensity. We found experimentally that the output beam diameter especially along the optical axis does not depend on the diameter of the input beam if it lies between 18 μm and 40 μm. The beams have the same peak intensities and the required applied electric field should have a value of about 3 kV/cm (*optimal focusing*). The self-bending becomes stronger for higher applied electric fields and smaller input beam intensities which is

connected with the increasing of the non-local response of the medium. The theoretical model confirmed the tendency of the experimental results only qualitatively and predicts larger displacements than the experimental ones.

The competition of the beam focusing and the beam self-bending velocities determines the experimental saturation time that decreases if the applied electric field and the input beam intensity increase.

Chapter 4

Self-action of light beams in sillenites

In this chapter we develop a theoretical model of the self-action of one-dimensional light beams in (110)-cut and $(11\bar{2})$ -cut sillenite crystals. The model takes into account the vector nature of the light field, the gyrotropy of the medium, the linear birefringence induced by the external field, and the additional photoelastic contribution to the modulation of optical properties by the space-charge field.

We discuss different orientations of the applied voltage and show that the additional photoelastic contribution plays a significant role in the photorefractive response of the medium and strong influences on the polarization of the propagated beam when the external electric field orientation is along the axis $[1\bar{1}1]$.

4.1 Self-action of light beams in (110)-cut sillenites

4.1.1 Theoretical model

Let us consider a photorefractive crystal of point group 23 in which a light beam with one-dimensional intensity distribution $I(x)$ at the input face (Figure 4.1) is propagated at a small angle to the z axis.

The external ac or dc electric field is applied along the x axis which makes an angle θ with the $[1\bar{1}0]$ crystallographic direction. The space-charge field formed in the crystal results in a self-action of the light beam. It has the dominating component $E_x(x, z)$. To describe this field taking into account only the local component of the photorefractive response, we take the expression:

$$E_x = -E_0 \frac{I_d}{I_d + I}, \quad (4.1)$$

where I_d is the ratio of the dark irradiance including the intensity of background illumination to the maximal intensity of the input beam.

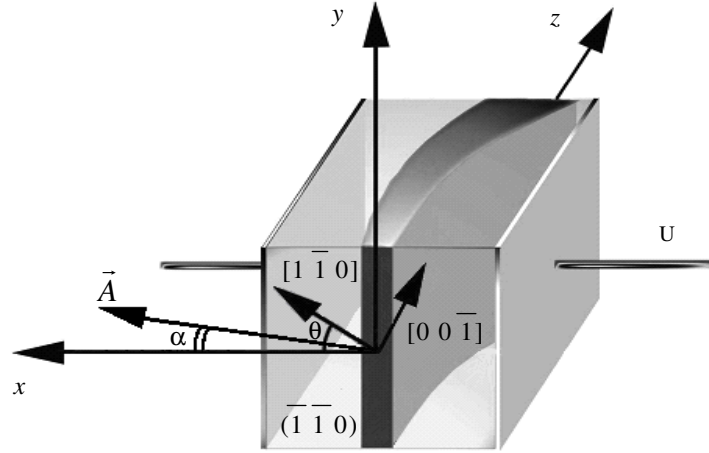


Figure 4.1: Orientation of the photorefractive crystal in which the light beam with the intensity distribution $I(x)$ at the input face is propagated. An external direct electric field U is applied along the axis x .

The optical properties of the crystal change in external and internal fields due to the linear electro-optic effect and additional elasto-optic contribution is connected with elastic crystal strains excited by the piezoelectric effect [107]. With allowance for the well-known relations [40, 41] the dielectric tensor components in a cubic crystal can be represented in the form:

$$\varepsilon_{ij} = n_0^2 \delta_{ij} \mp n_0^4 r_{41}^T \delta_{ijk} m_k E_0 + n_0^4 r_{41}^S \Delta b_{ij} E_x, \quad (4.2)$$

$$\Delta b_{ij} = \left[\delta_{ijk} m_k + \frac{1}{r_{41}^T} (P_{ijkl}^E m_l \gamma_{kn} e_{mnp} m_m m_p) \right], \quad (4.3)$$

where n is the refractive index of an unperturbed crystal; δ_{ij} and δ_{ijk} are the symmetric and antisymmetric unit tensors, respectively; r_{41}^T and r_{41}^S are the electro-optic coefficients of a mechanically clamped and free crystals respectively; P_{ijkl}^E are the photoelastic tensor components; γ_{kn} are the components of the tensor inverse of $\Gamma_{nk} = C_{nmkl}^E m_m m_l$; C_{nmkl}^E and e_{mnp} are the components of the elastic and piezoelectric constant tensors, respectively; and m_k are the direction cosines of the x axis in crystallographic coordinates. For symmetric

and antisymmetric unit tensors δ_{ij} and δ_{ijk} the following rule has to be used: $\delta_{ij} = 1$ if $i=j$ and $\delta_{ij} = 0$ otherwise, $\delta_{ijk} = 1$ if $i \neq j \neq k$ and $\delta_{ijk} = 0$ otherwise.

For the crystallographic system in figure 4.1 the vectors of the coordinate systems yield:

$$\begin{aligned}\bar{x}_0 &= \left(\frac{1}{\sqrt{2}} \cos(\theta), -\frac{1}{\sqrt{2}} \cos(\theta), \sin(\theta) \right), \\ \bar{y}_0 &= \left(-\frac{1}{\sqrt{2}} \sin(\theta), \frac{1}{\sqrt{2}} \sin(\theta), \cos(\theta) \right), \\ \bar{z}_0 &= \left(\frac{1}{\sqrt{2}}, \frac{1}{\sqrt{2}}, 0 \right),\end{aligned}\tag{4.4}$$

which depend on the angle θ and have to be used to formulate the problem in the given coordinates.

The analysis of the laser beam propagation in cubic photorefractive crystals having optical activity can be described by the wave equation for the electric vector of the optical field \vec{E} :

$$\nabla^2 \vec{E}(\vec{r}, t) + k_0^2 \hat{\epsilon} \vec{E} + i\rho [\bar{z}_0 \vec{E}] = 0,\tag{4.5}$$

where k_0 is the wave vector inside the medium, ρ is the constant of the optical activity, $\hat{\epsilon}$ is the symmetric dielectric permittivity tensor of the anisotropic material from equation (4.2).

The solution of the equation (4.5) for the (1+1)D case can be expressed using the exponent of the light monochromatic field in the standard form $i(kz - \omega t)$:

$$\vec{E}(x, t) = [\bar{x}_0 A_x(x, z) + \bar{y}_0 A_y(x, z)] \exp[i(kz - \omega t)].\tag{4.6}$$

With the help of equation (4.5) we obtain in the paraxial approximation the following equations for the components of the vector envelope of the light beam $A(x, z)$:

$$\begin{cases} i \frac{\partial A_x}{\partial z} + \frac{1}{2k_0 n_0} \frac{\partial^2 A_x}{\partial x^2} - \bar{x}_0 k_0^2 \hat{\epsilon}' [\bar{x}_0 A_x(x, z) + \bar{y}_0 A_y(x, z)] - i\rho A_y = 0, \\ i \frac{\partial A_y}{\partial z} + \frac{1}{2k_0 n_0} \frac{\partial^2 A_y}{\partial x^2} - \bar{y}_0 k_0^2 \hat{\epsilon}' [\bar{x}_0 A_x(x, z) + \bar{y}_0 A_y(x, z)] + i\rho A_x = 0, \end{cases}\tag{4.7}$$

where the tensor $\hat{\epsilon}'$ has the form:

$$\hat{\epsilon}'_{ij} = n_0^4 r_{41}^T \delta_{ijk} | m_k E_0 + n_0^4 r_{41}^S \Delta b_{ij} E_x.\tag{4.8}$$

After some manipulation the set of coupled equation (4.7) takes the form:

$$\left\{ \begin{array}{l} i \frac{\partial A_x}{\partial z} + \frac{1}{2k_0 n_0} \frac{\partial^2 A_x}{\partial x^2} + \frac{k_0 n_0^3}{2} r_{41}^T E_0 (\mu_1 A_x + \mu_2 A_y) + \\ \frac{k_0 n_0^3}{2} r_{41}^S E_{x1} (\eta_1 A_x + \eta_2 A_y) - i \rho A_y = 0, \\ i \frac{\partial A_y}{\partial z} + \frac{1}{2k_0 n_0} \frac{\partial^2 A_y}{\partial x^2} + \frac{k_0 n_0^3}{2} r_{41}^T E_0 (\mu_2 A_x + \mu_3 A_y) + \\ \frac{k_0 n_0^3}{2} r_{41}^S E_{x1} (\eta_2 A_x + \eta_3 A_y) + i \rho A_x = 0, \end{array} \right. \quad (4.9)$$

where coefficients μ_i and η_i depend on the direction of the crystallographic axes and in the complete form can be presented by the expressions:

$$\begin{aligned} \mu_1 &= \bar{x}_0 \left(\hat{\delta} \cdot \bar{x}_0 \right) \bar{x}_0 = 6(x_0^1 x_0^2 x_0^3), \\ \mu_2 &= \bar{x}_0 \left(\hat{\delta} \cdot \bar{x}_0 \right) \bar{y}_0 = 2(x_0^1 x_0^2 y_0^3 + x_0^1 x_0^3 y_0^2 + x_0^2 x_0^3 y_0^1), \\ \mu_3 &= \bar{y}_0 \left(\hat{\delta} \cdot \bar{x}_0 \right) \bar{y}_0 = 2(x_0^1 y_0^2 y_0^3 + x_0^2 y_0^1 y_0^3 + x_0^3 y_0^1 y_0^2), \end{aligned} \quad (4.10)$$

$$\begin{aligned} \eta_1 &= \bar{x}_0 \Delta \hat{b} \bar{x}_0 = \Delta b_{11} (x_0^1)^2 + \Delta b_{22} (x_0^2)^2 + \Delta b_{33} (x_0^3)^3 + \\ &+ 2\Delta b_{12} x_0^1 x_0^2 + 2\Delta b_{13} x_0^1 x_0^3 + 2\Delta b_{23} x_0^2 x_0^3, \\ \eta_2 &= \bar{x}_0 \Delta \hat{b} \bar{y}_0 = \Delta b_{11} x_0^1 y_0^1 + \Delta b_{22} x_0^2 y_0^2 + \Delta b_{33} x_0^3 y_0^3 + \Delta b_{12} x_0^1 y_0^2 + \\ &+ \Delta b_{13} x_0^1 y_0^3 + \Delta b_{23} x_0^2 y_0^3 + \Delta b_{21} x_0^2 y_0^1 + \Delta b_{31} x_0^3 y_0^1 + \Delta b_{32} x_0^3 y_0^2, \\ \eta_3 &= \bar{y}_0 \Delta \hat{b} \bar{y}_0 = \Delta b_{11} (y_0^1)^2 + \Delta b_{22} (y_0^2)^2 + \Delta b_{33} (y_0^3)^3 + \\ &+ 2\Delta b_{12} y_0^1 y_0^2 + 2\Delta b_{13} y_0^1 y_0^3 + 2\Delta b_{23} y_0^2 y_0^3, \end{aligned} \quad (4.11)$$

with $b_{12} = b_{21}$, $b_{13} = b_{31}$ and $b_{23} = b_{32}$ due to the symmetry properties. The tensor $\Delta \hat{b}$ of the additional photoelastic contribution to the modulation of optical properties by the space-charge field according to equation (4.3) has to be calculated taking into account the symmetry class of the cubic crystals. The photoelastic tensor, elastic and piezoelectric tensors of point group 23 have the form:

$$\begin{pmatrix} P_{11}^E & P_{12}^E & P_{13}^E & 0 & 0 & 0 \\ P_{13}^E & P_{11}^E & P_{12}^E & 0 & 0 & 0 \\ P_{12}^E & P_{13}^E & P_{11}^E & 0 & 0 & 0 \\ 0 & 0 & 0 & P_{44}^E & 0 & 0 \\ 0 & 0 & 0 & 0 & P_{44}^E & 0 \\ 0 & 0 & 0 & 0 & 0 & P_{44}^E \end{pmatrix}, \quad (4.12)$$

$$\begin{pmatrix} C_{11}^E & C_{12}^E & C_{12}^E & 0 & 0 & 0 \\ C_{12}^E & C_{11}^E & C_{12}^E & 0 & 0 & 0 \\ C_{12}^E & C_{12}^E & C_{11}^E & 0 & 0 & 0 \\ 0 & 0 & 0 & C_{44}^E & 0 & 0 \\ 0 & 0 & 0 & 0 & C_{44}^E & 0 \\ 0 & 0 & 0 & 0 & 0 & C_{44}^E \end{pmatrix}, \quad (4.13)$$

$$\begin{pmatrix} 0 & 0 & 0 & e_{14} & 0 & 0 \\ 0 & 0 & 0 & 0 & e_{14} & 0 \\ 0 & 0 & 0 & 0 & 0 & e_{14} \end{pmatrix}. \quad (4.14)$$

Using the symmetry of cubic crystals the components of the tensor $\hat{\Delta b}$ can be expressed as:

$$\begin{aligned} \Delta b_{11} &= \frac{e_{41}}{r_{41}^S} \{ p_{11} m_1 (\gamma_{11} m_2 m_3 + \gamma_{12} m_1 m_3 + \gamma_{13} m_1 m_2) + \\ &+ p_{12} m_2 (\gamma_{21} m_2 m_3 + \gamma_{22} m_1 m_3 + \gamma_{23} m_1 m_2) + p_{13} m_3 (\gamma_{31} m_2 m_3 + \gamma_{32} m_1 m_3 + \gamma_{33} m_1 m_2) \}, \\ \Delta b_{22} &= \frac{e_{41}}{r_{41}^S} \{ p_{13} m_1 (\gamma_{11} m_2 m_3 + \gamma_{12} m_1 m_3 + \gamma_{13} m_1 m_2) + \\ &+ p_{11} m_2 (\gamma_{21} m_2 m_3 + \gamma_{22} m_1 m_3 + \gamma_{23} m_1 m_2) + p_{12} m_3 (\gamma_{31} m_2 m_3 + \gamma_{32} m_1 m_3 + \gamma_{33} m_1 m_2) \}, \\ \Delta b_{33} &= \frac{e_{41}}{r_{41}^S} \{ p_{12} m_1 (\gamma_{11} m_2 m_3 + \gamma_{12} m_1 m_3 + \gamma_{13} m_1 m_2) + \\ &+ p_{13} m_2 (\gamma_{21} m_2 m_3 + \gamma_{22} m_1 m_3 + \gamma_{23} m_1 m_2) + p_{11} m_3 (\gamma_{31} m_2 m_3 + \gamma_{32} m_1 m_3 + \gamma_{33} m_1 m_2) \} \end{aligned}, \quad (4.15)$$

$$\begin{aligned} \Delta b_{12} &= m_3 + \frac{e_{41} P_{44}}{r_{41}^S} \{ m_2 (\gamma_{11} m_2 m_3 + \gamma_{12} m_1 m_3 + \gamma_{13} m_1 m_2) + \\ &+ m_1 (\gamma_{21} m_2 m_3 + \gamma_{22} m_1 m_3 + \gamma_{23} m_1 m_2) \}, \end{aligned}$$

$$\begin{aligned} \Delta b_{13} &= m_2 + \frac{e_{41} P_{44}}{r_{41}^S} \{ m_3 (\gamma_{11} m_2 m_3 + \gamma_{12} m_1 m_3 + \gamma_{13} m_1 m_2) + \\ &+ m_1 (\gamma_{31} m_2 m_3 + \gamma_{32} m_1 m_3 + \gamma_{33} m_1 m_2) \}, \end{aligned}$$

$$\Delta b_{23} = m_1 + \frac{e_{41} P_{44}}{r_{41}^S} \{m_3(\gamma_{21} m_2 m_3 + \gamma_{22} m_1 m_3 + \gamma_{23} m_1 m_2) + m_2(\gamma_{31} m_2 m_3 + \gamma_{32} m_1 m_3 + \gamma_{33} m_1 m_2)\}$$

Taking into account the symmetry of the C_{nmkl}^E tensor the components of the tensor Γ_{nk} are:

$$\begin{aligned}\Gamma_{11} &= C_{11}^E(m_1)^2 + C_{44}^E(m_2)^2 + C_{44}^E(m_3)^2, \\ \Gamma_{22} &= C_{11}^E(m_2)^2 + C_{44}^E(m_1)^2 + C_{44}^E(m_3)^2, \\ \Gamma_{33} &= C_{11}^E(m_3)^2 + C_{44}^E(m_2)^2 + C_{44}^E(m_1)^2, \\ \Gamma_{12} &= C_{12}^E m_1 m_2 + C_{44}^E m_1 m_2, \\ \Gamma_{13} &= (C_{12}^E + C_{44}^E) m_1 m_3, \\ \Gamma_{23} &= (C_{12}^E + C_{44}^E) m_2 m_3,\end{aligned}\tag{4.16}$$

where $\Gamma_{12} = \Gamma_{21}$, $\Gamma_{13} = \Gamma_{31}$ and $\Gamma_{23} = \Gamma_{32}$. The parameters of tensor γ_{kn} are being calculated by means of the inverse matrix $(\Gamma)^{-1}$.

The coefficients μ_i and η_i for the orientation (110) of the crystal using (4.4) are determined by expressions:

$$\begin{aligned}\mu_1 &= -3 \sin \theta \cos^2 \theta, \\ \mu_2 &= -\cos \theta (3 \sin^2 \theta - 1), \\ \mu_3 &= \sin \theta (3 \cos^2 \theta - 1),\end{aligned}\tag{4.17}$$

$$\begin{aligned}\eta_1 &= \frac{1}{2}(\Delta b_{11} + \Delta b_{22} - 2\Delta b_{12}) \cos^2 \theta + \Delta b_{33} \sin^2 \theta + \frac{1}{\sqrt{2}}(\Delta b_{13} - \Delta b_{23}) \sin 2\theta, \\ \eta_2 &= \frac{1}{4}(\Delta b_{11} + \Delta b_{22} - 2\Delta b_{33} - 2\Delta b_{12}) \sin 2\theta - \frac{1}{\sqrt{2}}(\Delta b_{13} - \Delta b_{23}) \cos 2\theta, \\ \eta_3 &= \frac{1}{2}(\Delta b_{11} + \Delta b_{22} - 2\Delta b_{12}) \sin^2 \theta + \Delta b_{33} \cos^2 \theta - \frac{1}{\sqrt{2}}(\Delta b_{13} - \Delta b_{23}) \sin 2\theta,\end{aligned}\tag{4.18}$$

where the following designations have been introduced:

$$\begin{aligned}
\Delta b_{11} &= \frac{e_{14}}{r_{41}^s} \cos^2 \theta \sin \theta \frac{(p_{11} + p_{12})A + p_{13}B}{C}, \\
\Delta b_{22} &= \frac{e_{14}}{r_{41}^s} \cos^2 \theta \sin \theta \frac{(p_{11} + p_{13})A + p_{12}B}{C}, \\
\Delta b_{33} &= \frac{e_{14}}{r_{41}^s} \cos^2 \theta \sin \theta \frac{(p_{12} + p_{13})A + p_{11}B}{C}, \\
\Delta b_{23} &= -\Delta b_{13} = \frac{1}{\sqrt{2}} \cos \theta \left[1 - \frac{e_{14}}{r_{41}^s} p_{44}^E \frac{(2A \sin^2 \theta + B \cos^2 \theta)}{C} \right], \\
\Delta b_{12} &= \sin \theta \left[1 - \frac{2e_{14}}{r_{41}^s} p_{44}^E \frac{A \cos^2 \theta}{C} \right], \\
\Delta b_{13} &= -\Delta b_{23},
\end{aligned} \tag{4.19}$$

$$\begin{aligned}
A &= (C_{12} - C_{44}^E) \cos^2 \theta - 2C_{11} \sin^2 \theta, \\
B &= 4(C_{12} + C_{44}^E) \sin^2 \theta - (C_{11} + C_{12}) \cos^2 \theta - 2C_{44}^E, \\
C &= (C_{11} \sin^2 \theta + C_{44}^E \cos^2 \theta) [(C_{11} + C_{12}) \cos^2 \theta + 2C_{44}^E] - 2(C_{12} + C_{44}^E)^2 \sin^2 \theta \cos^2 \theta.
\end{aligned} \tag{4.20}$$

In formulas (4.19) and (4.19), the piezoelectric coefficient e_{14} , elasto-optic constants p_{mn} and elasticity moduli C_{mm} are used in matrix designations.

The third term in the set of equations (4.17)-(4.20) determines the induced linear birefringence by the external electric field. The magnitude of this term is determined by the coefficients μ_1 , μ_2 and μ_3 whose dependences on the orientation angle θ are shown in figure 4.2. These coefficients do not depend on the type of cubic photorefractive crystals unlike the coefficients η_1 , η_2 , and η_3 determining the magnitude and sign of the photorefractive nonlinearity (the fourth term in the set of equations 4.9). The orientational dependences of these coefficients, calculated using the material constants presented in [35, 43] (Table 4.1), are given in figure 4.3 for BTO and BSO crystals.

Comparing figures 4.2 and 4.3 one can notice that the orientational dependencies of nonlinear coefficients $\mu_i(\theta)$ and $\eta_i(\theta)$ on the orientation angle θ are similar. At the orientations corresponding to the extrema of both dependences the magnitude of the coefficients μ_i and η_i have the quantitative difference. This difference is associated with the additional contribution of the piezoelectric and photoelastic effects to the optical

properties of the crystal by the space-charge field [35, 43] induced in this case by a light beam. The best conditions for implementation of self-action are achieved for an external field applied along the $[1\bar{1}1]$ direction at $\theta = 35.26^\circ$.

| | $\text{Bi}_{12}\text{TiO}_{20}$ | $\text{Bi}_{12}\text{SiO}_{20}$ |
|---|--|---|
| Photoelastic tensor P_{ijkl}^E | $P_{11}^E = -0.06$ $P_{12}^E = 0.2$ $P_{13}^E = 0.2$ $P_{44}^E = -0.009$ | $P_{11}^E = -0.16$ $P_{12}^E = 0.13$ $P_{13}^E = 0.12$ $P_{44}^E = -0.015$ |
| Elastic tensor C_{nmkl}^E | $C_{11}^E = 12.5 \times 10^{10}$ $C_{12}^E = 2.75 \times 10^{10}$ $C_{44}^E = 2.42 \times 10^{10}$ | $C_{11}^E = 12.96 \times 10^{10}$ $C_{12}^E = 2.99 \times 10^{10}$ $C_{44}^E = 2.45 \times 10^{10}$ |
| Piezoelectric tensor e_{mnp} | $e_{14} = 1.1$ | $e_{14} = 1.12$ |
| Electro-optic coefficients of a free crystals of r_{41}^S | $r_{41}^S = 5.28 \times 10^{-12}$ | $r_{41}^S = 5 \times 10^{-12}$ |

Table 4.1: Material constants of BTO and BSO crystals.

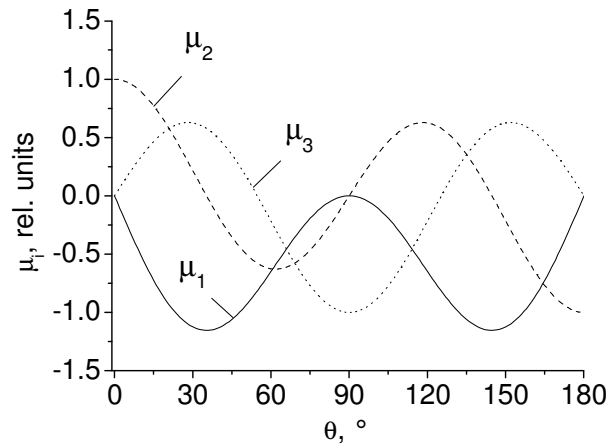


Figure 4.2: Dependences of the coefficients μ_1 , μ_2 and μ_3 on the orientation angle θ .

In this case, the coefficients μ_1 and η_1 determine, respectively, the induced birefringence and the x -component of the light beam polarization has the maximal nonlinear self-action.

It should be noticed that in a BTO crystal a larger additional photoelastic contribution leads to a larger coefficient $|\eta_1|=1.419$ than in BSO ($|\eta_1|=1.182$) for an external field orientation along the axis $[1\bar{1}1]$. However, the coefficient η_3 characterizing the nonlinear self-action due to the y component of the polarization vector has a larger absolute value for the BSO crystal ($|\eta_3^{BSO}|=1.419, |\eta_3^{BTO}|=0.266$) at $\theta=35.26^\circ$.

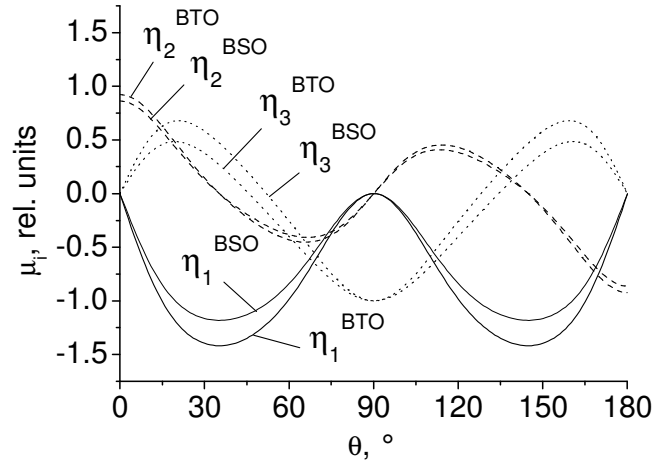


Figure 4.3: Dependences of the coefficients η_1 , η_2 , and η_3 on the orientation angle θ in bismuth titanate (BTO) and bismuth silicate (BSO) crystals.

Choose of the optimal orientation of the crystal makes it possible to reach a maximal photorefractive response of the medium. However the polarization of the input light beam has to be taken into consideration to increase the nonlinear properties of the crystal. At the orientation of the external applied electric field along axes of type $[1\bar{1}0]$ ($\theta=0^\circ$) the nonlinear photorefractive response reaches the maximal value for an orientation of the light polarization vector at an angle $\alpha=45^\circ$ with this direction. In this case only the coefficients μ_2 and η_2 in the set of equations (4.9) differ from zero. These coefficients correspond to the cross correlation between the polarization components A_x and A_y of the light vector, and the maximal nonlinear response of the medium can be realised only at $\alpha=45^\circ$. For $\theta=35.26^\circ$ (the external electric field is applied along the direction $[1\bar{1}1]$) the coefficients μ_1 and η_1 have maximal magnitudes and the light polarization vector has to be aligned along the direction of the beas field.

4.1.2 Numerical simulation

BTO crystal

The propagation of a light beam ($\lambda = 633$ nm) with a Gaussian distribution of the input amplitude (the waist radius is $x_0 = 25$ μm) was numerically analyzed using equations (4.9), (4.17)-(4.20) on the basis of the finite-difference Douglas scheme [113]. In the calculation, the BTO crystal parameters (the size $d = 15$ mm along the z axis and $\rho = 6$ $^\circ/\text{mm}$) were taken to be the same as in [29]. In [29] Shepelevich *et al.* used a theoretical model taking into account only the induced birefringence and optical activity that corresponds to the following set of coupled equations:

$$\begin{cases} i \frac{\partial A_x}{\partial z} + \frac{1}{2k_0 n_0} \frac{\partial^2 A_x}{\partial x^2} + \frac{k_0 n_0^3}{2} r_{41} E_{SC1} (\mu_1 A_x + \mu_2 A_y) - i \rho A_y = 0, \\ i \frac{\partial A_y}{\partial z} + \frac{1}{2k_0 n_0} \frac{\partial^2 A_y}{\partial x^2} + \frac{k_0 n_0^3}{2} r_{41} E_{SC1} (\mu_2 A_x + \mu_3 A_y) + i \rho A_x = 0. \end{cases} \quad (4.21)$$

Figure 4.4 shows the dependence of the output beam waist radius on the applied electric field for $I_d = 0.1I_0$ taking into account the induced birefringence and the additional photoelastic contribution.

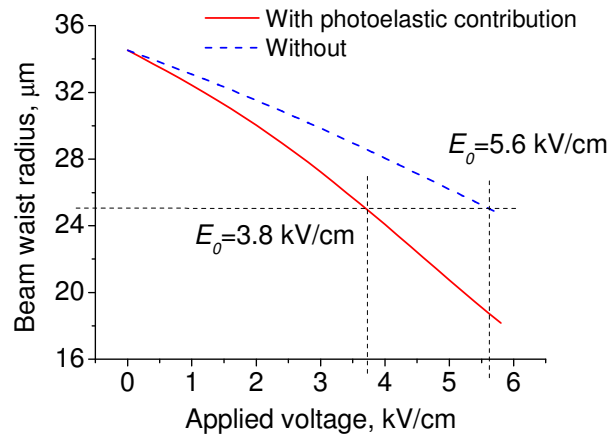


Figure 4.4: Output beam waist radius in dependence on the applied voltage with and without the additional photoelastic contribution to the optical properties of the medium, $I_d = 0.1I_0$.

The analysis shows that the additional photoelastic contribution decreases substantially the magnitude of the external field necessary for the realisation of the quasi-soliton beam. Taking into account of the photoelastic contribution decreases the necessary field strength from $E_0 = 5.6$ kV/cm down to 3.8 kV/cm.

The increase of the intensity of the dark irradiance decreases the necessary magnitude of the applied voltage to reach a quasi-soliton regime. From figure 4.5 we can see that in the presence of the additional photoelastic contribution the quasi-soliton beam is realised at the external applied electric field 3 kV/cm. The theoretical model of Shepelevich *et al.* predicts a value of 5.1 kV/cm.

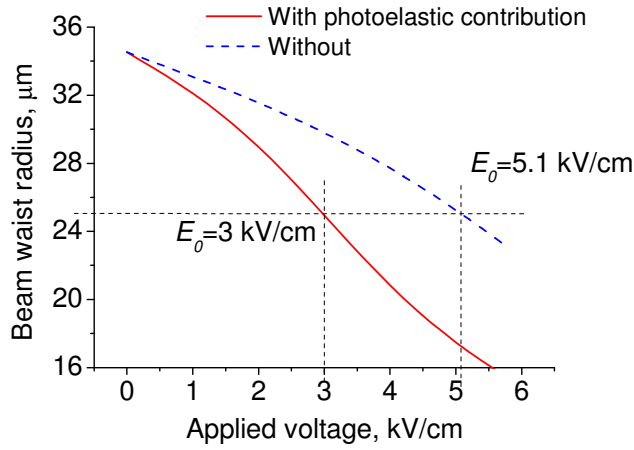


Figure 4.5: Output beam waist radius in dependence on the applied voltage with and without additional photoelastic contribution to the optical properties of the medium, $I_d=1I_0$.

Comparing figures 4.4 and 4.5 we can see that the increase of the dark irradiance intensity ten times decreases the magnitude of the applied voltage to observe the quasi-soliton. In the first case the taking into account of the additional photoelastic contribution decreases the necessary value of the electric field amplitude about 1.47 times. In the last case this ratio increases up to 1.7 times. It means that the intensity of the dark irradiance strongly influences on the magnitude of the additional photoelastic contribution to the modulation of the optical properties of the medium. Thereby for the developed theoretical model the accuracy of the numerical determination of the external parameters can be enhanced in some cases more than twice.

In equation (4.9) the amplitude of the external applied voltage influences on the linear birefringence induced in the crystal (terms μ_i) by the external applied electric field. The amplitude of the space-charge field E_x depends on the applied voltage amplitude E_0 and on the dark irradiance intensity I_d . It is responsible for the laser beam self-action (terms η_i). If one takes into account no additional photoelastic contribution the amplitude of the space-charge field influences simultaneously on the linear birefringence and on the laser beams

self-action that doesn't permit to separate these effects in the theoretical model by Shepelevich *et al.* [29]. In our theoretical model the change of the dark irradiance intensity influences only on the laser beam self-action through the terms η_i . The separation of effects of the induced birefringence and the formed space-charge field to the optical properties of the medium makes it possible to decrease the amplitude of the applied electric field necessary to observe the quasi-soliton regime in the crystal.

Figure 4.6 shows the dependence of the output beam waist radius on the ratio I_d at the applied voltage 3 kV/cm for both theoretical models. In the absence of the additional photoelastic contribution the minimum of the dashed curve reaches the value of the output beam waist radius 29 μm at $I_d = 0.3I_0$. The minimum of the solid curve is shifted on $0.2I_0$ to the right with a value of 24 μm . For the theoretical model by Shepelevich the quasi-soliton regime cannot be realised for any value of the ratio I_d but for the solid curve the quasi-soliton exists at $I_d = 0.2I_0$. The maximal difference 5 μm is observed at $I_d = 0.5I_0$ that corresponds to the minimum of the solid curve.

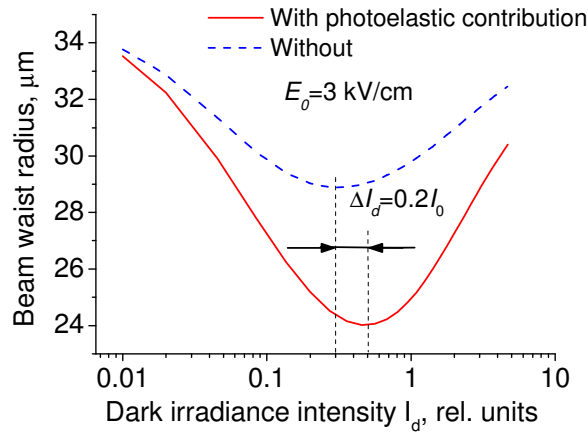


Figure 4.6: Output beam waist radius in dependence on the I_d at the amplitude of the applied electric field 3 kV/cm.

The ratio between output beam radii r_2/r_1 in dependence on I_d for both theoretical models is presented in figure 4.7. The growth of the amplitude of the applied voltage leads to the increase of this ratio and at the applied voltage 6 kV/cm the additional photoelastic contribution decreases the output beam waist radius almost 1.7 times at the maximum of the curve. This fact is important if the input beam waist radius has a rather small value.

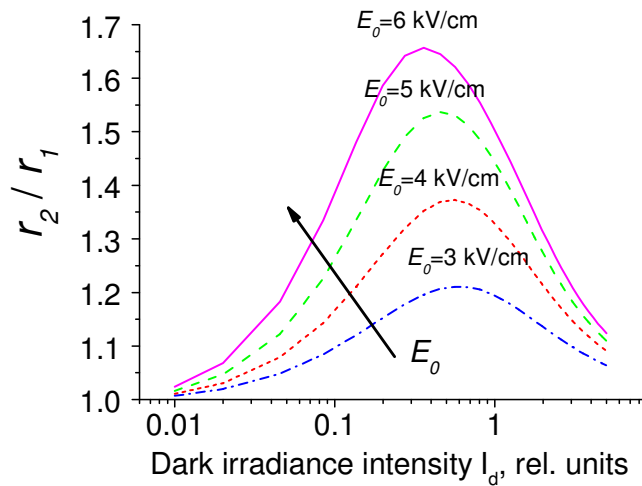


Figure 4.7: Ratio of output beam waist radii in dependence on the I_d at the amplitude of the applied electric field 3 kV/cm.

The ratio of output beam waist radii r_2/r_1 for the input $r_0 = 10 \mu\text{m}$ in dependence on the applied voltage is presented in figure 4.8.

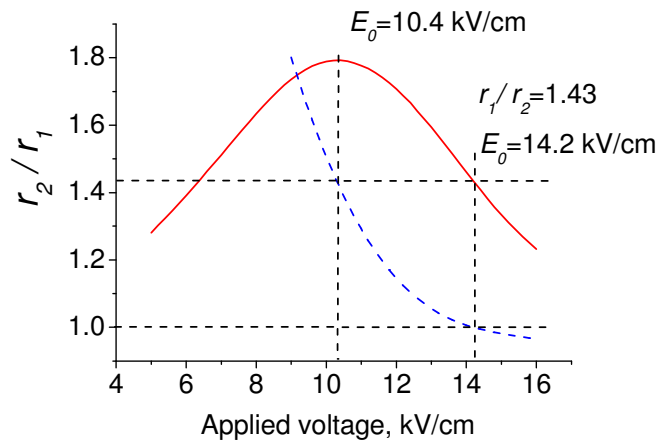


Figure 4.8: Ratio of output beam waist radii (solid curve) and r_1/r_0 (dash curve) in dependence on the value of the applied electric field amplitude for the input beam waist radius $r_0=10 \mu\text{m}$ and for $I_d=0.5I_0$.

At the $E_0=10.4 \text{ kV/cm}$ the ratio r_2/r_1 has the value 1.8 and when the output beam radius is equal to the input one this ratio reaches the value $r_2/r_1 = 1.43$. Such large contribution of the additional photoelastic effect to the optical properties of the photorefractive cubic

crystal has to be taken into consideration in the case of a small input beam waist radius and under a large amplitude of the applied electric field.

BSO crystal

The major difference between BSO and BTO crystals is the value of the optical activity. The BSO crystal has the value of the optical activity at about $\rho = 22$ °/mm [64]. The rapid rotation of the polarization leads to the well known effect of breathing solitons [27, 28]. Authors have used the orientations of the applied external electric field along crystallographic axes [001] and [110] that requires extreme large value of the electric field amplitude to observe photorefractive spatial solitons. If the external electric field applied along the crystallographic axis $[1\bar{1}1]$ the distribution of the power between polarization components in the BTO crystal influences weakly on the beam self-focusing due to maximal values of nonlinear coefficients η_1 and η_3 responsible for photorefractive response of the crystal. But the large value of the optical activity increases the necessary value of the applied voltage to reach the same self-focusing effect as in BTO crystals. Figure 4.9 shows the dependence of the output beam waist radius on the applied voltage for the propagation of a light beam ($\lambda = 633$ nm) with the Gaussian distribution of the input amplitude (the waist radius is $x_0 = 25$ μm) for BTO and BSO crystals for the same crystal length 15 mm.

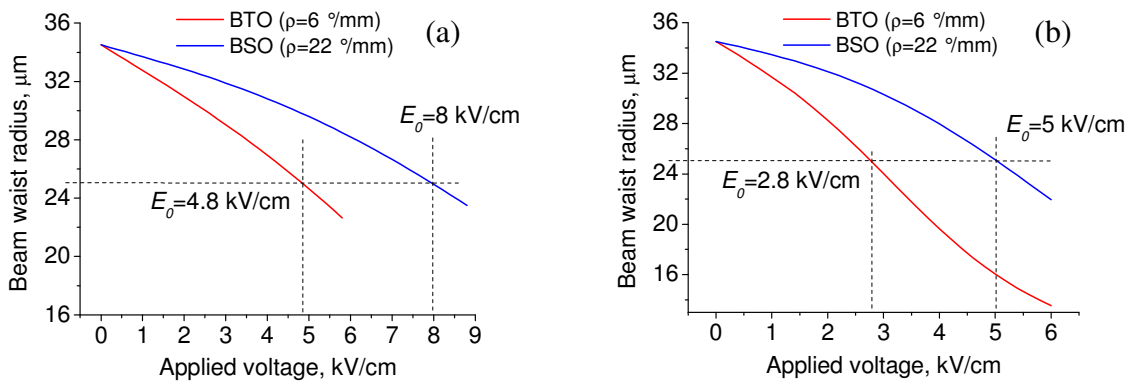


Figure 4.9: Output beam waist radius in dependence on the amplitude of the applied electric field for the BTO and BSO crystals without (a) and with (b) an accounting of the additional photoelastic contribution, $I_d=0.5I_0$.

The propagating laser beam reaches a quasi-soliton regime in the BTO crystal for the

smaller value of the applied voltage $E_0 = 4.8$ kV/cm and at $E_0 = 8$ kV/cm for the BSO (Figure 4.9a). The taking into account of the additional photoelastic contribution decreases the necessary electric field 1.7 times for the BTO crystal and 1.6 times for the BSO one. The difference between the two theoretical models is rather large and both crystals have about the same decreasing factor of the necessary electric field to observe the quasi-soliton regime.

In the common case the increase of the optical activity leads to the increase of the applied voltage for the same self-focusing effect due to the difference between absolute values of the nonlinear coefficients η_1 and η_3 . The transfer of the total power of the propagating laser beam in the y -component of the polarization leads to the decreasing of the effective beam self-focusing effect. In the set of equations (4.9) the absolute value of the coefficient η_3 2.5 times less than for η_1 that decreases the nonlinear response of the photorefractive crystal by the same factor. The behavior of the intensity of both polarization components for two crystals in the presence of the additional photoelastic contribution is shown in figure 4.10.

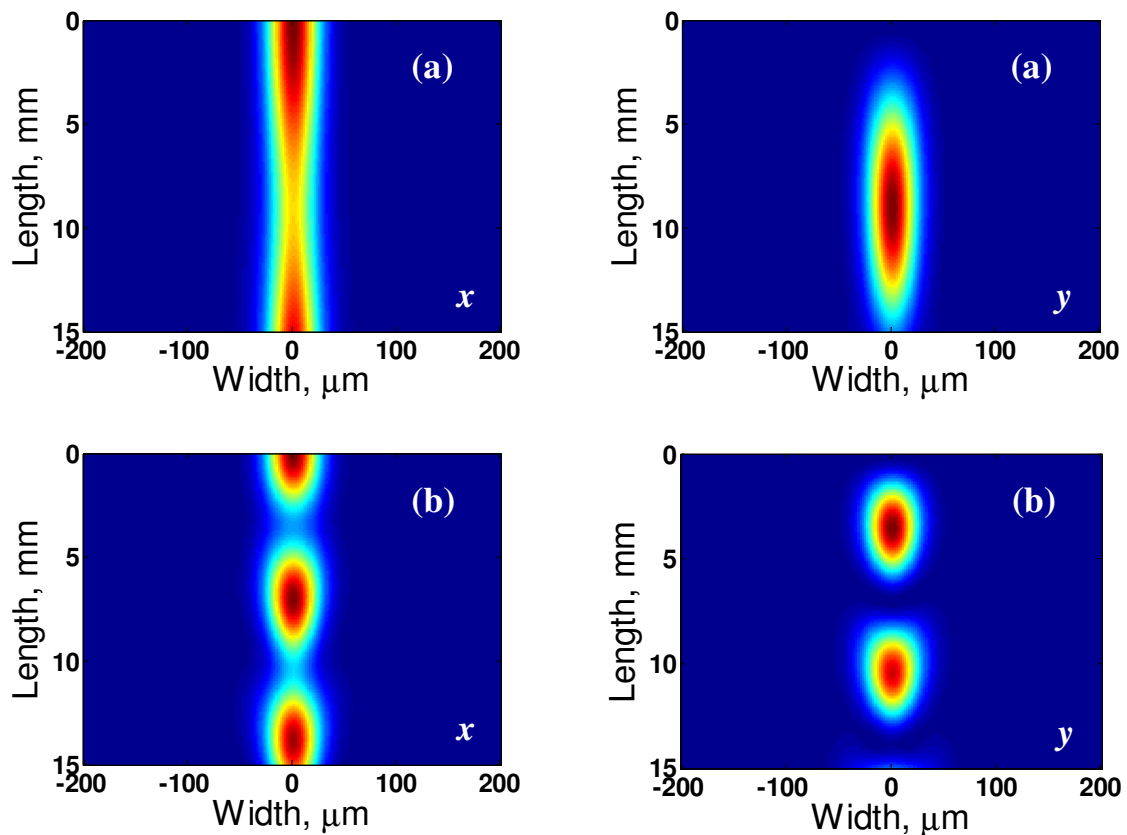


Figure 4.10: Intensity distribution of the x - and y -components of the quasi-soliton beam in BTO (a) and BSO (b) crystals.

Comparing figures 4.10a and 4.10b we can see that in the BTO crystal the self-focusing occurs generally due to the x -component of the polarization and there is only one region with a length of about 10 mm where the x -component vanishes. In the BSO crystal already both components influence on the laser beam self-action that reduces the influence of the nonlinear response of the photorefractive medium.

Taking into account the additional photoelastic contribution leads to the increase of the rotating velocity of the polarization vector of the propagated beam which is shown in figure 4.11 by the maximal normalized intensity.

The rather large value of the applied electric field changes strongly the polarization state of the propagating light beam [27, 28]. The narrow input beam requires an increase of the applied voltage to compensate the essential diffraction. As we have shown the quasi-soliton regime for the input waist radius 10 μm can be realised in the BTO crystal for $E_0=14.2$ kV/cm if the electric field is applied along the crystallographic axis $[\bar{1}\bar{1}1]$. The large magnitude of the optical activity of the BSO crystal decreases the nonlinear response that leads to the increase of the amplitude of the electric field to observe the quasi-soliton regime. The dependence of the output beam waist radius on the applied voltage is shown in figure 4.12. The quasi-soliton is observed at a value of the electric field of about 19 kV/cm.

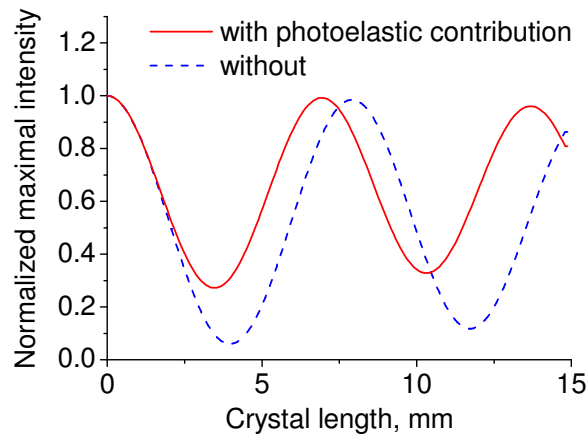


Figure 4.11: Maximal normalized intensity of the propagated laser beam in the x -component of the polarization with (solid curve) and without (dashed curve) the additional photoelastic contribution.

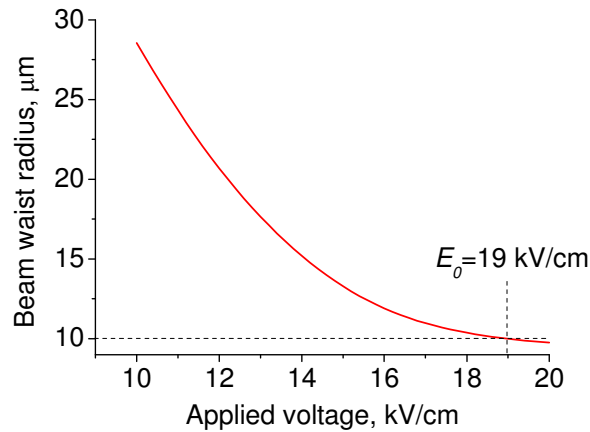


Figure 4.12: Output beam waist radius in dependence on the applied voltage in the BSO crystal at $r_0=10 \mu\text{m}$, $I_d=0.5I_0$.

Maps of the polarization orientation during the laser beam propagation in this case for both theoretical models are presented in figure 4.13a, b. Both maps are very different at edges of the propagated beam as well as in the region of the light illumination. Due to the accounting of the additional photoelastic contribution the vector of the polarization rotates rather rapidly. Coefficients μ_i in the set of equations (4.9) are responsible only for the induced birefringence and in the theoretical model of Shepelevich *et al.* [29] (the set of equations 4.21) they are responsible also for the nonlinear response. The induced space-charge field switches on the influence of coefficients η_i in the set of coupled equations (4.9) that gives the additional contribution to the optical nonlinear response of the medium and to the induced birefringence. As magnitudes of coefficients μ_i and η_i don't differ strongly (Figures 4.2 and 4.3) for any orientation of the applied electric field the induced birefringence near the beam centre could be magnified about two times in comparing with Shepelevich's model.

Without the influence of the additional photoelastic effect the polarization vector of the beam center (Figure 4.13c, d) makes only 1.5 full rotations. Our theoretical model predicts 3.5 full rotations.

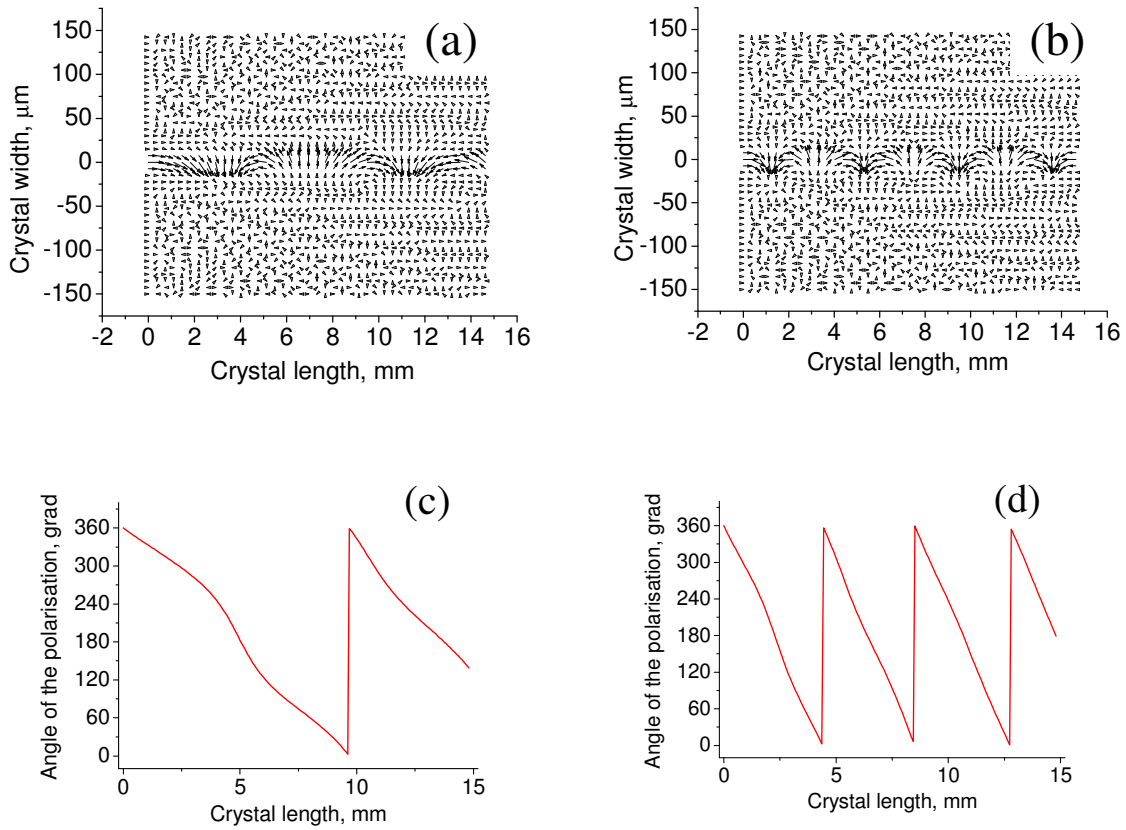


Figure 4.13: Evolution of the polarization vector orientation (a, b) and the polarization angle of the beam centre (c, d) during the laser beam propagation in a BSO crystal at the $r_0=10\ \mu\text{m}$, $E_0=19\ \text{kV/cm}$ with (a, c) and without (b, d) influence of the photoelastic effect.

But the map representation is not suitable to demonstrate the polarization state while the induced birefringence modifies it from the linear polarization to the elliptical one. The polarization dynamics in this case can be easily analysed by means of the Poincare sphere. We consider the projection of the S_1 - S_2 plane instead of the volumetric sphere while it is the only possible representation to show the whole polarization trajectory (Figure 4.14). In the absence of an external applied electric field both theoretical models show that the beam has a linear polarization along the propagation direction. In this case there is only an influence of the essential optical activity and the polarization vector turns itself with a speed of $22^\circ/\text{mm}$. The increase of the applied bias up to $5\ \text{kV/cm}$ changes the linear polarization to the elliptical one and the polarization dynamic shows more than one complete turn around the sphere, especially in the theoretical model of Shepelevich *et al.* Our model predicts the strong change of the polarization state and the acceleration of the polarization rotation. The induced birefringence strongly bends the polarization trajectory which approaches once the S_3 axis (circular polarization).

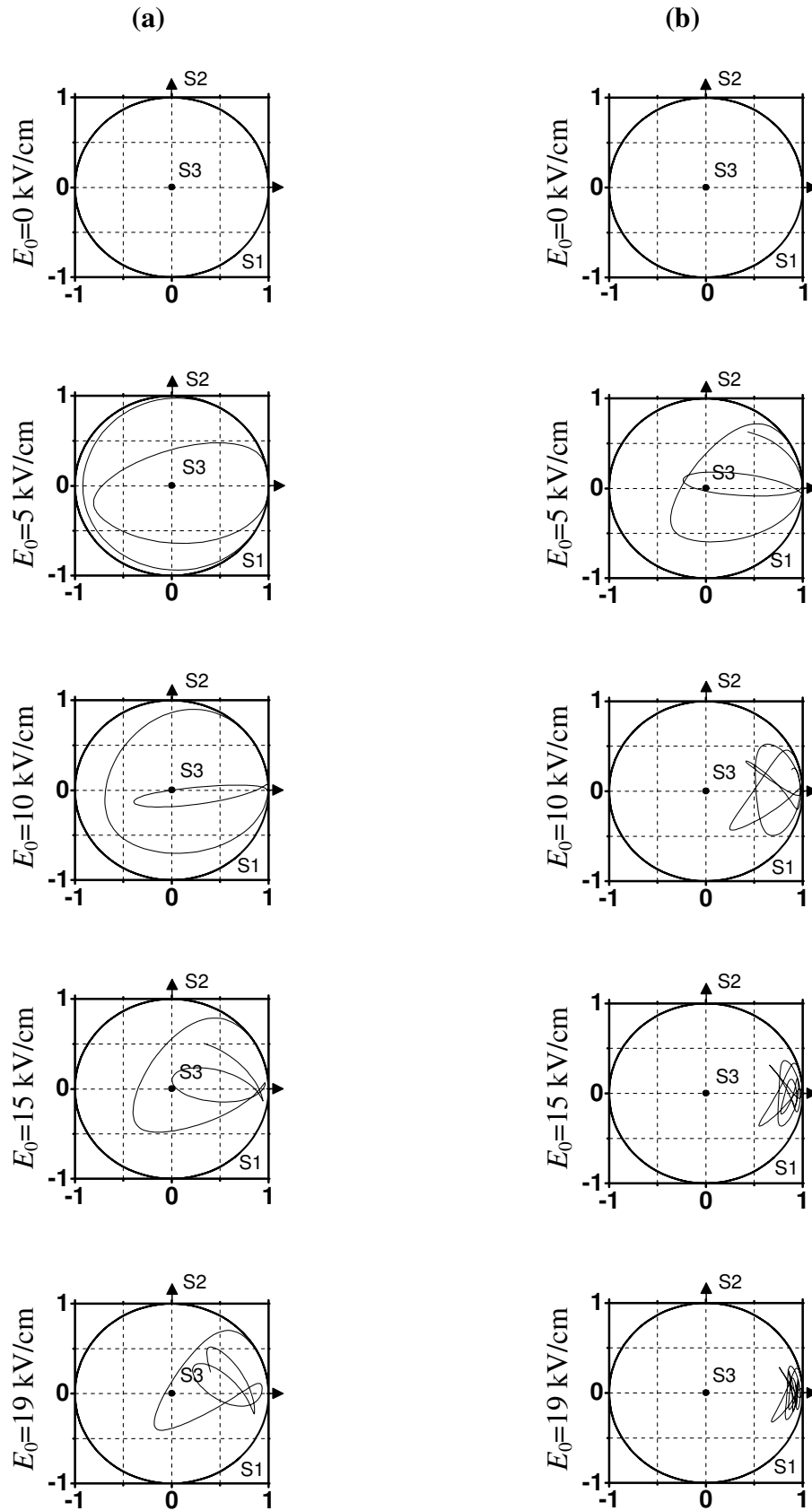


Figure 4.14: Polarization dynamics of the beam for increasing of the applied voltage without (a) and without (b) the accounting of the additional photoelastic effect.

The further increase of the external bias distorts the polarization trajectory and at $E_0 = 15$ kV/cm Shepelevich's model shows about the same results as we can observe in our model at $E_0 = 5$ kV/cm. Increasing more the bias, the dynamics is more concentrated at the region $S_1 > 0$ for both theoretical models. It means that the polarization doesn't rotate anymore completely but vibrates around the x axis. Observing all obtained trajectories for $E_0 > 0$ we see that all of them rotate around a stable state for the plane $S_2 = 0$. It is clear that the quasi-soliton regime can be realised if the change of the polarization state tends to small perturbations around the direction of the applied electric field. This fact is demonstrated by the last image in figure 4.13b at $E_0 = 19$ kV/cm. The induced birefringence reduces the fluctuation of the polarization trajectory around the x axis (S_1 state) that makes it possible to compensate the essential diffraction of the x -component of the polarization and we can affirm that the pure solitonic state is reached. Although the polarization vector in figure 4.13b makes about 3.5 full rotations and the ellipse of the polarization is extended along the axis x .

Already at $E_0 = 10$ kV/cm the dynamics is completely concentrated at the region $S_1 > 0$ and with an increase of the bias the whole trajectory approaches the state $S_1 = 1$. If one takes into account no additional contribution of the photoelastic effect (Figure 4.13a) even at $E_0 = 19$ kV/cm the polarization in one place of the trajectory is very near to the circular but generally has the elliptical form. It means that the amplitude of the external applied electric field has to be grown to align the polarization to the linear state that could lead to the overfocusing of the propagated beam and to the distortion of the beam intensity distribution.

The necessary value of the applied bias to reach a quasi-soliton regime is 24 kV/cm. The beam intensity distribution along the crystal in this case is presented in figure 4.15a. Although the outputs beam waist radius is equal to the input one and the form of the intensity distribution changes quite significantly along the propagation distance. It is easy to see that there arise any additional beams which propagate under an angle to the straight direction which reduce the whole power of the main beam. It leads to the narrowing of the written channel and to the unequal intensity distribution at the edges of the output beam. Our theoretical model predicts almost straight channels formed by the focused propagated beam (Figure 4.15b). This large difference between theoretical models is connected with the behaviour of the polarization. As we have shown before, the quasi-soliton regime can be reached if the polarization state tends to the linear one along the direction of the applied

electric field. The separation of effects of the induced birefringence and the nonlinear response of the medium in the set of equations (4.9) gives us an ability to take into consideration the change of the polarization of the propagated laser beam independently on both effects. The model of Shepelevich *et al.* (Equation 4.21) mixes both effects that by turn significantly distort the polarization behaviour.

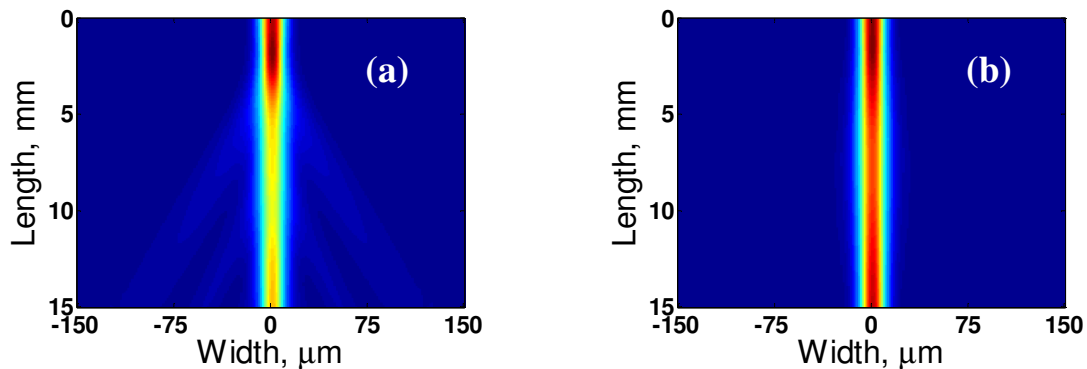


Figure 4.15: Evolution of the beam intensity distribution for the quasi-soliton regime without (a) and with (b) the additional photoelastic contribution.

4.1.2 Conclusion

Thus the additional photoelastic contribution to the optical properties of the photorefractive cubic medium in some cases can reduce the necessary value of the electric field amplitude to observe the same magnitude of the self-action effect as in the simple theoretical model by a factor of 1.7. It means that the accuracy of the numerical determination of external parameters can be enhanced up to 60% in some cases. We have also shown that the increase of the applied voltage leads to the increase of the influence of the photoelastic contribution on the self-focusing of the laser beam. It is especially important if the input beam waist radius has a rather small value. The new theoretical model predicts also the strong change in the polarization behavior of the propagated laser beam in comparing with old one. This is reached by the separating of effects of the induced birefringence and the nonlinear response of the photorefractive medium.

The presented theoretical model predicts an ability to observe quasi-solitons in cubic photorefractive crystals with a large magnitude of optical activity if the laser beam has small input waist radius. The theoretical model developed by Shepelevich *et al.* does not permit to obtain the same result.

4.2 Self-action of light beams in (112)-cut sillenites

4.2.1 Theoretical model

We shall consider a crystal with symmetry 23, in which a light beam with an intensity distribution $I(x)$ on the input face propagates along the z axis (Figure 4.16) coinciding with the crystallographic direction $[1\bar{1}\bar{2}]$.

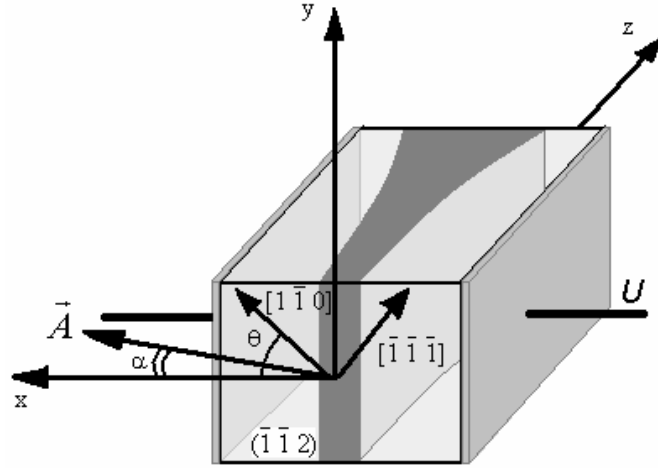


Figure 4.16: Photorefractive crystal orientation under an applied external dc electric field U in which a light beam with intensity distribution $I(x)$ at the input face propagates.

The external ac or dc electric field was applied along the x axis which makes an angle θ with the crystallographic direction $[1\bar{1}0]$. In the presented crystallographic system the vectors of the coordinate systems have the relations:

$$\begin{aligned}\vec{x}_0 &= \left(\frac{\sin(\theta)}{\sqrt{3}} + \frac{\cos(\theta)}{\sqrt{2}}, \frac{\sin(\theta)}{\sqrt{3}} - \frac{\cos(\theta)}{\sqrt{2}}, \frac{\sin(\theta)}{\sqrt{3}} \right), \\ \vec{y}_0 &= \left(\frac{\sin(\theta)}{\sqrt{2}} - \frac{\cos(\theta)}{\sqrt{3}}, \frac{\sin(\theta)}{\sqrt{2}} + \frac{\cos(\theta)}{\sqrt{3}}, -\frac{\cos(\theta)}{\sqrt{3}} \right), \\ \vec{z}_0 &= \left(\frac{1}{\sqrt{6}}, \frac{1}{\sqrt{6}}, -\sqrt{\frac{2}{3}} \right).\end{aligned}\tag{4.22}$$

The set of equations describing the laser beam propagation in cubic photorefractive crystals of $(11\bar{2})$ -cuts can be obtained using the same method as in section 4.1. In this case the coefficients μ_i and η_i entering in the set of equations (4.9) are given by:

$$\begin{aligned}
\mu_1 &= -\frac{\sin \theta}{\sqrt{3}}(5 \cos^2 \theta - 2), \\
\mu_2 &= -\frac{\cos \theta}{\sqrt{3}}(5 \sin^2 \theta - 1), \\
\mu_3 &= \frac{\sin \theta}{\sqrt{3}}(5 \cos^2 \theta - 1),
\end{aligned} \tag{4.23}$$

$$\begin{aligned}
\eta_1 &= \frac{\sin^2 \theta}{3} [\Delta b_{11} + \Delta b_{22} + \Delta b_{33} + 2(\Delta b_{12} + \Delta b_{13} + \Delta b_{23})] + \\
&+ \frac{\cos^2 \theta}{2} (\Delta b_{11} + \Delta b_{22} - 2\Delta b_{12}) + \frac{\sin 2\theta}{\sqrt{6}} (\Delta b_{11} - \Delta b_{22} + \Delta b_{13} - \Delta b_{23}), \\
\eta_2 &= \frac{\sin 2\theta}{12} [\Delta b_{11} + \Delta b_{22} - 2\Delta b_{33} - 10\Delta b_{12} - 4(\Delta b_{13} + \Delta b_{23})] - \\
&- \frac{\cos 2\theta}{\sqrt{6}} (\Delta b_{11} - \Delta b_{22} + \Delta b_{13} - \Delta b_{23}), \\
\eta_3 &= \frac{\sin^2 \theta}{2} (\Delta b_{11} + \Delta b_{22} - 2\Delta b_{12}) + \frac{\cos^2 \theta}{2} [\Delta b_{11} + \Delta b_{22} + \Delta b_{33} + 2(\Delta b_{12} + \Delta b_{13} + \Delta b_{23})] - \\
&- \frac{\sin 2\theta}{\sqrt{6}} (\Delta b_{11} - \Delta b_{22} + \Delta b_{13} - \Delta b_{23})
\end{aligned} \tag{4.24}$$

4.2.2 Numerical simulation

Dependences of coefficients $\mu_i(\theta)$ and $\eta_i(\theta)$ for the $(11\bar{2})$ -cut are presented in figures 4.17 and 4.18. For the orientation angle $\theta = 0^\circ$ ($\vec{E}_0 \parallel [1\bar{1}0]$), as in samples with conventional orientation, only the coefficients μ_2 and η_2 responsible for the cross correlation between the x and y components of the polarization vector are nonzero. However in the considered case their absolute values ($|\mu_2| = 0.577$, $|\eta_2^{BTO}| = 0.533$ and $|\eta_2^{BSO}| = 0.657$) are much lower ($|\mu_2| = 1$, $|\eta_2^{BTO}| = 0.923$ and $|\eta_2^{BSO}| = 1.137$), than for the (110) -cut at the same direction of the applied field.

When the field is applied along the crystallographic axis $[1\bar{1}0]$, the difference in the coefficients μ_2 , η_2 for $\{110\}$ and $\{112\}$ -cuts influences considerably on the observation conditions of the soliton-like laser beam propagation. For each of these cuts, at a given field direction, the screening nonlinearity reaches its maximum for a polarization vector

orientation at the angle $\alpha = \pm 45^\circ$ to the x axis. The calculation shows that the soliton-like beam propagation with such input polarization and with input beam waist $25 \mu\text{m}$ can be observed in a $(11\bar{2})$ -cut BTO crystal for a field strength $E_0 \approx 8.8 \text{ kV/cm}$, whereas for the (110) -cut it is possible already for $E_0 \approx 5.1 \text{ kV/cm}$.

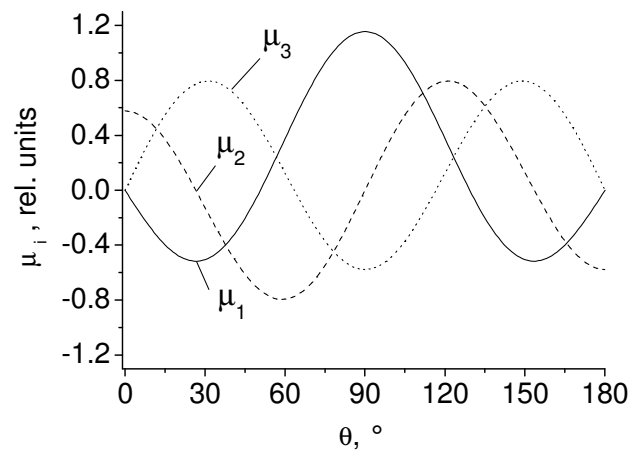


Figure 4.17: Dependences of the coefficients μ_1 , μ_2 , and μ_3 on the orientation angle θ .

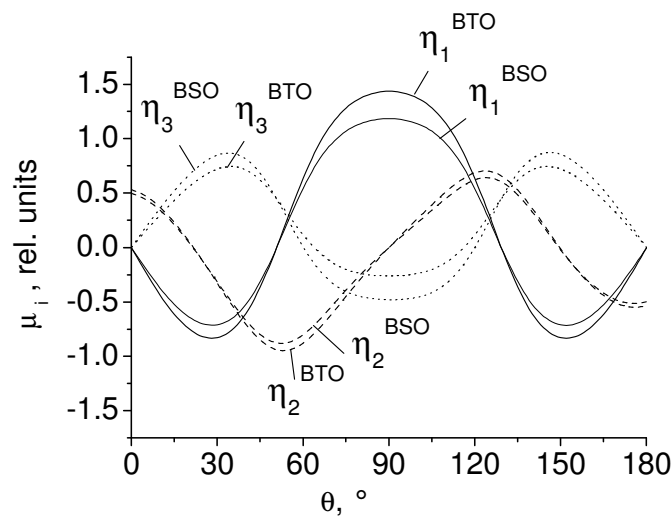


Figure 4.18: Dependences of the coefficients η_1 , η_2 , and η_3 on the orientation angle θ in bismuth titanate (BTO) and bismuth silicate (BSO) crystals.

The maximal nonlinear response of the medium is reached at the orientation of the applied electric field along the crystallographic axis $[001]$ ($\theta = 90^\circ$). In this case the values

of coefficients η_i and μ_i have the same magnitude as for the crystals of (110)-cuts at $\theta = 35.26^\circ$.

4.2.3 Conclusion

We have developed a theoretical model of self-action of one-dimensional light beams in $(11\bar{2})$ -cut sillenite crystals. At the same orientations of the applied electric field as for the (110)-cut the magnitude of the nonlinear response strongly differs. But $(11\bar{2})$ -cut sillenite crystals show same properties if the electric field is applied along the crystallographic axis $[001]$ ($\theta = 90^\circ$). This correspond to the orientation $[1\bar{1}1]$ ($\theta = 35.26^\circ$) in the (110)-cut.

The advantage of using $(11\bar{2})$ -cut crystals is the possibility of counter interaction of propagating light.

Chapter 5

Self-bending of laser beams in photorefractive crystals

In this chapter we study the self-bending effect of a laser beam in single-axis BaTiO₃ crystals as well as in cubic BTO and BSO ones. We consider the influence of the additional elasto-optic contribution to changes of the dielectric permittivity on the magnitude of the beam deviation for a speckled extraordinary light beam in photorefractive BaTiO₃. The real trajectory of the speckled beam is calculated.

Results of theoretical analyses and numerical calculations of the influence of natural optical activity and linear birefringence, induced by an external alternating-sign electric field, on the self-action of light beams with one dimensional input intensity distribution propagating in sillenite crystals are presented. The theoretical model is confirmed by the experiment.

5.1 Self-bending in BaTiO₃

Following the simple model of Lyubomudrov and Shkunov [56], we investigate the trajectories for a self-bent extraordinary beam in BaTiO₃, including the elasto-optic contribution to the changes of the dielectric permittivity for the photorefractive gratings. We neglect the roto-optic contribution because of the weak linear birefringence of BaTiO₃.

5.1.1 Basic equations

Figure 5.1 shows the curved path geometry for pump beam propagation in BaTiO₃, where α_0 and α are the entrance and local angles of the beam inside the crystal.

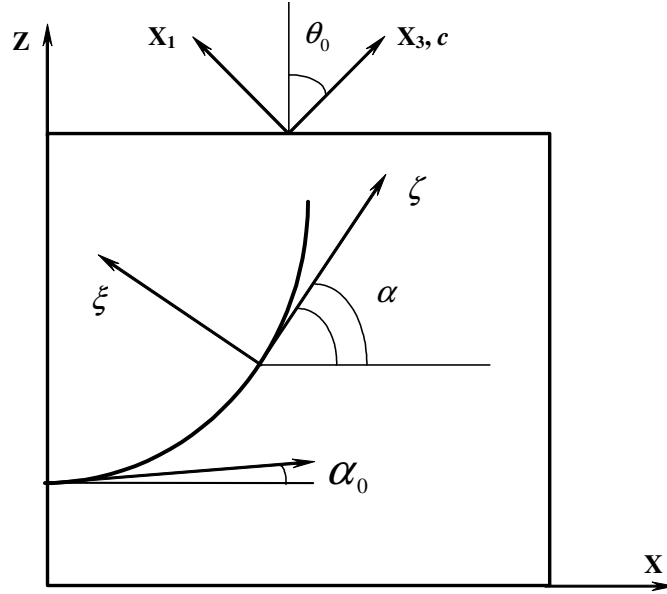


Figure 5.1: Geometric configuration for self-bending of the laser beam in the crystal with an arbitrary orientation of the optical axis c in the (010) crystallographic plane.

In order to extend the configuration from References [56] and [108] we consider an arbitrary orientation of the optical axis c in the (010) crystallographic plane. In the diffusion regime without trap saturation the trajectory of the whole pump beam can be calculated from the following set of equations [56]:

$$\frac{d\alpha}{dx} = \frac{1}{\cos\alpha} \frac{d\alpha}{d\zeta} = k\Delta\theta_f^2 \frac{\gamma(\beta)}{\cos\alpha}, \quad (5.1)$$

$$z(x) = \int_0^x \operatorname{tg}\alpha(x_1) dx_1, \quad (5.2)$$

where $k = 2\pi/\lambda$ is the magnitude of the light wave vector in vacuum, $\Delta\theta_f$ is the angular half-width divergence of the speckled beam, λ is the wavelength, $\beta = \alpha + \theta_0$, and θ_0 is the angle between the axes c and z (Figure 5.1). The nonlinearity coefficient $\gamma(\beta)$ for a beam with the extraordinary polarization can be represented as [56]:

$$\gamma(\beta) = -\frac{1}{2} k \left(\frac{k_B T}{e} \right) \frac{1}{\epsilon_0} \Delta\epsilon_{ij} m_i m_j, \quad (5.3)$$

where m_i and m_j are the components of the unit vector \mathbf{m} which is perpendicular to the local beam direction inside the crystal. For an arbitrary orientation of the optical axis c in the (010) crystallographic plane the unit vector \mathbf{m} is:

$$m_1 = \sin(\beta), \quad m_2 = 0, \quad m_3 = \cos(\beta). \quad (5.4)$$

In this case the nonlinearity coefficient $\gamma(\beta)$ takes the form:

$$\gamma(\beta) = -\frac{1}{2}k \left(\frac{k_B T}{e} \right) \left[\Delta\epsilon_{11}(\beta) \sin^2 \beta + \Delta\epsilon_{33}(\beta) \cos^2 \beta + 2\Delta\epsilon_{13}(\beta) \sin \beta \cos \beta \right] \frac{1}{\epsilon_0}, \quad (5.5)$$

where $k_B T$ is the thermal energy, e is the charge of the mobile charge carriers, and ϵ_0 is the vacuum permittivity. The change in the dielectric permittivity tensor, $\Delta\epsilon_{ij}$, for the photorefractive grating with the unit amplitude of space-charge field in a non-centrosymmetric crystal can be written as the sum of the electro-optic and elasto-optic contributions [34, 35]:

$$\Delta\epsilon_{ij} = -\frac{\epsilon_{im} \epsilon_{jn}}{\epsilon_0} \left(r_{mnp}^S m_p + P_{mnkl}^E m_l \gamma_{ks} e_{psr} m_p m_r \right), \quad (5.6)$$

where ϵ_{im} is the dielectric permittivity tensor at optical frequencies in absence of space-charge field; r_{mnp}^S and P_{mnkl}^E , respectively, are the electro-optic tensor in a clamped crystal and the elasto-optic tensor for a constant electric field; G_{ks} are the components of the tensor $G = \Gamma^{-1}$ inverse to the Christoffel's tensor Γ with the components $\Gamma_{sc} = C_{sqkt}^E m_q m_t$; C_{sqkt}^E and e_{psr} , respectively, are the tensor of elastic constant for a constant electric field and the piezoelectric stress tensor. The photoelastic, elastic and piezoelectric tensors of point group 4mm are presented below:

$$\begin{pmatrix} P_{11}^E & P_{12}^E & P_{13}^E & 0 & 0 & 0 \\ P_{13}^E & P_{11}^E & P_{12}^E & 0 & 0 & 0 \\ P_{12}^E & P_{13}^E & P_{11}^E & 0 & 0 & 0 \\ 0 & 0 & 0 & P_{44}^E & 0 & 0 \\ 0 & 0 & 0 & 0 & P_{44}^E & 0 \\ 0 & 0 & 0 & 0 & 0 & P_{66}^E \end{pmatrix}, \quad (5.7)$$

$$\begin{pmatrix} C_{11}^E & C_{12}^E & C_{13}^E & 0 & 0 & 0 \\ C_{12}^E & C_{11}^E & C_{13}^E & 0 & 0 & 0 \\ C_{13}^E & C_{13}^E & C_{33}^E & 0 & 0 & 0 \\ 0 & 0 & 0 & C_{44}^E & 0 & 0 \\ 0 & 0 & 0 & 0 & C_{44}^E & 0 \\ 0 & 0 & 0 & 0 & 0 & C_{66}^E \end{pmatrix}, \quad (5.8)$$

$$\begin{pmatrix} 0 & 0 & 0 & 0 & e_{15} & 0 \\ 0 & 0 & 0 & e_{14} & 0 & 0 \\ e_{31} & e_{31} & e_{33} & 0 & 0 & e_{36} \end{pmatrix}. \quad (5.9)$$

Using the approach described in Refs. 37 and 116, we derive the following expressions for $\Delta\epsilon_{11}$, $\Delta\epsilon_{33}$ and $\Delta\epsilon_{13}$ in BaTiO₃ crystal:

$$\begin{aligned} \Delta\epsilon_{11} &= n_0^4 \left(r_{13}^S \cos\beta + \frac{p_{11}^E (\Gamma_{33} e_1' - \Gamma_{13} e_3') \sin\beta + p_{13}^E (\Gamma_{11} e_3' - \Gamma_{13} e_1') \cos\beta}{\Gamma_{11} \Gamma_{33} - \Gamma_{13}^2} \right), \\ \Delta\epsilon_{33} &= n_e^4 \left(r_{33}^S \cos\beta + \frac{p_{31}^E (\Gamma_{33} e_1' - \Gamma_{13} e_3') \sin\beta + p_{33}^E (\Gamma_{11} e_3' - \Gamma_{13} e_1') \cos\beta}{\Gamma_{11} \Gamma_{33} - \Gamma_{13}^2} \right), \\ \Delta\epsilon_{13} &= n_0^2 n_e^2 \left(r_{42}^S \sin\beta + \frac{p_{44}^E (\Gamma_{33} e_1' - \Gamma_{13} e_3') \cos\beta + p_{33}^E (\Gamma_{11} e_3' - \Gamma_{13} e_1') \sin\beta}{\Gamma_{11} \Gamma_{33} - \Gamma_{13}^2} \right), \end{aligned} \quad (5.10)$$

where n_0 and n_e are the ordinary and extraordinary indices of refraction. The relevant components of the Christoffel's tensor Γ_{sc} and vectors e_i' are given by [37]:

$$\begin{aligned} \Gamma_{11} &= C_{11}^E \sin^2 \beta + C_{44}^E \cos^2 \beta, \\ \Gamma_{33} &= C_{44}^E \sin^2 \beta + C_{33}^E \cos^2 \beta, \end{aligned} \quad (5.11)$$

$$\begin{aligned} \Gamma_{13} &= (C_{13}^E + C_{44}^E) \sin\beta \cos\beta, \\ e_1' &= (e_{15} + e_{31}) \sin\beta \cos\beta, \\ e_3' &= e_{15} \sin^2 \beta + e_{33} \cos^2 \beta, \end{aligned} \quad (5.12)$$

where r_{mn}^S are the clamped electro-optic constants, p_{mn}^E are the elasto-optic constants, C_{mn}^E are the elastic constants, and e_{mn} are the piezoelectric stress constants in the matrix contracted notations.

5.1.2 Results and discussion

Figure 5.2 shows the calculated curved trajectory followed by the speckled beam ($\lambda = 633$ nm, $\Delta\theta_f = 0.076$) for various values of the incident angle φ_0 specified at the entrance face outside the 0°-cut crystal. The solid curve in figure 5.2 corresponds to the calculation on the basis of exact equations (5.3) and (5.10)-(5.12). For comparison we plot these curved

trajectories without considering the additional elasto-optic contribution ($p_{mn}^E = 0$) by using clamped (dash-dotted curve) and unclamped (dashed curve) electro-optic constants of BaTiO₃ crystal. We have used the following material parameters of the BaTiO₃ crystal for $\lambda = 633$ nm from Ref. 117: $n_0 = 2.412$, $n_e = 2.360$, $r_{13}^S = 10.2$ pm/V, $r_{33}^S = 40.6$ pm/V, $r_{42}^S = 730$ pm/V, $p_{11}^E = 0.5$, $p_{13}^E = 0.2$, $p_{31}^E = 0.07$, $p_{33}^E = 0.77$, $e_{31} = -0.7$ C/m², $e_{33} = 6.7$ C/m², $e_{15} = 34.2$ C/m², $C_{11}^E = 2.22 \cdot 10^{11}$ N/m², $C_{13}^E = 1.11 \cdot 10^{11}$ N/m², $C_{33}^E = 1.51 \cdot 10^{11}$ N/m², $C_{44}^E = 0.61 \cdot 10^{11}$ N/m², $r_{13}^T = 8$ pm/V, $r_{33}^T = 105$ pm/V, $r_{42}^T = 1300$ pm/V.

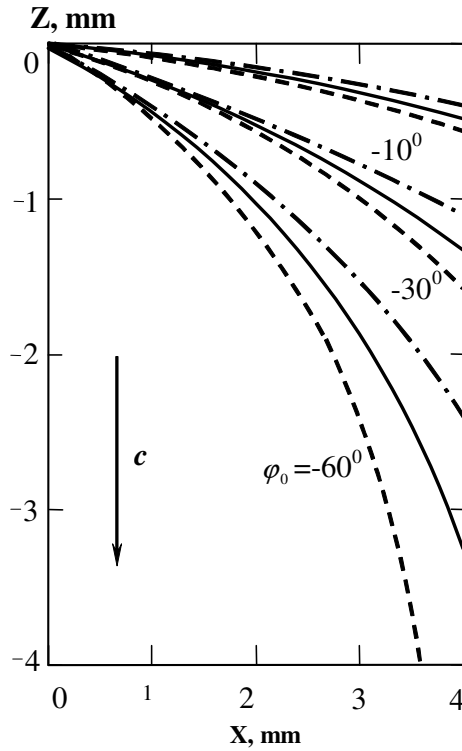


Figure 5.2: Trajectories of the self-bent beam for various values of the incident angle φ_0 in the 0⁰-cut BaTiO₃ crystal at the angular half-width divergence of the speckled beam $\Delta\theta_f = 0.076$ and for the angle between the axes c and z $\theta_0 = 180^0$. The solid curves correspond to the calculation with elasto-optic contribution. The dash-dotted and the dashed curves indicate results calculated without elasto-optic contribution ($p_{mn}^E = 0$) by using electro-optic coefficients for clamped and unclamped crystals, respectively.

It can be seen from figure 5.2 that the real trajectory of the speckled beam lies in the range between two curves that are commonly calculated on the base of the clamped or the unclamped electro-optic coefficients. The form of the beam trajectory is dictated by the angular dependence of the nonlinear coefficient $\gamma(\beta)$ and the initial angle $\alpha_0 + \theta_0$ at the

entrance face of the crystal. In figure 5.3 we show the dependence of the real non-linear coefficient with the elasto-optic contribution γ on β and, as a comparison, the nonlinear coefficients γ^S and γ^T which are calculated for $p_{mn}^E = 0$ by using clamped and unclamped electro-optic constants. It is clear that $\gamma^S(\beta)$ and $\gamma^T(\beta)$, respectively, indicate the overestimated and underestimated magnitudes of the nonlinear response relative to $\gamma(\beta)$.

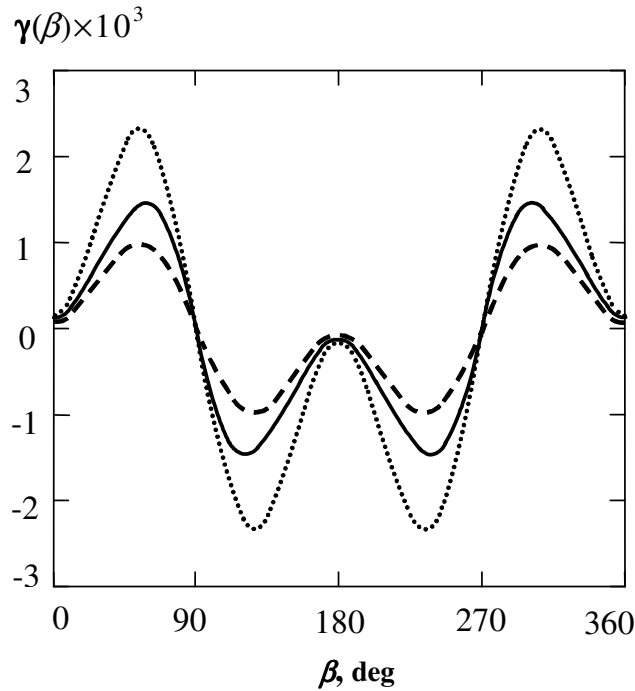


Figure 5.3: Orientation dependence of the nonlinear coefficient $\gamma(\beta)$ in BaTiO₃ with elasto-optic contribution (solid curve) and without one for the calculation by clamped (dashed curve) and unclamped (dotted curve) electro-optic coefficients.

Figure 5.5 shows the trajectory of the self-bending beam in the 45⁰-cut crystal. In that case a curvature of an initial part of the beam trajectories is far in excess of curve for the corresponding incident angles in the 0⁰-cut sample (Figure 5.2). This distinction is due to the dissimilar initial values of nonlinear coefficient $\gamma(\alpha_0 + \theta_0)$ (Figures 5.1 and 5.3). Note that calculated trajectory tends to be aligned along the direction of the optical axis c [56] in this approach.

The view of self-bent beams in a sample with the $(00\bar{1})$ input face is shown in figure 5.6. The negative or positive sign of the nonlinear coefficient $(90^0 + \theta_0)$ at $\alpha_0 > 0$ or $\alpha_0 < 0$ leads to the convex upwards or convex downwards trajectories of the beam.

The behavior of the beams in such nonlinear medium closely resembles that in a positive gradient lens. However, the pattern of the beams in the crystal with (001) entrance

face (Figure 5.6) indicates that the properties of negative lens for speckled beam is exhibited in that case.

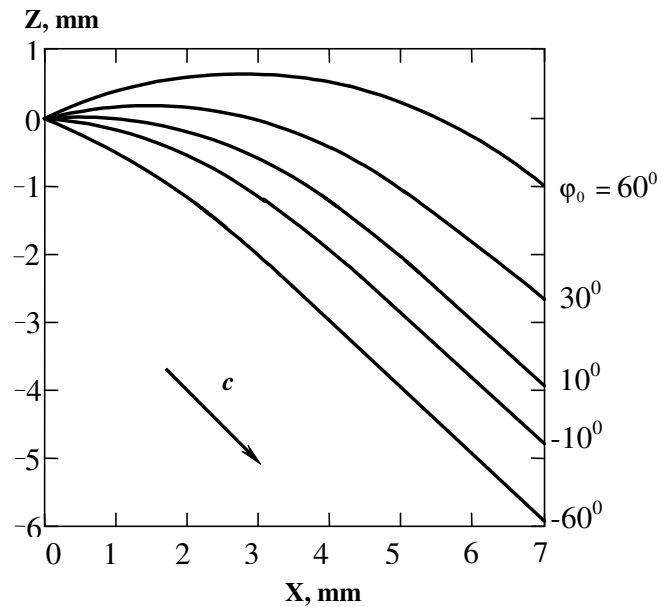


Figure 5.4: Trajectories of the self-bent beam for various values of the incident angle φ_0 in the 45° -cut BaTiO_3 crystal at $\Delta\theta_f = 0.076$ and $\theta_0 = 135^\circ$. The curves calculated with elasto-optic contribution.

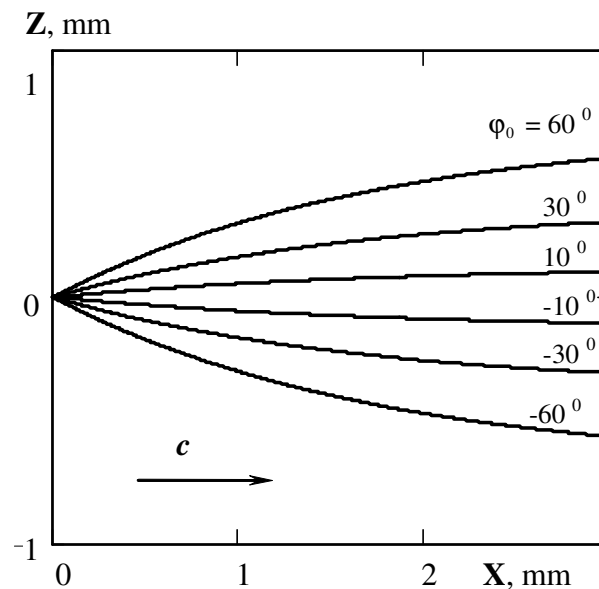


Figure 5.5: Trajectories of the self-bent beam for various values of the incident angle φ_0 in the 45° -cut BaTiO_3 crystal at $\Delta\theta_f = 0.076$ and $\theta_0 = 135^\circ$. The curves calculated with elasto-optic contribution.

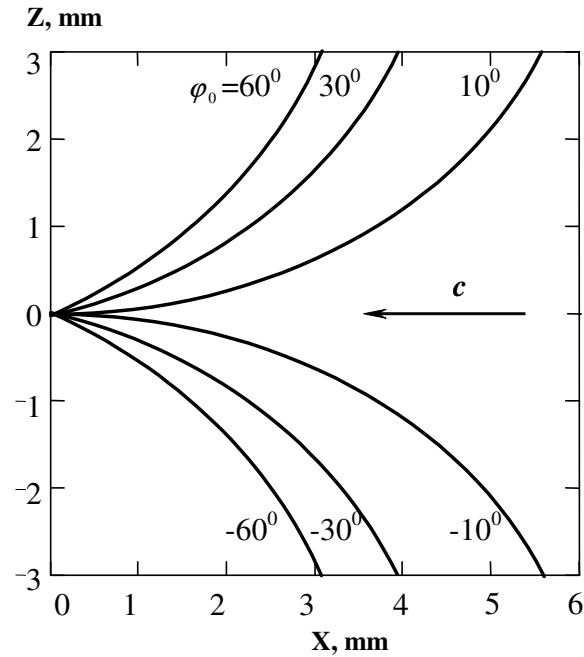


Figure 5.6: Trajectories of the self-bent beam for various values of the incident angle φ_0 in the BaTiO_3 crystal at $\Delta\theta_f = 0.076$ and $\theta_0 = -90^\circ$. The curves calculated with elasto-optic contribution.

5.1.3 Conclusion

We have considered the self-bending effect for a speckled extraordinary light beam in BaTiO_3 on the base of a model that takes into account the additional elasto-optic contribution. The analytical expressions for the nonlinearity coefficient have been derived. The substantial influence of the elasto-optic effect on the beam self-bending was demonstrated. It was shown that BaTiO_3 crystals exhibit the property of a positive or negative gradient lens depending on whether the speckled laser beam propagates along the optical axis \mathbf{c} or in the opposite direction.

5.2 Self-bending in cubic photorefractive crystals

5.2.1 Theoretical model

The nonlocal nonlinearity in cubic photorefractive crystals is strongly amplified in an external alternating field [61]. Self-bending of a light beam propagating in a cubic photorefractive crystal with an applied square-wave electric field was considered by Borodin *et al.* [62], who disregarded the optical activity of the crystal.

Let us consider a (110)-cut photorefractive crystal of point group 23 as in section 4 (Figure 4.1) in which a light beam with one-dimensional intensity distribution $I(x)$ at the input face is propagated at a small angle to the z axis.

The alternating square-wave electric field with amplitude E_0 and period T is applied along the x axis which has an angle θ with the [110] direction. To describe the dominating component $E_x(x, z)$ of the space-charge far from the saturation of traps, we take the expression

$$E_x = -\frac{L_E E_0}{I_d + I} \frac{dI}{dx} \quad (5.13)$$

obtained for the monopolar photorefractive crystal model [89] by averaging over the period of applied voltage taking into account that E_x undergoes small variations around the steady-state value [114]. Here $L_E = \mu\tau_R E_0$ is the drift length, μ is the mobility, and τ_R is the recombination time of charge carriers, I_d is the dark irradiance including the intensity of background illumination. From equation (5.13) it follows that for the employed linear model, the nonlocal component of the field in the crystal E_x grows quadratically with the amplitude E_0 of the external square-wave field. The set of equations (4.9) in this case has to be rewritten as follows:

$$\begin{cases} i \frac{\partial A_x}{\partial z} + \frac{1}{2k_0 n_0} \frac{\partial^2 A_x}{\partial x^2} \pm \frac{k_0 n_0^3}{2} r_{41}^T E_0 (\mu_1 A_x + \mu_2 A_y) + \\ \frac{k_0 n_0^3}{2} r_{41}^S E_x (\eta_1 A_x + \eta_2 A_y) - i \rho A_y = 0, \\ i \frac{\partial A_y}{\partial z} + \frac{1}{2k_0 n_0} \frac{\partial^2 A_y}{\partial x^2} \pm \frac{k_0 n_0^3}{2} r_{41}^T E_0 (\mu_2 A_x + \mu_3 A_y) + \\ \frac{k_0 n_0^3}{2} r_{41}^S E_x (\eta_2 A_x + \eta_3 A_y) + i \rho A_x = 0, \end{cases} \quad (5.14)$$

where the sign of the third terms of both equations specifies the positive or negative half-cycles of the alternating square-wave electric field.

5.2.2 Results of numerical analysis

BTO crystal

To analyze the evolution of spatial and polarization structures of the light beam, the system of equations (5.14) was integrated numerically using the Douglas scheme [113, 115], and

the space charge field was then averaged over the period of the applied alternating voltage. In calculations, it was assumed that the Gaussian light beam with the wavelength $\lambda = 633$ nm, plane wavefront, intensity distribution $I(x) = I_0 \exp(-x^2/x_0^2)$, and beam waist radius $x_0 = 15$ μm was incident at the input face of the crystal. The crystal parameters $\mu\tau_R = 2 \cdot 10^{-12}$ m^2/V and $\rho = 6.5$ $^\circ/\text{mm}$ were typical for the BTO crystal, and material constants are from [43].

The third term in equation (5.14) determines the linear birefringence induced in the crystal by the electric field, and the fourth term specifies the nonlocal nonlinearity of the diffusion type resulting in the self-bending of the light beam. The values of these terms are determined by the coefficients μ_1, μ_2, μ_3 and η_1, η_2, η_3 , respectively, depending on the orientation angle θ (Figure 5.7).

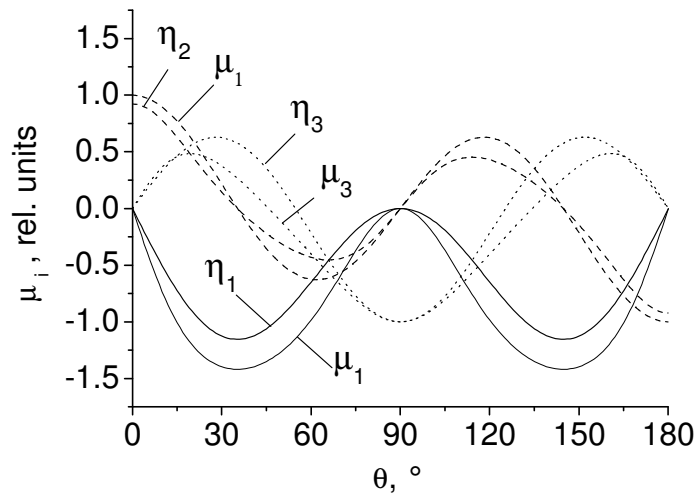


Figure 5.7: Dependences of the coefficients μ_1, μ_2, μ_3 and η_1, η_2, η_3 on the orientation angle θ .

We note that without the piezoeffect ($e_{14} = 0$), when the elasto-optic contribution to the modulation of the optical characteristics of the medium is absent, the electro-optic constants of clamped and unclamped crystals are equal ($r_{14}^S = r_{14}^T$), and the orientation dependences of the corresponding coefficients must coincide: $\eta_i(\theta) = \mu_i(\theta)$. From figure 5.7 it can be seen that at the orientation angle $\theta = 35.26^\circ$ (the x axis coincides with the $[1\bar{1}1]$ crystallographic direction), the coefficients μ_2 and η_2 , specifying cross correlation between x - and y -components of polarization, are equal to zero. The coefficients describing induced birefringence and nonlinear self-action for the x -component of polarization in this

case reach maximal negative values: $\mu_1 = -1.155$ and $\eta_1 = -1.419$, while the appropriate coefficients for the y -component of polarization are positive and their absolute values are much smaller: $\mu_3 = 0.577$ and $\eta_3 = 0.266$. The opposite signs of the nonlinear coefficients η_1 and η_3 cause self-bending of light beams with x - and y -components of polarization toward opposite sides. This is illustrated in figure 5.8 which shows the input (curve 1) and output light intensity distributions (curves 2–6) for the crystal with a thickness of 18 mm in the alternating field with the amplitude $E_0 = 12.5$ kV/cm for the indicated values of the dark irradiance I_d . We note that the light intensity distributions in the crystal are averaged over the period of the applied alternating field. The maximal deviation of about $75 \mu\text{m}$ of the beam center of gravity at the exit from the crystal is observed at a dark irradiance $I_d = 10^{-5}I_0$ and $I_d = 10^{-3}I_0$ (curves 2 and 3) for the input polarization vector making the angle $\alpha = 0$ with the x axis (Figure 4.1).

An increase of the dark irradiance for the same input polarization reduces the self-bending effect and increases the degree of asymmetry of the beam intensity distribution (curves 4 and 5). When the input polarization vector has the angle $\alpha = 90^\circ$ (curve 6), the beam is displaced toward the opposite direction from the center on much shorter distance.

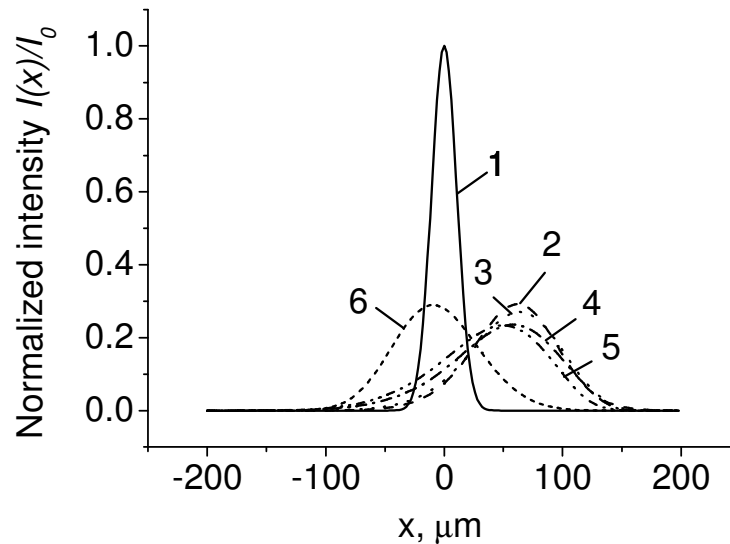


Figure 5.8: Input (curve 1) and output (curves 2–6) beam intensity distributions for the dark irradiance $I_d = 10^{-5}I_0$ (curve 2), $10^{-3}I_0$ (curves 3 and 6), $0.03I_0$ (curve 4), and $0.1I_0$ (curve 5) and the input polarization vector at the angle $\alpha = 0$ (curves 2–5) and 90° (curve 6).

The circular polarization of the input beam has to reduce the self-bending effect. Figure 5.9 illustrates the input (curve 1) and output light intensity distributions (curves 2, 3) for

the right (curve 2) and for the left (curves 3) circular polarizations at $I_d = 10^{-5}I_0$. The behaviors of the beam self-bending has the same tendency as for the input polarization vector at the angles $\alpha = 0$ and 90° (Figure 5.8). The displacement of the output light intensity distributions for the right circular polarization is stronger as for the left one and gives the magnitude of about $50 \mu\text{m}$ that is $25 \mu\text{m}$ less than for the curves 2 and 3 in figure 5.8. The decrease of the beam displacement is observed also in photorefractive cubic crystals having a large magnitude of the optical activity (for example in BSO crystals with $\rho=22^\circ/\text{mm}$ [64]). The rapid rotation of the polarization plane reduces the magnitude of the nonlocal response of the photorefractive medium due to the redistribution of the energy between x and y components of the polarization vector.

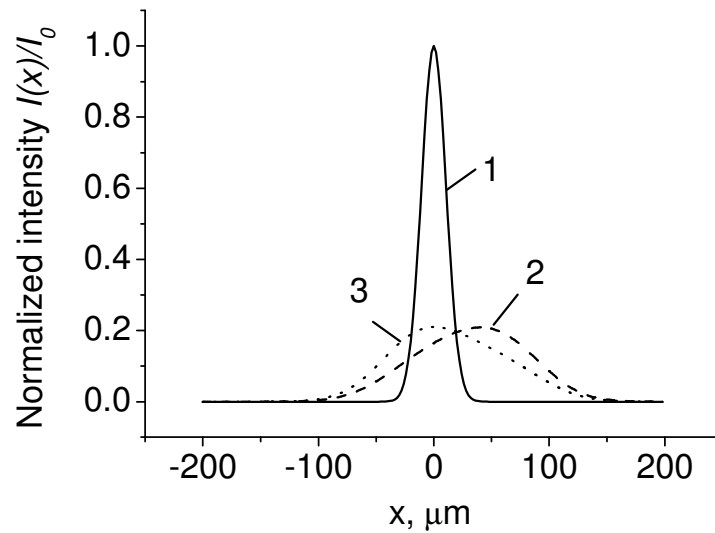


Figure 5.9: Input (curve 1) and output (curves 2, 3) beam intensity distributions for the dark irradiance $I_d = 10^{-5}I_0$ for the right (curve 2) and left (curve 3) circular polarizations.

At the orientation angle $\theta=0$, only the coefficients $\mu_2 = 1$ and $\eta_2 = 0.923$ are nonzero. In this case, the correlation between the x - and y -components of the polarization vector is maximal, whereas the nonlinearity reaches its maximum when this vector is directed at the angle $\alpha = \pm 45^\circ$ to the x axis (see equation 5.14). Characteristically, at $\rho = 0$ in the coordinate system $x'y'$ coinciding with these axes, the nonlinear terms have identical values but opposite signs at $\alpha = 45$ and -45° . Thus, for the input linear polarization plane oriented at angles $\pm 45^\circ$ to the x axis, the light beam will be bent in the crystal in the opposite directions (Figure 4.1). In figure 5.10, the output light intensity distributions for

this case (curves 2–6) correspond to the same crystal sizes and applied field amplitudes as in figure 5.10 with the dark irradiance $I_d = 10^{-3}I_0$.

It can be seen that the magnitude of beam displacement from the center is determined by the orientation of the input polarization vector and changes from +45 to $-45 \mu\text{m}$ when the angle α changes from $+45$ to -45° . We note that for the polarization vector oriented at the angles $\alpha = \pm 22.5^\circ$, the output intensity distributions have an asymmetric form, whereas for the symmetrical output beam, the output intensity distributions have a maximal width when the angle $\alpha = 0^\circ$. These differences are due to the transformation of light beam polarization in the crystal and the corresponding changes in the effective nonlinear coefficient which are responsible for the self-action effect. Figure 5.11 shows the evolution of the cross sectional intensity distributions for the x - and y -components of the light field accompanying the propagation of beams with different input linear polarization states through the crystal with the orientation angle $\theta = 0$.

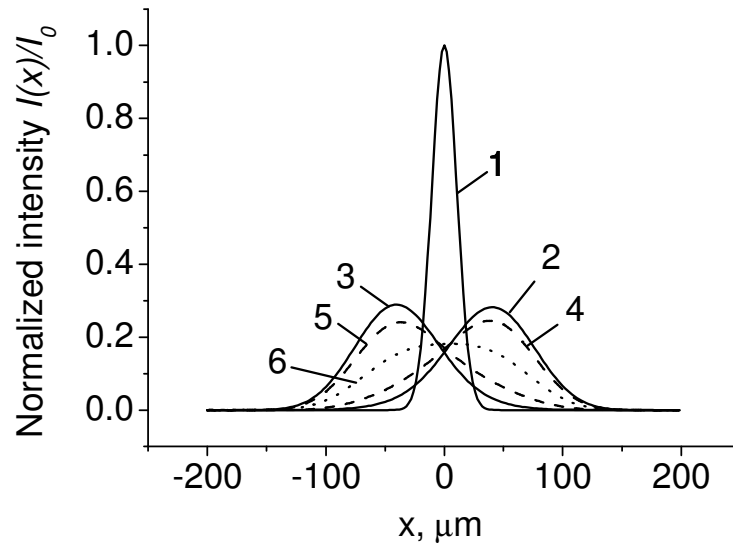


Figure 5.10: Input (curve 1) and output (curves 2–6) beam intensity distributions for the input polarization vector at angles $\alpha = -45$ (2), $+45$ (3), -22.5 (4), $+22.5$ (5) and 0° (6) and the dark irradiance $I_d = 10^{-3}I_0$.

At the input polarization angle $\alpha = -45^\circ$ (Figures 5.11a and b), the amplitudes of both x - and y -components of the light field and the nonlinear terms corresponding to them are identical: $\partial A_x/\partial z, \partial A_y/\partial z \sim i\eta_2(\partial I(x)/\partial x)(\sqrt{I(x)}/\sqrt{2})/[I_d + I(x)]$ at $z = 0$ (see equation 5.14). Therefore, both components deviate in the same direction and the behavior of the beam as a whole differs only slightly from that predicted by the scalar model [62]. Another

pattern of the evolution of light field polarization components is observed for the input polarization angle $\alpha = 0$ (Figures 5.11c and d).

For the single x -component excited in the crystal at $z = 0$, the nonlinear term vanishes. The occurrence of the y -component at $z > 0$ is caused by two reasons. First, by the rotation of the polarization vector due to the optical activity of the crystal $\partial A_y / \partial z \sim -\rho A_x(x, z)$ (see equation 5.14). Second, the nonlinear cross-polarization term is equal to $i\eta_2(\partial I(x)/\partial x)\sqrt{I(x)}/[I_d + I(x)]$ and reaches the maximal values at the slopes of the intensity distribution function. As a result of the joint action of these effects, the intensity distribution of the arising y -components is shifted to the left from the crystal center at $x = 0$ (Figure 5.11d). The same sign of the nonlinear term, as at $\alpha = -45^\circ$, leads to the deviation to the right part of both polarization components of the beam. Exactly the superposition of both y - and x - components of polarization arising on the left and deviating to the right from the crystal center produces a broadening of the total light beam intensity distributions symmetrical around $x = 0$.

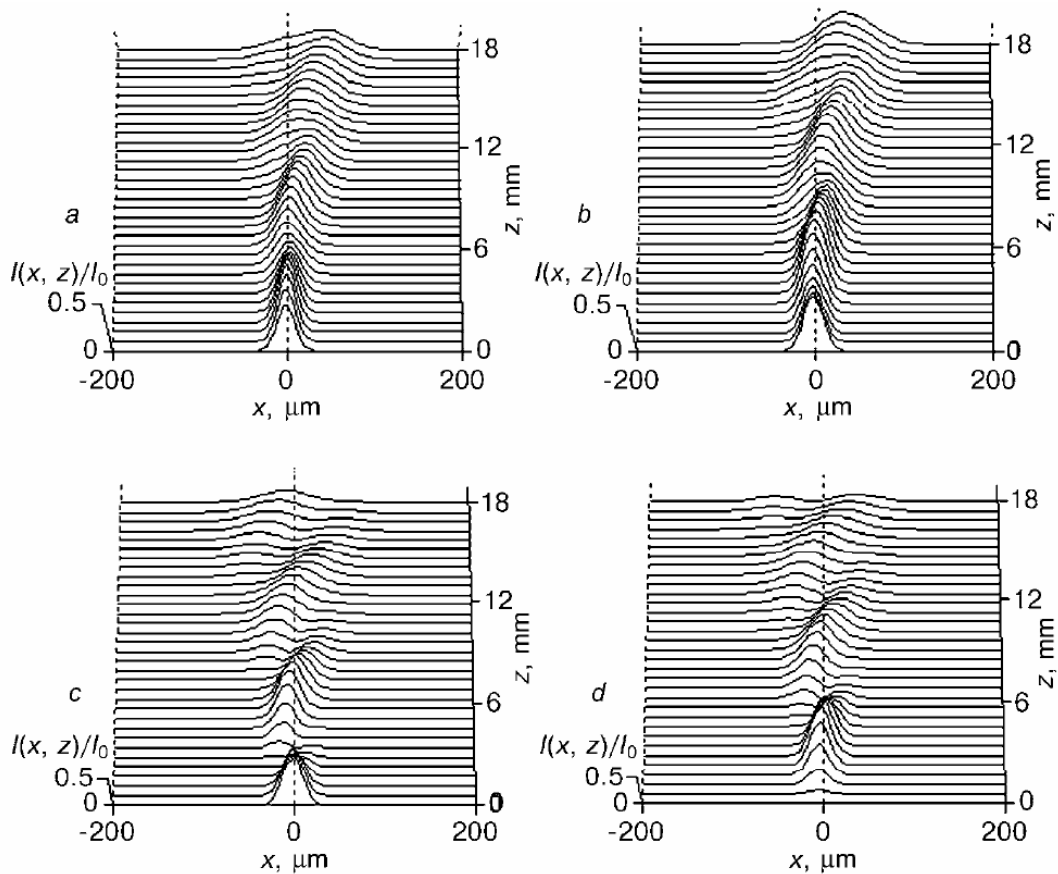


Figure 5.11: Evolution of the x - (a and c) and y -components (b and d) of the light beam for the input polarization vector $\alpha = -45^\circ$ (a and b) and 0° (c and d).

The polarization dynamics of the propagated beam for both cases can be easily and more understandable presented on the Poincare sphere (Figure 5.12). The input linear polarization in figure 5.12a during the beam propagation is transformed to the elliptical polarization or returns again to the linear one and once reaches a circular nature. It is easy to see that the dynamics of the polarization change is more concentrated at the region $S_1 > 0$, $S_2 < 0$ and tends to the linear state more and more for the angle α varying between 0 and -45° to the axis x . The change of the polarization dynamics in the region $S_1 > 0$, $S_2 < 0$ provides the same sign for the amplitudes of both x - and y -components of the light field (as we have shown before) that leads to the deviation of both components toward one side. For $\alpha = 0^\circ$ (Figure 5.12b) the state of the polarization changes first from linear to elliptical one and back to the linear at the region $S_2 > 0$. In the region $S_2 < 0$ the polarization repeats the same behaviour as in the region $S_2 > 0$. This process repeats during the beam propagation again and again. The transition of the polarization state from the region $S_2 > 0$ to the $S_2 < 0$ changes the sign of polarization components that influences on the direction of the self-bending. Thus x - and y -components of the light field deviate in the region $S_2 > 0$ to the left and for $S_2 < 0$ to the right. That produces a broadening of the total light beam intensity distributions symmetrically around $x = 0$ as we have shown before in figure 5.11c and d.

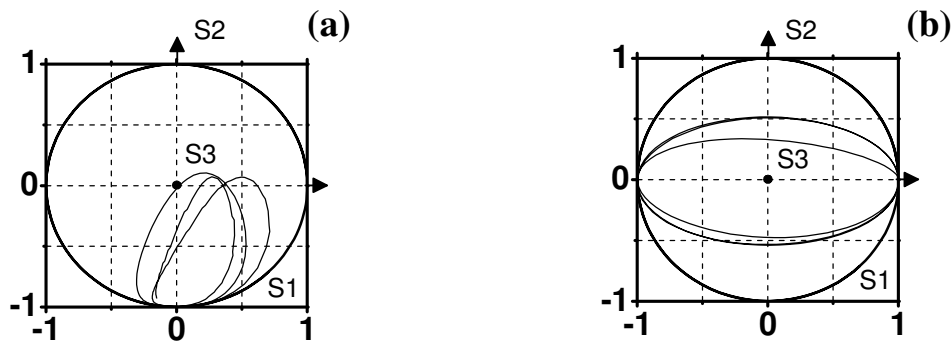


Figure 5.12: Polarization dynamics of the beam at $E_0 = 12.5$ kV/cm and $I_d = 10^{-3}I_0$ for the input polarization -45° (a) and 0° (b).

The maximal deviation of the propagated beam occurs at the orientation angle $\theta = 35.26^\circ$ and for the input polarization vector at the angle $\alpha = 0$. The self-bending depends weakly on the intensity of the dark irradiance but can be strongly enhanced by the increase of the magnitude of the applied alternating electric field (Figure 5.13). The dependence of the output beam displacement on the applied voltage has an exponential form and at $E_0 =$

14 kV/cm for $I_d = 10^{-5}I_0$ the displacement magnitude reaches a value of about 5 of the input waist beam radius.

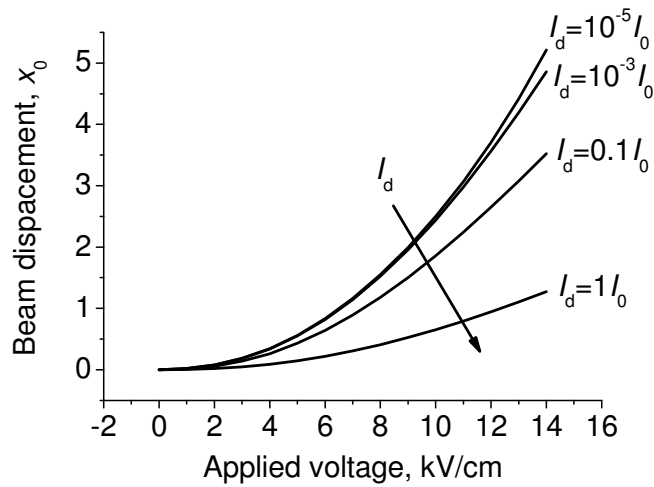


Figure 5.13: Relative displacement of the output beam in dependence on the value of the applied alternating square-wave electric field for $I_d = 10^{-5}I_0$, $10^{-3}I_0$, $0.1I_0$ and I_0 .

The increase of the dark irradiance intensity reduces the self-bending magnitude and influences on the output beam broadening effect (Figure 5.8). As the output intensity distribution has no more Gaussian shape the waist radius could be used only for the quantitative estimation of the characteristics of the output beam. The dependence of the output beam waist radius on the dark irradiance intensity at $E_0 = 14$ kV/cm is illustrated in figure 5.14.

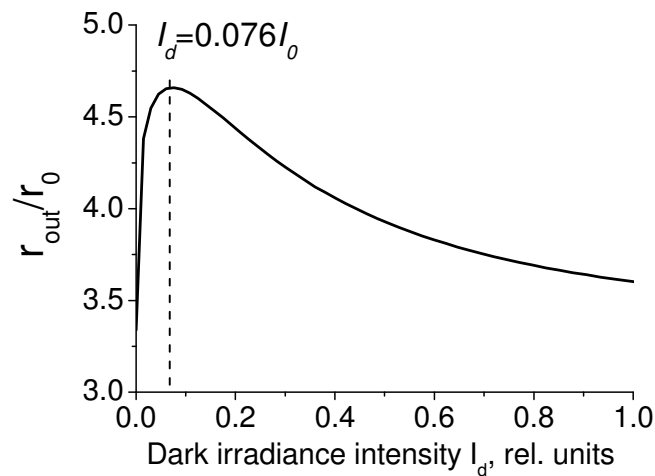


Figure 5.14: Relative output beam waist radius in dependence on the dark irradiance intensity at $E_0 = 14$ kV/cm.

The curve has a maximum at $I_d = 0.076I_0$ where the relative output beam waist radius is about $4.3r_0$. The change of the I_d strongly influences on the magnitude of the space charge field (Equation 5.13) and for slighting small values input beam intensity plays no role in the nonlocal photorefractive response of the crystal. On the other hand the growth of the dark irradiance intensity up to I_{max} reduces the induced space-charge field. Thus the self-bending of the laser beam under an applied alternating electric field occurs without dark irradiance that is not possible for the applied dc electric field. The further increase of the bias field leads to the distortion of the output beam intensity distribution (Figure 5.15). At $E_0 = 15$ kV/cm the displacement becomes so strong that the beam divides into several beams having different propagation angles. This fact is connected with the energy redistribution between the angular components of the angular spectrum of the beam. The self-bending effect occurs while all components of the spectrum have different self-bending magnitudes [56] and the strong bent of the propagating trajectory of the whole beam leads to the extension of the angular spectrum.

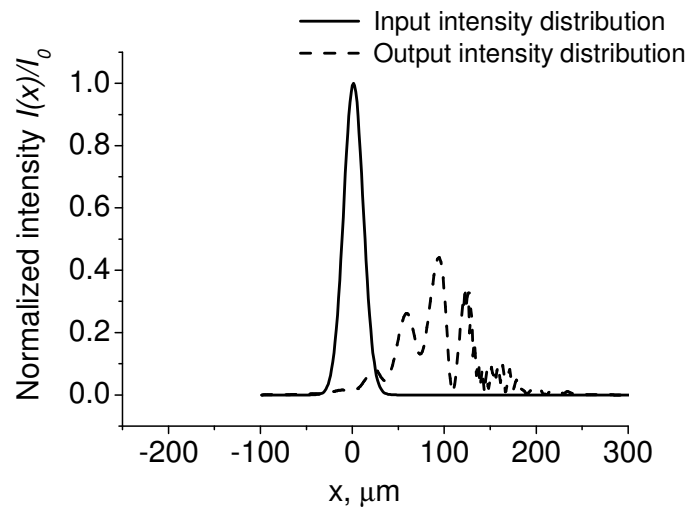


Figure 5.15: Displacement of the output beam at $E_0 = 15$ kV/cm. and $0.1I_0$.

From equation (5.13) it is easy to see that the magnitude of the space-charge field depends also on the spatial derivative of the intensity distribution and the decrease of the input beam waist radius has to enhance significantly the nonlocal response of the photorefractive medium that leads to the stronger bending of the propagating beam trajectory. The figure 5.16 illustrates the dependence of the output beam displacement on the magnitude of the input beam waist radius. At the input beam waist radius $10 \mu\text{m}$ the

displacement reaches the value of about $10x_0$. The increase of the input beam aperture decreases the self-bending magnitude and at $x_0 = 30 \mu\text{m}$ the displacement reaches the value of about x_0 .

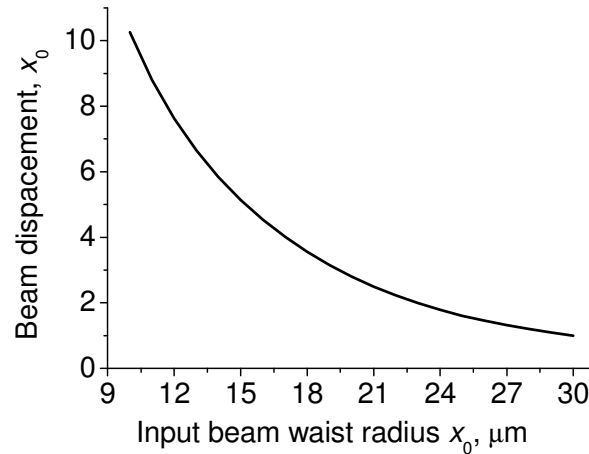


Figure 5.16: Relative displacement of the output beam in dependence on the input beam radius $I_d = 10^{-5}I_0$ and $E_0 = 14 \text{ kV/cm}$.

BSO crystal

The other types of cubic sillenite crystals such as the BSO and BGO have a large magnitude of the optical activity up to $22^\circ/\text{mm}$ [64]. The comparative analyses of the beam self-bending effect in BTO and BSO crystals at $\theta = 35.26^\circ$ is presented in figure 5.17.

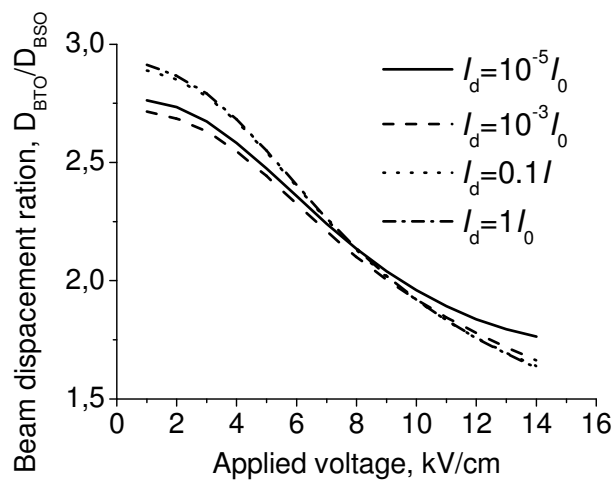


Figure 5.17: Ratio between displacements in both BTO and BSO crystals in dependence on the applied electric field for $I_d = 10^{-5}I_0$, $10^{-3}I_0$, $0.1I_0$ and $1I_0$.

The dependences show the ratio between displacements in both crystals $D_{\text{BTO}}/D_{\text{BSO}}$ versus the applied electric field for different values of the dark irradiance intensity. The maximal ratio $D_{\text{BTO}}/D_{\text{BSO}}=3$ for $I_d = 1I_0$ is observed at the smallest values of the bias electric field 2 kV/cm. With the increase of the applied voltage up to 14 kV/cm this ratio tends to 1.5. The further increase of the bias field leads to the instability in the beam intensity distribution which occurs because of the strong self-bending effect that was illustrated in figure 5.15. However the increase of the dark irradiance intensity influences weakly on this ratio. At the magnitude of the applied electric field in the range of 8 kV/cm the ratio $D_{\text{BTO}}/D_{\text{BSO}}$ has the same factor for all values of I_d . At $E_0=1$ kV/cm and $E_0=14$ kV/cm the difference between beam displacements ratios for different values of I_d is not more than 0.2.

The polarization dynamics of the propagated beam for different values of the applied electric field in BTO and BSO crystals are illustrated in figure 5.18. The difference between polarization dynamics can be already observed at $E_0 = 4$ kV/cm. For the BTO crystal the polarization state rotates completely in the region $S_1>0$ and with increase of the bias electric field the polarization tends to the linear state. It means that the influence of the optical activity on the propagated beam decreases that allows to neglect the vector nature of the light field and the rotation of the polarization plane. But thanks to the high optical activity the dynamics of the polarization change in the BSO crystal is significantly stronger than in the BTO crystal. For the applied voltage 4 kV/cm the polarization in the BSO differs insignificantly from the linear one. Increasing of the bias up to 8 kV/cm makes the beam polarization in some points close to the circular state. The further growth of the applied voltage shifts the curve of the polarization state in the region $S_1>0$ where it changes from linear to elliptical one. The strong distortion of the polarization state in the BSO crystal leads to the decrease of the influence of the nonlocal response on the beam self-bending effect. The effective self-bending at $\theta = 35.26^\circ$ can be reached if there is no significant rotation of the polarization plane as it is shown in the BTO crystal at $E_0 = 12$ kV/cm. But due to the high magnitude of the optical activity of the BSO crystal the polarization state changes from linear to the elliptical one along the beam propagation distance and this change decreases the displacement. A similar behavior is observed in the BTO crystal (Figure 5.9) if the laser beam has the circular polarization.

Thereby the scalar theoretical model describing the laser beams self-bending developed by Borodin *et al.* [62] is valid only for cubic photorefractive crystals having insignificant

optical activity and if the laser beam is linearly polarized along the crystallographic axis $[1\bar{1}1]$ and the applied electric field has a rather high magnitude.

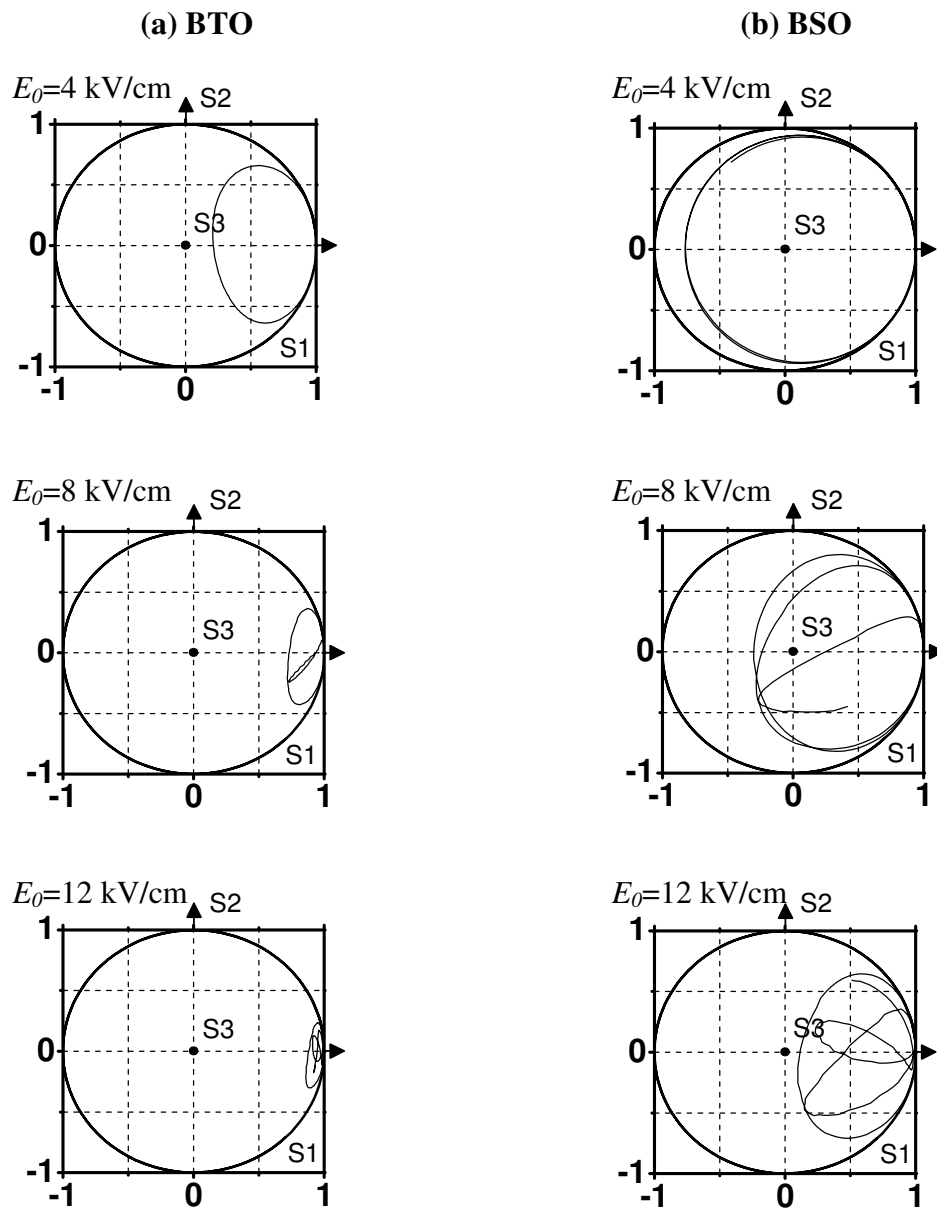


Figure 5.18: Polarization dynamics of the beam at different values of the applied electric field for $I_d = 10^{-5}I_0$ and for the input polarization 0° in BTO (a) and BSO (b) crystals.

5.2.3 Experimental results

A BTO crystal with a specific rotation of $6.5^\circ \text{ mm}^{-1}$ at the He-Ne laser wavelength was used in the experiment. The experimental setup is shown in figure 5.19. An external meander-shaped electric field with an amplitude of 10 kV/cm was applied to the crystal

side faces along the x axis making an angle θ with the $[1\bar{1}0]$ crystallographic direction. For the given crystal orientation $\theta = 0$, the crystal thickness is 6.93 mm. A light beam of the He-Ne laser ($\lambda = 632.8$ nm) with waist $x_0 = 15$ μm was focused by a cylindrical lens (CL) in the x direction to the input face of the crystal and propagated along the z axis coinciding with the $[110]$ crystallographic direction. The light beam intensity distribution on the output face of the crystal was observed by means of the objective and the CCD camera. The input polarization was controlled by the first polarizer (P1) placed behind the laser beam source.

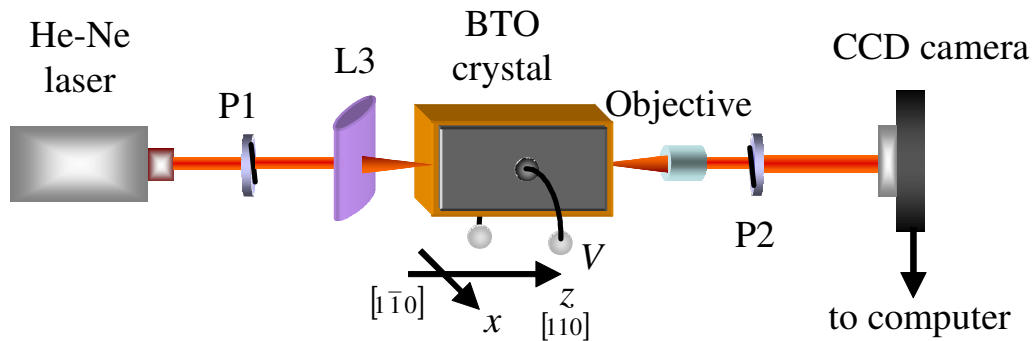


Figure 5.19: Schematic diagram of the experimental setup for observing self-bending of the laser beam in the photorefractive crystal.

The experiment was performed in two steps. At first, the output intensity distribution was measured, and then the polarization characteristics of the light beam were measured using the second polarizer (P2). The numerical simulation and experimental results for the parameters of this crystal are shown in figures 5.20a and 5.20b, from which it follows that, for the input Gaussian distribution $I_0(x)$ (Figure 5.20, curve 1), the output beam with distribution $I(x)$ is deflected to opposite directions (curves 2 and 3) at light polarizations of 45° and -45° . The experimental intensity distribution for both cases of the input beam polarization is shown in figure 5.20b (curve 2 and 3).

The amplitude of the applied external field for the numerical simulation and experimental study was selected so that the deflection of the trajectory of the light beam from the propagation axis in the crystal with a thickness $d = 6.93$ mm was noticeable; $E_0 = 10$ kV/cm. According to the results of the numerical analysis, the shapes of the output light distributions with a halfwidth of 30 μm are identical for beams with input polarizations of 45° and -45° , but their deflection directions from the center are different. The experimentally measured light beam halfwidth was larger, about 50 μm . The

deflection of beams of both polarizations was $15\ \mu\text{m}$, which is equal to the calculated one.

To analyze the polarization structure of the light beam the input polarization was taken as 45° . The light beam components were separated by polarizer P2. The results of numerical integration and measurement of the intensity distribution for x and y components are shown in figures 5.20c and 5.20d, respectively. For $\pm 45^\circ$ polarizations, the amplitudes of x and y light field components excited in the crystal are equal at $z = 0$ and the corresponding nonlinear perturbations of both components in the crystal have the same magnitude. Therefore, both components during propagation deflect to the same side (to the right for 45° and to the left for -45°), and the behavior of the beam as a whole differs slightly from that predicted by the scalar model [62].

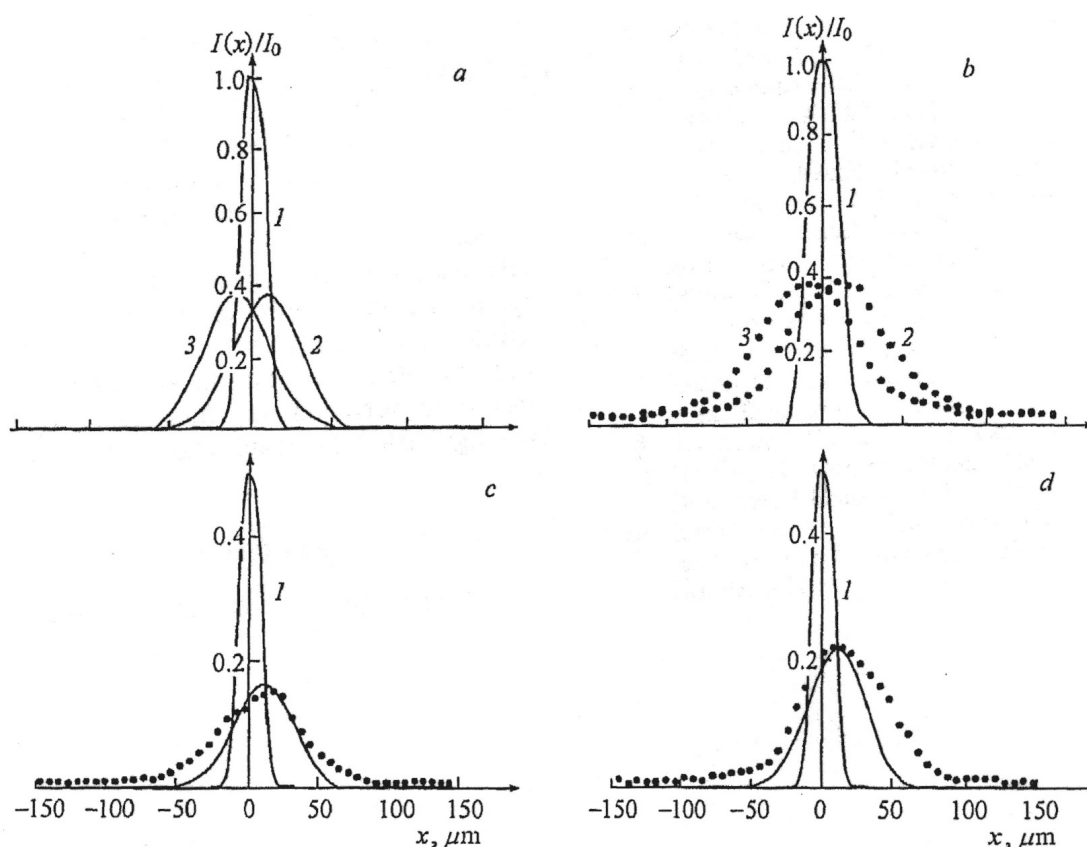


Figure 5.20: Normalized output distributions of the beam intensity $I(x)/I_0(x)$, obtained experimentally (dots) and by numerical solution (solid curves) for the input distribution (1). Beam intensity distribution at input polarizations of 45° (2) and -45° (3). Output distribution of the light beam intensity for x (c) and y (d) components of the light field vector.

5.2.4 Conclusion

Thus, formulas have been derived that in the paraxial approximation describe the propagation of a light beam with a one-dimensional input intensity distribution through cubic optically active photorefractive crystals of point group 23 with applied external alternating electric field. The employed model takes into account the vector nature of the light field and the additional elasto-optic contribution connected with elastic strains accompanying light-induced internal spatially inhomogeneous electric fields in piezocrystals. Numerical analysis of the propagation of a Gaussian beam in bismuth titanium oxide and bismuth silicate oxide crystals demonstrated the feasibility of control of the self-bending direction and the form of the beam on the output face of the crystal by changing the orientation of the sample relatively to the crystal axes and variation of the input polarization state of light. The high optical activity of the bismuth silicate oxide crystal requires the accounting of the vector nature of the light field that is not possible in the scalar theoretical model developed by Borodin *et al.* [62].

The experimental study demonstrated the adequacy of the theoretical model and chosen numerical solution, which allows their application for solving other problems of nonlinear photorefractive physics, in particular, quasi-soliton propagation and the behavior of a randomly polarized light beam for both high and low intensities which were studied in the fourth chapter.

Chapter 6

Conclusion

New effects of the laser beam self-action in photorefractive crystals were observed and studied theoretically in single-axis and cubic electro-optic crystals. The work contains results of experimental and theoretical investigations of these effects which give us an opportunity to use obtained results for further researches of the laser beam propagation in photorefractive media. Developed theoretical models take into account the additional photoelastic contribution to the modulation of optical properties by the space-charge field in the photorefractive medium that enhances the accuracy of the numerical simulation that results in the increase of the efficiency of the numerical determination of external parameters to observe the quasi-soliton regime up to 60% in some cases. This model separates the influence of effects of the induced birefringence and the nonlinear electro-optic response of the medium. Taking into consideration the optical activity for the investigation of laser beam self-bending effects in cubic electro-optic crystals demonstrated the ability to control the self-bending magnitude and the form of the beam on the output face of the crystal by changing the orientation of the sample relatively to the crystal axes and variation of the input polarization state of light. The experimental study demonstrating the laser beam self-bending in the bismuth titanate oxide crystal under the applied electric field shows the adequacy of the theoretical model for the investigation of the self-action effects in cubic photorefractive crystals as beam self-focusing and self-bending.

Self-action of laser beams in SBN. The experimental investigation of the influence of the external applied voltage, parameters of the input beam and dark irradiance intensity let us to find the new effect of the *optimal focusing* of the laser beam in single-axis strontium barium niobate crystals. We have shown that the output beam diameter especially along the optical axis does not depend on the diameter of the input beam if it lies between 18 μm and 40 μm . The obtained results were proved theoretically and the numerical calculation

confirmed the tendency of the experimental results only qualitatively and predicts larger displacements than the experimental ones.

Beam self-focusing in sillenite crystals. A new theoretical model for the laser-beam self-action in sillenite photorefractive crystals of point group 23 taking into account the additional contribution of the photoelastic effect to the optical properties of the medium was developed and investigated. The comparative analyse of the laser beam self-focusing for the simple vector model by Shepelevich *et al.* [29] and for our vector model was carried out for bismuth titanate and bismuth silicate oxide crystals. The magnitude of the local photorefractive response and the induced birefringence were studied for different orientations of the applied direct electric field and it was shown that the maximal nonlinearity of the optical properties of the medium is reached at the orientation of the applied voltage along the crystallographic direction $[1 \bar{1} 1]$ and with linearly polarized input beams along this axis. The taking into account of the additional photoelastic effect for this orientation reduces the value of the bias electric field to observe the quasi-soliton regime by a factor of 1.8 in some cases. The large difference between results of both theoretical models gives us the right to confirm that the developed theoretical model is more adequate in comparison with existing ones to investigate the self-action effect in cubic photorefractive crystals especially for the orientation of the applied voltage along the crystallographic direction $[1 \bar{1} 1]$.

For crystals with a large magnitude of the optical activity (for example, BSO) the numerical results showed that considerable differences in the behavior of the polarization state of the propagated beam for both theoretical models occur even at a small magnitude of the bias electric field amplitude that influences on the conditions of the observing of the quasi-soliton regime. We have also shown that the increase of the applied voltage enhances these differences and taking into consideration of the additional photoelastic contribution lets to observe theoretically the quasi-soliton laser beam propagation for a small waist radius of the input beam which is impossible for the theoretical model developed by Shepelevich *et al.* This fact is connected with an ability to separate the effects of the induced birefringence and nonlinear response of the medium in our theoretical model that make it possible to take into consideration the change of the polarization independently for both effects.

We have also considered the cut $(11\bar{2})$ where the maximal nonlinear photorefractive response is reached for the orientation of the applied electric field along $[001]$ direction and has the same magnitude as for the direction of the bias field along $[\bar{1}\bar{1}1]$ in (110) -cut crystals. The advantage of the $(11\bar{2})$ -cut is an ability to investigate the interaction of counter propagating light.

Beam self-bending effect. The bent of the trajectory of the propagated beam was studied in single-axis photorefractive BaTiO_3 crystal and in cubic electro-optic media. We have developed a theoretical model to investigate the beam selfbending effect for a speckled extraordinary light beam in photorefractive barium titanate at an arbitrary orientation of the optical axis c . The model takes into account the additional elasto-optic contribution to changes of the dielectric permittivity. It was demonstrated that the additional photoelastic effect has a substantial influence on beam self-bending. Due to the possibility to take into consideration the arbitrary orientation of the optical axis we have shown that BaTiO_3 crystals exhibit the property of positive or negative gradient lens depending on whether the speckled laser beam propagates along the optical axis c or in the opposite direction.

The self-bending effect in cubic photorefractive sillenite crystals occurs only under an applied external alternating square-wave electric field that makes it possible to investigate the influence of the optical activity and the input beam polarization on the bent of propagated beam trajectory. The maximal displacement of the light is observed for the orientation of the applied voltage along the crystallographic axis $[\bar{1}\bar{1}1]$ for the linearly polarized input beam along this direction. The circularly polarized beam bends only for the right rotation but with the lower displacement. At the orientation of the bias electric field along $[\bar{1}\bar{1}0]$ it becomes possible to control the beam self-bending direction by changing of the input polarization. In this case for the polarization vector of the linearly polarized beam oriented at angles $\pm 45^\circ$ to the x axis, the light beam will be bent in the crystal in the opposite directions.

It was also shown that the intensity of the dark irradiance, the value of the applied electric field and the input beam waist radius strong influence on the self-bending magnitude. The change of dark irradiance intensity leads to the slight influence on the essential beam diffraction. The rather high amplitude of the applied electric field strong influences on the distortion the output beam intensity due to the redistribution of the

energy between the angular components of the angular spectrum. The beam displacement increases also with the reducing of the input beam waist radius while it enhances the nonlocal response of the photorefractive medium. However the large optical activity of the BSO crystal decreases the self-bending effect and only with the increasing of the applied voltage tends to the same magnitude as in BTO. Investigating the polarization dynamics in both BTO and BSO crystals we have shown that the scalar model of the laser beam self-bending developed by Borodin *et al.* [62] is valid only for the BTO crystal under a high applied electric alternating field along the crystallographic axis $[1\bar{1}1]$ if the propagated laser beam has the linear polarization along this direction.

The experimental results demonstrated the adequacy of the theoretical model and confirmed an ability to observe the bending of the laser beam in the opposite directions for the input linear polarization plane oriented at angles $\pm 45^\circ$ to the x axis at the orientation of the bias electric field in the BTO crystal along the $[1\bar{1}0]$ axis. Thus the new theoretical model taking into account the additional photoelastic effect allows to solve the considered problems of nonlinear photorefractive physics as soliton propagation and the behavior of a randomly polarized light beam for both high and low intensities.

References

1. M. Segev, B. Crosignani, A. Yariv, B. Fisher, *Spatial solitons in photorefractive media*, Phys. Rev. Lett. **68** (1992), 923.
2. B. Crosignani, M. Segev, D. Engin, P. Di. Porto, A. Yariv, G. Salamo, *Self-trapping of optical beams in photorefractive media*, J. Opt. Soc. Am. B. **10** (1993), 446.
3. D. N. Christodoulides, M.I. Carvalho, *Compression, self-bending and collapse of Gaussian beam in photorefractive crystals*, Opt. Lett. **19** (1994), 1714.
4. M. D. Castillo, A. Aguilar, J. J. Mondragon, S. Stepanov, V. Vysloukh, *Spatial solitons in photorefractive $Bi_{12}TiO_{20}$ with drift mechanism of nonlinearity*, App. Phys. Lett. **64** (1994), 408.
5. G. C. Valley, M. Segev, B. Crosignani, A. Yariv, M. M. Fejer, M. C. Bashaw, *Dark and bright photovoltaic spatial solitons*, Phys. Rev. A **50** (1994), R4457.
6. M. Segev, G. C. Valley, B. Crosignany, P. Di. Porto, A. Yariv, *Steady-state spatial screening solitons in photorefractive material with external applied field*, Phys. Rev. Lett. **73** (1994), 3211.
7. D. N. Christodoulides, M. I. Carvalho, *Bright, dark and grey spatial soliton states in photorefractive media*, J. Opt. Soc. Am. B **12** (1995), 1628.
8. N. Fressengeas, Maufof, and G. Kugel, *Temporal behavior of bidimensional photorefractive bright spatial solitons*, Phys. Rev. E **54** (1996), 6866.
9. A. Zozulya and D. Z. Anderson, *Propagation of an optical beam in a photorefractive medium in the presence of a photogalvanic nonlinearity or an externally applied electric field*, Phys. Rev. A **51** (1995), 1520.
10. G. Lesaux, G. Roosen, and A. Brun, *Observation and analysis of the fast photorefractive process in BSO*, Opt. Comm. **56** (1986), 374.

11. B. Crosignani, P. Di. Porto, A. Degasperis, M. Segev, S. Trillo, *Three dimensional optical beam propagation and solitons in photorefractive crystals*, J. Opt. Soc. Am. B. **14** (1997), 3078.
12. M. Shih, M. Segev, G. Valley, G. Salamo, B. Crosignani, P. DiPorto, *Observation of 2-dimensional steady-state photorefractive screening solitons*, Electron. Lett. **31** (1995), 826.
13. M. Shih, P. Leach, M. Segev, M. Garrett, G. Salamo, G. Valley, *Two-dimensional steady-state photorefractive screening solitons*, Opt. Lett. **21** (1996), 324.
14. G. C. Duree Jr., J. L. Shiltz, G. J. Salamo, M. Segev, A. Yariv, B. Crosignani, P. Di Porto, E. J. Sharp, and R. R. Neurgaonkar, *Observation of self-trapping of an optical beam due to the photorefractive effect*, Phys. Rev. Lett. **71** (1993), 533.
15. S. R. Singh, D. N. Christodoulides, *Evolution of spatial optical solitons in biased photorefractive media under steady-state conditions*, Opt. Comm. **118** (1995), 569.
16. T. H. Coskun, D. N. Christodoulides, M. Mitchell, Zh. Chen, and M. Segev, *Dynamics of incoherent bright and dark self-trapped beams and their coherence properties in photorefractive crystals*, Opt. Lett. **23** (1998), 418.
17. V. Aleshkevich, Y. Kartashov, V. Vysloukh, *Self-bending of the coupled spatial soliton pairs in a photorefractive medium with drift and diffusion nonlinearity*, Phys. Rev. E **63** (2001), 0166030.
18. J. Maufoy, N. Fressengeas, D. Wolfersberger, and G. Kugel, *Simulation of the temporal behavior of soliton propagation in photorefractive media*, Phys. Rev. E **59** (1999), 6116.
19. M. Wesner, C. Herden, R. Pankrath, D. Kip, and P. Moretti, *Temporal development of photorefractive solitons up to telecommunication wavelengths in strontium-barium niobate waveguides*, Phys. Rev. E **64** (2001), 036613.
20. M. Segev, B. Crosignani, P. Di Porto, A. Yariv, G. Duree, G. Salamo, and E. Sharp, *Stability of photorefractive spatial solitons*, Opt. Lett. **19** (1994), 1296.
21. M. Facao and D. F. Parker, *Stability of screening solitons in photorefractive media*, Phys. Phys. Rev. E **68** (2003), 016610.
22. J. Liu, *Existence and property of spatial solitons in a photorefractive dissipative system*, J. Opt. Soc. Am. B **20** (2003), 1732.
23. M. Morin, G. Duree, G. Salamo, and M. Segev, *Waveguides formed by quasi-steady-state photorefractive spatial solitons*, Opt. Lett. **20** (1995), 2066.

24. D. Kip, M. Wesner, V. Shandarov, and P. Moretti, *Observation of bright spatial photorefractive solitons in a planar strontium barium niobate waveguide*, Opt. Lett. **23** (1998), 921.
25. S. R. Singh and D. N. Christodoulides, *Effects of optical activity on photorefractive spatial solitons in a biased $Bi_{12}TiO_{20}$ crystal*, J. Opt. Soc. Am. B **13** (1996), 719.
26. N. Fressengeas, D. Wolfersberger, J. Maufroy, and G. Kugel, *Experimental study of the self-focusing process temporal behavior in photorefractive $Bi_{12}TiO_{20}$* , J. Appl. Phys. **85** (1999), 2062.
27. E. Fazio, V. Babin, M. Bertolotti, and V. Vlad, *Solitonlike propagation in photorefractive crystals with large optical activity and absorption*, Phys. Rev. E **66** (2002), 016605.
28. E. Fazio, W. Ramadan, A. Belardini, A. Bosco and M. Bertolotti, *(2+1)-dimensional soliton formation in photorefractive $Bi_{12}SiO_{20}$ crystals*, Phys. Rev. E **67** (2003), 026611.
29. V. V. Shepelevich, R. Kowarschik, A. Kiessling, V. Matusevich, A. Goluba, *Effect of optical activity on the self-focusing of light beams in cubic photorefractive crystals*, Quantum Electron. **33** (2003), 446.
30. E. Fazio, W. Ramadan, M. Bertolotti, A. Petris, and V. I. Vlad, *Complete characterization of (2+1)D soliton formation in photorefractive crystals with strong optical activity*, J. Opt. A: Pure Appl. Opt. **5** (2003), 119.
31. V. V. Shepelevich, A. A. Golub, R. Kowarschik., A. Kiessling, V. Matusevich, *Interaction of screening solitons in cubic optically active photorefractive crystals*, Quantum Electron. **35** (2005), 351.
32. E. Weidner, A. Kiessling, and R. Kowarschik, *Stable self-focused beams in a photorefractive $Bi_{12}TiO_{20}$ crystal*, Opt. Express **12** (2004), 4993.
33. G. Duree, M. Morin, G. Salamo, M. Segev, B. Crosignani, P. DiPorto, E. Sharp, A. Yariv, *Dark Photorefractive Spatial Solitons and Photorefractive Vortex Solitons*, Phys. Rev. Lett. **74** (1995), 1978.
34. A. A. Izvanov, A. E. Mandel, N. D. Khat'kov, S. M. Shandarov, *The influence of piezoeffect on hologram recording and restoration processes in photorefractive crystals*, Optoelectronics, Instrumentation and Data Processing **2** (1986), 80.
35. S. I. Stepanov., S. M. Shandarov, N. D. Khat'kov, *Photoelastic contribution to photorefractive effect in cubic crystals*, Sov. Phys. Solid State **29** (1987), 1754.

36. P. Günter and M. Zgonik, *Clamped-unclamped electro-optic coefficient dilemma in photorefractive phenomena*, Opt. Lett. **16** (1991), 1826.
37. S. Shandarov, *Influence of piezoelectric effect on photorefractive gratings in electro-optic crystals*, Appl. Phys. A. **55** (1992), 91.
38. G. Pauliat, P. Mathey, and G. Roosen, *Influence of piezoelectricity on the photorefractive effect*, J. Opt. Soc. Am. B **8** (1991), 1942.
39. V. V. Shepelevich; S. M. Shandarov; A. E. Mandel, *Light diffraction by holographic gratings in optically active photorefractive piezocrystals*, Ferroelectrics **110** (1990), 235.
40. V. I. Volkov, Yu. F. Kargin, N. V. Kukhtarev, A. V. Privalko, T. I. Semenets, S. M. Shandarov, V. V. Shepelevich, *Influence of the photoelasticity on self-diffraction of light in electro-optic crystals*, Soviet Journal of Quantum Electronics **21** (1991), 1122.
41. H. C. Ellin, L. Solymar, *Light scattering in bismuth silicate: matching of experimental results*, Opt. Comm. **130** (1996), 85.
42. S. M. Shandarov, A. Emelyanov, O. V. Kobozev, and A. Reshet'ko, *Photorefractive properties of doped sillenite crystals*, Proc. SPIE **2801** (1996), 221.
43. O. V. Kobozev, S.M. Shandarov, R. V. Litvinov, Yu. F. Kargin and V. V. Volkov, *Photorefractive effect in sillenite crystals with shallow traps in a sign-alternating electric field*, Physics of the Solid State **40** (1998), 2037.
44. E. Shamonina, K. H. Ringhofer, B. I. Sturman, V. P. Kamenov, G. Cedilnik, M. Esselbach, A. Kiessling, R. Kowarschik, A. A. Kamshilin, V. V. Prokofiev, and T. Jaaskelainen, *Giant momentary readout produced by switching electric fields during two-wave mixing in sillenites*, Opt. Lett. **23** (1998), 1435.
45. B. I. Sturman, E. V. Podivilov, K. H. Ringhofer, E. Shamonina, V. P. Kamenov, E. Nippolainen, V. V. Prokofiev, and A. A. Kamshilin, *Theory of photorefractive vectorial coupling in cubic crystals*, Phys. Rev. E **60** (1999), 3332.
46. K. Shcherbin, S. Odoulov, R. Litvinov, E. Shandarov, and S. Shandarov, *Contribution of nonlinear absorption and elasto-optic effect in photorefractive grating recording in GaAs*, J. Opt. Soc. Am. B **13** (1996), 2268.
47. M. Zgonik, K. Nakagawa, and P. Günter, *Electro-optic and dielectric properties of photorefractive BaTiO₃ and KNbO₃*, J. Opt. Soc. Am. B **12** (1995), 1416.

48. G. Montemezzani, A. A. Zozulya, L. Czaia, and D. Z. Anderson, *Origin of the lobe structure in photorefractive beam fanning*, Phys. Rev. A **52** (1995), 1791.
49. P. Mathey, *Photorefractive-gain dependence on piezoelectric and photoelastic effects in barium titanate*, Phys. Rev. E **55** (1997), 7782.
50. M. Plesovskikh, S. M. Shandarov, A. G. Mart'yanov, A. E. Mandel', N. I. Burimov, E. A. Shaganova, Yu. F. Kargin, V. V. Volkov, A. V. Egorysheva, *Vector two-wavelength interaction on reflection holographic gratings in cubic gyrotropic photorefractive crystals*, Quantum Electron. **35** (2005), 163.
51. J. Feinber, *Self-pumped, continuous-wave phase conjugator using internal reflection*, Opt. Lett. **7** (1982), 486.
52. A. M. Smout, R. W. Eason, *Bistability and noncommutative behavior of multiple-beam self-pulsing and self-pumping in BaTiO₃*, Opt. Lett. **12** (1987), 51.
53. M. D. Ewbank, *Mechanism for photorefractive phase conjugation using incoherent beams*, Opt. Lett. **13** (1988), 47.
54. J. Feinber, *Asymmetric self-defocusing of an optical beam from the photorefractive effect*, J. Opt. Soc. Am. B. **72** (1982), 46.
55. A. Esayan, A. Zozulya, V. Tikhonchuk, *Self-curvature of a light beam in a photorefractive crystal*, Lebedev Phys. Short Commun. Phys. **5** (1982), 45.
56. O. V. Lyubomudrov, V. V. Shkunov, *Self-bending specklons in photorefractive crystals*, J. Opt. Soc. Am. B. **11** (1994), 1403.
57. A. Brignon, S. Breugnot, J. P. Huignard, *Very high-gain two-wave mixing in BaTiO₃ with a self-bent pump beam*, Opt. Lett. **20** (1995), 1689.
58. M. Segev, Y. Ophir, B. Fischer, *Nonlinear multi two-wave mixing, the fanning process and its bleaching in photorefractive media*, Opt. Comm. **77** (1990), 265.
59. M. Segev, Y. Ophir, B. Fischer, *Photorefractive self-defocusing*, Appl Phys. Lett. **56** (1990), 1086.
60. A. A. Zozulya, M. Saffman, and D. Z. Anderson, *Propagation of light beams in photorefractive media: fanning, self-bending, and formation of self-pumped four-wave-mixing phase conjugation geometries*, Phys. Rev. Lett. **73** (1994), 818.
61. S. I. Stepanov, M. P. Petrov, *Efficient unstationary holographic recording in photorefractive crystals under an external alternating electric field*, Opt. Comm. **53** (1995), 292.

62. M. V. Borodin, N.I. Nazhestkina, S.M. Shandarov, R.V. Litvinov, *Self-Bending of the light beam trajectory in photorefractive crystals in an external alternating-sign electric field*, Russian Physics Journal **44** (2001), 1050.
63. M. P. Shaskol'skaya, ed., *Acoustic Crystals [in Russian]*, Nauka, Moscow, 1982.
64. M. P. Petrov, S. I. Stepanov, and A. V. Khomenko, *Photorefractive Crystals in Coherent Optical Systems*, Springer-Verlag, Berlin, 1991.
65. A. M. Glass, *Photorefractive Effect*, Opt. Eng. **17** (1978), 470.
66. G. C. Valley and M. B. Klein, *Optimal properties of photorefractive materials for optical data processing*, Opt.Eng. **22** (1983), 704.
67. G. C. Valley, M. B. Klein, R. A. Mullen, D. Rytz, and B. Wechsler, *Photorefractive Materials*, Annu. Rev. Mater. Sci. **18** (1988), 165.
68. M. Cronin-Golomb, B. Fischer, J. White, and A. Yariv, *Theory and applications of four-wave mixing in photorefractive media*, IEEE J. Quantum Electron. **QE-20** (1984), 12.
69. G. C. Valley, M. Segev, B. Crosignani, A. Yariv, M. M. Fejer, M. C. Bashaw, *Dark and bright photovoltaic spatial solitons*, Phys. Rev. A **50** (1994), R4457.
70. M. Segev, G. C. Valley, B. Crosignany, P. Di. Porto, A. Yariv, *Steady-state spatial screening solitons in photorefractive material with external applied field*, Phys. Rev. Lett. **73** (1994), 3211.
71. D. N. Christodoulides, M. I. Carvalho, *Bright, dark and grey spatial soliton states in photorefractive media*, J. Opt. Soc. Am. B **12** (1995), 1628.
72. J. Feinberg and G. D. Bacher, *Phase-locking lasers with phase conjugation*, Appl. Phys. Lett. **48** (1986), 570.
73. D. A. Rockwell and C. G. Giuliano, *Coherent coupling of laser gain media using phase conjugation*, Opt. Lett. **11** (1986), 147.
74. M. Segev, S. Weiss, and B. Fischer, *Coupling of diode laser arrays with photorefractive passive phase conjugate mirrors*, Appl. Phys. Lett. **50** (1986), 1397.
75. S. Sternklar, S. Weiss, M. Segev, and B. Fischer, *Beam coupling and locking of lasers using photorefractive four-wave mixing*, Opt. Lett. **11** (1986), 528.
76. M. Cronin-Golomb, A. Yariv, and I. Ury, *Coherent coupling of diode lasers by phase conjugation*, Appl. Phys. Lett. **48** (1986), 1240.

77. J. O. White, G. C. Valley, and R. A. McFarlane, *Coherent coupling of pulsed dye oscillators using nonlinear phase conjugation*, Appl. Phys. Lett. **50** (1987), 880.
78. M. A. Kramer, S. Sifuentes, and C. M. Clayton, *Phase locking of ring dye lasers using incoherent beam coupling*, Appl. Opt. **27** (1988), 1374.
79. C. J. Gaeta, R. C. Lind, W P. Brown, and C. R. Giuliano, *Coupled cw dye lasers using intracavity four-wave mixing*, Opt. Lett. **13** (1988), 1093.
80. D. Statman and B. Liby, *Two-beam cross coupling from mutually incoherent lasers*, J. Opt. Soc. Am. B **6** (1989), 1884.
81. T. Tschudi, A. Herden, J. Goltz, H. Klumb, F. Laeri, and J. Albers, *Image amplification by two-and four-wave mixing in BaTiO₃ photorefractive crystals*, IEEE J. Quantum Electron. **QE-22** (1986), 1493.
82. J. A. Khoury and R. W Eason, *Photorefractive deconvolution techniques for optical differentiation of images*, J. Mod. Opt. **36** (1989), 369.
83. P. Yeh, *Introduction to photorefractive nonlinear optics*, John Wiley and Sons, Inc., New York, 1993.
84. M. D. Castillo, J. J. Sanchezmondragon, S. I. Stepanov, M. B. Klein, B. A. Wechsler, *Probe beam wave-guiding induced by spatial dark solitons in photorefractive BTO crystal*, Rev. Mex. Fis. **41** (1995), 1.
85. M. Segev, M. Shih, G.C. Valley, *Photorefractive screening solitons of high and low intensity*, J. Opt. Soc. Am. B **13** (1996), 706.
86. Z. Chen, M. Mitchell, M. Shih, M. Segev, M. Garrett, G. Valley, *Steady-state dark photorefractive screening solitons*, Opt. Lett. **21** (1996), 629.
87. Z. Chen, M. Shih, M. Segev, D. Wilson, R. Muller, P. Maker, *Steady-state vortex-screening solitons formed in biased photorefractive media*, Opt. Lett. **22** (1997), 1751.
88. M. Castillo, J. Sanchez-Mondragon, S. Stepanov, M. Klein, B. Wechsler, *(1+1)-dimensional dark spatial solitons in photorefractive Bi₁₂TiO₂₀ crystal*, Opt. Comm. **118** (1995), 515.
89. N. V Kukhtarev, V. B. Markov, S. G. Odulov, M. S. Soskin, and V L. Vinetskii, *Holographic storage in electro-optic crystals. I. Steady state*, Ferroelectrics **22** (1979), 961.

90. G. C. Duree, G. Salamo, M. Segev, A. Yariv, B. Crosignani, Di. Porto, E. J. Sharp, *Dimensionality and size of photorefractive spatial solitons*, Opt. Lett. **19** (1994), 1195.
91. G. Pauliat, C. Besson, G. Rosen, *Polarization properties of two-wave mixing under an alternating electric field in BSO crystals*, IEEE J. Quantum Electron. **QE-25** (1989), 1736.
92. K. Walsh, A. K. Powell, C. Stace, and T. J. Hall, *Techniques for the enhancement of space-charge fields in photorefractive materials*, J. Opt. Soc. Am. B **7** (1990), 288.
93. A. Grunnet-Jepsen, C. H. Kwak, I. Richter, L. Solymar, *Fundamental space-charge fields for applied alternating electric fields in photorefractive materials*, J. Opt. Soc. Am. B **11** (1994), 124.
94. M. Zairi, W.H. Steier, P. M. Ranon, M. B. Klein, S. Trivedi, *Enhancement of the photorefractive gain at 1.3–1.5 μm in CdTe using alternating electric fields*, J. Opt. Soc. Am. B **9** (1992), 1461.
95. S. I. Stepanov, M. P. Petrov, *Photorefractive Materials and Their Applications I. Fundamental Phenomena*, ed. by P. Günter, J. P. Huignard, Springer, Berlin, Heidelberg, 1988.
96. A. A. Kamshilin, V. V. Prokofiev, T. Jaaskelainen, *Beam fanning and double phase conjugation in a fiber-like photorefractive sample*, IEEE J. Quantum Electron. **QE-31** (1995), 1642.
97. A. A. Kamshilin, H. Tuovinen, V. V. Prokofiev, T. Jaaskelainen, *Phase conjugate mirrors on the base of $\text{Bi}_{12}\text{TiO}_{20}$ photorefractive fiber*, Opt. Mater. **4** (1995), 399.
98. J. Takacs, L. Solymar, *Subharmonics in $\text{Bi}_{12}\text{SiO}_{20}$ with an applied ac electric field*, Opt. Lett. **17** (1992), 247.
99. C.H. Kwak, M. Shamonin, J. Takacs, L. Solymar, *Spatial subharmonics in photorefractive $\text{Bi}_{12}\text{SiO}_{20}$ crystal with a square wave applied field*, Appl. Phys. Lett. **62** (1993), 328.
100. R. V. Litvinov, S. M. Shandarov, D. V. Yakimov, A. V. Reshet'ko, S. N. Pitchenko, Yu. F. Kargin, V. V. Volkov, *Generation of spatial subharmonics of a photorefractive grating in bismuth silicate crystals in an alternating electric field*, Tech. Phys. **42** (1997), 1400.

101. A. A. Kamshilin, E. Raita, V. V. Prokofiev, T. Jaaskelainen, *Nonlinear self-channeling of a laser beam at the surface of a photorefractive fiber*, Appl. Phys. Lett. **67** (1995), 3242.
102. A. A. Kamshilin, E. Raita, A. V. Khomenko, *Intensity redistribution in a thin photorefractive crystal caused by strong fanning effect and internal reflections*, J. Opt. Soc. Am. B **13** (1996), 2536.
103. H. Meng, G. Salamo, M. Shih, and M. Segev, *Coherent collisions of photorefractive solitons*, Opt. Lett. **22** (1997), 448.
104. W. Krolikowski, N. Akhmediev, B. Luther-Davies, and M. Cronin-Golomb, *Self-bending photorefractive solitons*, Phys. Rev. E **54** (1996), 5761.
105. S. Gatz and J. Herrmann, *Propagation of optical beams and the properties of two-dimensional spatial solitons in media with a local saturable nonlinear refractive index*, J. Opt. Soc. Am. B **14** (1997), 1795.
106. W. Krolikowski, N. Akhmediev and B. Luther-Davies, *Effect of natural optical activity on the propagation of photorefractive solitons*, Opt. Comm. **132** (1996), 179.
107. J. Nye, Physical Properties of Crystals, *Their Representation by Tensors and Matrices*, Clarendon Press, Oxford, 1964.
108. P. A. Marques, J. J. Sanchez Mondragon, S. I. Stepanov, V. Vysloukh, *Transient self-bending of the laser beams in photorefractive crystals with drift nonlinearity*, Phys. Rev. A. **54** (1996), R2563.
109. J. Petter, C. Weilmann, C. Denz, A. Stepken, and F. Kaiser, *Self-bending of photorefractive solitons*, Opt. Comm. **170** (1999), 291.
110. D. Kip, M. Wesner, C. Herden, and V. Shandarov, *Interaction of spatial photorefractive solitons in a planar waveguide*, Appl. Phys. B **68** (1999), 971.
111. W. Krolikowski, B. Luther-Davies, C. Denz, and Th. Tschudi, *Annihilation of photorefractive solitons*, Opt. Lett. **23** (1998), 97.
112. S. F. Ashby, T. A. Manteuffel and P. E. Saylor, *A taxonomy for conjugate gradient methods*, Siam J. Numer. Anal. **27** (1990), 1542.
113. L. Sun and G. L. Yip, *Modified finite-difference beam-propagation method based on the Douglas scheme*, Opt. Lett. **18** (1993), 1229.

-
114. S. M. Shandarov, N. I. Nazhestkina, O. V. Kobozev and A. A. Kamshilin, *Nonlinearity of a response in photorefractive crystals with a square-wave applied field*, Appl. Phys. B **68** (1991), 1007.
 115. A. R. Mitchell, *Computational Methods in Partial Differential Equations*, John Wiley and Sons, London, 1969.
 116. S. M. Shandarov, V. V. Shepelevich, N. D. Khat'kov, *Measurement of inductivity tensor in cubic photorefractive piezoelectric crystals under the influence of the holographic grating electric field*, Opt. Spectr. **70** (1991), 1068.
 117. M. Zgonik, P. Bernasconi, M. Duelli, R. Schlessler, P. Günter, M. H. Garrett, D. Rytz, Y. Zhu, X. Wu, *Dielectric, elastic, piezoelectric, electro-optic, and elasto-optic tensors of BaTiO₃ crystals*, Phys. Rev. B **50** (1994), 5941.

Ehrenwörtliche Erklärung

Ich erkläre hiermit ehrenwörtlich, daß ich die vorliegende Arbeit selbständig, ohne unzulässige Hilfe Dritter und ohne Benutzung anderer als der angegebenen Hilfsmittel und Literatur angefertigt habe. Die aus anderen Quellen direkt oder indirekt übernommenen Daten und Konzepte sind unter Angabe der Quelle gekennzeichnet.

Weitere Personen waren an der inhaltlich-materiellen Erstellung der vorliegenden Arbeit nicht beteiligt. Insbesondere habe ich hierfür nicht die entgeltliche Hilfe von Vermittlungs- bzw. Beratungsdiensten (Promotionsberater oder andere Personen) in Anspruch genommen. Niemand hat von mir unmittelbar oder mittelbar geldwerte Leistungen für Arbeiten erhalten, die im Zusammenhang mit dem Inhalt der vorgelegten Dissertation stehen.

Die Arbeit wurde bisher weder im In- noch im Ausland in gleicher oder ähnlicher Form einer anderen Prüfungsbehörde vorgelegt.

Die geltende Promotionsordnung der Physikalisch-Astronomischen Fakultät ist mir bekannt.

Ich versichere ehrenwörtlich, dass ich nach bestem Wissen die reine Wahrheit gesagt und nichts verschwiegen habe.

Jena, den 27. April 2010

Oleg Kashin

Acknowledgement

I would like to express the deepest appreciation to Prof. Dr. R. Kowarschik and Dr. V. Matusevich for inviting me to the Institute of Applied Optics of Friedrich-Schiller University Jena and giving me opportunities for successful finishing my PhD work. Without their guidance and persistent help this dissertation would not have been possible.

Advices and experiences of Prof. Dr. R. Kowarschik were invaluable during the writing of this work that enabled me to terminate my PhD studies.

I am heartily thankful to my supervisor, Dr. V. Matusevich, whose encouragement and guidance helped me to realise my plans.

I owe my deepest gratitude to Prof. S. M. Shandarov from Tomsk State University of Control Systems and Radioelectronics being co-author and ideologist of almost all reviewed articles on which this work is based. Without his invaluable help this work would not have been possible.

In addition, I would like to appreciate K. Pismennaya, who performed the experiment for the third chapter of my dissertation.

I would like to thank also Dr. A. Kiessling for the usefull discussion of some results of my researches.

I am grateful to Dr. N. Burimov and V. Datsyuk from Tomsk State University of Control Systems and Radioelectronics for their advices.

Lastly, I am indebted to my many of my colleagues who supported me in any respect during the completion of this work.

I wish to avail myself of this opportunity, express a sense of gratitude and love to my wife, son and my beloved parents for their warm encouragement and for everything that has helped me during my researches.

I would like to thank the Deutsche Forschungsgemeinschaft for financial support during my PhD study within the research Unit 532 "Nonlinear spatio-temporal dynamics in dissipative and discrete optical systems".

Curriculum Vitae

Name: Oleg Kashin
Date of birth: 16 June 1981
Place of birth: Asino, Russia
1988 – 1998 School № 8, Asino
1998 – 2003 Tomsk State University of Control Systems and Radioelectronics, Diploma
2003 – 2006 Tomsk State University of Control Systems and Radioelectronics, The Department of electronic devices, PhD student
2006 – 2010 Fridrich Schiller University of Jena, Institute of Applied Optics, PhD student

Jena, 27 April 2010

Oleg Kashin